THESIS ON NATURAL AND EXACT SCIENCES B117

Dispersion Analysis of Wave Motion in Microstructured Solids

TANEL PEETS

TUT PRESS

TALLIN UNIVERSITY OF TECHNOLOGY
Faculty of Science
Institute of Cybernetics

The dissertation was accepted for the defence of the degree of Doctor of Philosophy (Applied Mechanics) on 5 October 2011

Supervisor:
Jüri Engelbrecht, DSc, Professor, Institute of Cybernetics at Tallinn University of Technology, Tallinn, Estonia

Opponents:
Hui-Hui Dai, PhD, Professor, City University of Hong Kong, Hong Kong, PR China

Jiří Plešek, PhD, Deputy Director of the Institute of Thermomechanics AS CR, Prague, Czech Republic

Defence of the thesis: 5 December 2011

Declaration:
Hereby I declare that this doctoral thesis, my original investigation and achievement, submitted for the doctoral degree at Tallinn University of Technology, has not been submitted for any academic degree.

Tanel Peets

ISSN 1406-4723
ISBN 978-9949-23-185-0 (publication)
ISBN 978-9949-23-186-7 (PDF)

LOODUS- JA TÄPPISTEADUSED B117

Lainete dispersioon mikrostruktuuriga materjalides

TANEL PEETS

TTÜ
KIRJASTUS

Contents

List of Figures

List of Publications

Publication I: T. Peets, M. Randrüüt, and J. Engelbrecht. On modelling dispersion in microstructured solids. *Wave Motion*, 45:471–480, 2008

Publication II: T. Peets and K. Tamm. Dispersion analysis of wave motion in microstructured solids. In T.-T. Wu and C.-C. Ma, editors, *IUTAM Symposium on Recent Advances of Acoustic Waves in Solids: Proceedings, Taipei, Taiwan, May 25-28, 2009*, volume 26 of *IUTAM Bookseries*, pages 349–354. Springer, Dordrecht, 2010

Publication III: A. Berezovski, J. Engelbrecht, and T. Peets. Multiscale modeling of microstructured solids. *Mechanics Research Communications*, 37(6):531–534, 2010

Approbation:

Tanel Peets, 'Dispersiooni modelleerimine mikrostruktuuriga materjalide jaoks', XIII Estonian Mechanics days, Tallinn, Sept 15–16, 2008.

Tanel Peets (speaker), Kert Tamm, 'Dispersion Analysis on Wave Motion in Microstructured Solids', Symposium on Recent Advances of Acoustic Waves in Solids, Taiwan, May 25–28, 2009 (invited presentation).

Tanel Peets, 'Internal scales and dispersive properties of microstructured materials', The Seventh IMACS International Conference on Nonlinear Evolution Equations and Wave Phenomena: Computation and Theory, The University of Georgia, Athens, USA, April 04–07, 2011.

Introduction

Modern science has always been interested in the internal structure of the matter. Besides the quest for elementary particles, many technological applications are, however, based on the concept of continuity and the phenomena on the macroscale are explained by making use of the averaged properties of the underlying microstructure. In molecular physics, for example, the temperature of the material is recognised as the average kinetic energy of molecules.

In case of contemporary materials science, the microstructure of the material is not specifically characterised by atoms, but is set on a scale that is in the order of micrometres. This microstructure is not only used for explaining various properties of materials, but is also used for engineering of solids as it is done in case of functionally graded materials or composites. In general, microstructured materials like alloys, crystallites, ceramics, functionally graded materials, etc. have gained wide application in modern technologies.

Classical theories of wave motion in solids aim to smooth out the inhomogeneities created by the underlying microstructure. These theories have played an important role in the development of the materials science and have been used in many applications. Contemporary technology is, however, characterised by high–frequency and high–intense impacts. In this case the wavelengths are comparable to the internal scale of the microstructure and that is why the internal structure of a material becomes important in engineering applications. Consequently, there is an urgent need to understand how the wave processes are influenced by the underlying microstructure.

One of the most important effects created by the microstructure is dispersion, which in a nutshell means that the speed of the wave is not constant but depends on the wave number of the harmonics. This is due to the length scale that the internal structure brings into the models. If the wavelength of the wave is much larger than the internal scale, the waves do not 'feel' the internal structure and the classical theories give good predictions. When the wavelengths approach the internal scale, the wave propagation becomes strongly influenced by the underlying microstructure [15].

Moreover, in case of the microstructure, the dispersion is not only characterised by the variation in the speed of the wave, but also in the emergence of high frequency, so-called optical dispersion branches, which reflect the additional degrees of freedom due to the microstructure. The presence of the optical branches brings more modes of wave propagation into the model, hence making the wave propagation considerably more complex. The classical theories of homogeneous continua fail to predict the existence of the optical dispersion branches.

Over the previous decades many theories of microstructured solids have been proposed. In the present thesis we follow the ideas of Mindlin who has interpreted the

microstructure ‘as a molecule of a polymer, a crystallite of a polycrystal, or a grain of a granular material’ [25]. The one-dimensional version of the Mindlin model, derived by Engelbrecht et al. [12], and its hierarchical approximation will serve as a basis for our analysis. Based on the separation of the macro- and microstructure of a material, this model, called the Mindlin–Engelbrech–Pastrone model, is characterised by a clear physical structure of the governing equation.

The aim of the present thesis is to analyse the dispersion properties in case of the full and the hierarchical model. The latter is much simpler than the full model and has a clear structure of two wave operators that could be compared with the classical wave equation. There is a need to provide a deeper insight into the appearance of the optical dispersion branches and to analyse whether they create any measurable effect that needs to be accounted for in real experiments. As the hierarchical approximation excludes the effects of the optical dispersion branch, then the possible influence of the optical dispersion branch are of great importance when estimating the applicability of the hierarchical approximation. Although the present work is theoretical, it is related the possible practical applications of nondestructive testing of materials.

The results of the thesis are represented in three scientific papers. In Publication I [26] the dispersion relations are derived and analysed. In Publication II [27] the effect of the optical dispersion branch is described. Multiscale extensions of the Mindlin–Engelbrecht–Pastrone model are derived and the corresponding dispersion properties are analysed in Publication III [6]. In addition, two papers, one devoted to the solutions of the boundary value problem and the other to the solutions of the initial value problem, have been submitted for publication.

The thesis is organised as follows. Section 1 gives an overview of the dispersive models of wave motion. In Section 2 the Mindlin–Engelbrecht–Pastrone model is introduced along with multiscale extension and hierarchical approximation and Section 3 is devoted to the dispersion analysis of the derived models. The boundary value problem is analysed is Section 4 and the initial value problem is analysed in Section 5. Conclusions can be found in Section 6.

Acknowledgements

I would like to thank my supervisor Prof. Jüri Engelbrecht for introducing me to the field of wave propagation in microstructured solids and for his support and guidance.

I would also like to thank my colleagues at CENS, especially my roommate Kert Tamm for fruitful discussions in various topics. Some of the ideas in this thesis have sprung from our discussions.

Financial support from the Estonian Science Foundation is appreciated.

I would like to thank my family. Especially my grandmother who inspired me in pursuing a scientific career and my father and mother who have supported me in the choices I have made.

Last but not least, my greatest gratitude goes to my wife Mari-Liis. This thesis would have not been possible without her support and patience.

1. Overview of dispersive models of wave motion

Realistic mathematical models describing the propagation of deformation waves in solids should include also the description of dispersive and/or dissipation effects. Here we focus on dispersive effects.

There are two main sources of dispersion – geometrical and physical. Waves in a slender rod, for example, are dispersive due to the geometry of the rod. Waves in microstructured solids, on the other hand, are dispersive because different harmonic components of the wave 'feel' the microstructure differently. In order to model wave motion in these environments, the geometrical or physical structure of the material must be taken into account.

The mathematical models proposed for describing waves in microstructured solids can be divided into two groups – one group of models is based on lattice theories [3, 8, 22, 24] and the group on continuum theory [12, 14, 21, 25].

In the discrete approach the microstructure is treated as point masses with well-defined distribution and interactions between the particles. The particles may move from equilibrium positions and allow elastic wave propagation. Since discrete models bear certain resemblance to the atomic scale, the lattice models are very appealing in modelling the dynamics of crystal lattices [8, 20].

If the wave motion is set on the scale that is much larger than the distance between the particles of the lattice, the motion of the lattice can be described by a PDE, i.e., the model can be continualised. In principle continualisation means the approximation of the local (discrete) operator by a nonlocal one [2]. Many continualisation methods have been proposed. These methods are most often based on Taylor series expansion, but also other methods like Padé approximants and composite equations have been introduced [2]. This approach is attractive from the physical point of view because the 'atomic' scale is used in order to model wave propagation at the macroscale.

In the microcontinuum approach the classical continuum theory is enhanced in a way that matter is envisioned as a collection of deformable cells. These deformable cells bring new internal degrees of freedom to the equations of wave motion and their influence is also reflected in the number of dispersion curves. Straightforward modelling of microcontinuum means assigning physical properties to every volume element dV in a solid, introducing the dependence on coordinates X^k. A much more effective way, however, is to separate the macro- and microstructure and to formulate the conservation laws are formulated for both structures separately [12, 14, 25]. In principle there is no limit for the number of embedded microstructures and hence the microcontinuum approach is useful in modelling the effects of different scales [6, 12].

1.1. Infinite 1D chain of particles

Although theories of wave propagation in crystal lattices can be traced back all the way to Isaac Newton, who attempted to derive a formula for the speed of sound [8], the model of the infinite one-dimensional chain of particles is associated with Max Born and Theodore von Karman.

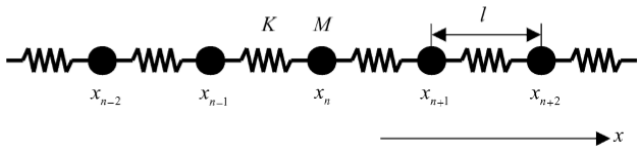

Figure 1: Infinite 1D chain of particles. Reproduced from [24].

The Born–Karman model is a chain of identical point masses m with some proposed topology and interaction between the particles. This interaction is usually defined by springs of stiffness K (Fig. 1) or by interaction energy between the masses. Mathematically these two views are equivalent, because the equations of motion will include either the spring constant explicitly or the second derivative of energy, which has the same dimensions as the spring constant.

The coordinate of each particle is given by $x_n = nd + \psi_n$, where d is the lattice spacing and ψ_n is a quantity that is propagated as a wave if the physical problems admit a solution of the type

$$\psi_n = Ae^{i(kX_n - \omega t)}, \tag{1}$$

where $X_n = nd$. This will lead to the well-known dispersion relation

$$\omega^2 = \frac{4K}{m}\sin^2\left(\frac{kd}{2}\right), \tag{2}$$

where only nearest-neighbour interactions have been accounted for. Since ω is not a linear function of k, it is clear that waves in one-dimensional crystal lattices are dispersive. The dispersion relation of (2) is depicted in Fig. 2. If more particles are allowed to interact with each other, the dispersion curves will change in a short wave limit [3].

It is clear from Eq. (2) and Fig. 2 that the frequency ω is a periodic function of kd with a period of 2π in kd. This is a general and direct consequence of the periodic and discontinuous structure. Therefore it is sufficient to study the dispersion relation $\omega = f(kd)$ inside one period of kd. The obvious choice is

$$-\pi \leq kd \leq \pi \tag{3}$$

This condition is also known as the first Brillouin zone. The limitation (3) also means that $\lambda \geq 2d$. The shortest wavelength is thus equal to twice the distance between

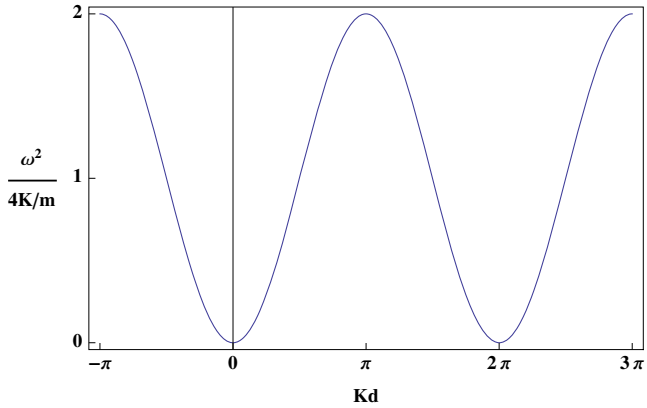

Figure 2: Dispersion curve for Eq. (2) (Born–Karman Model).

particles and corresponds to a certain critical frequency or cutoff frequency ω_m that is characteristic of the structure. In many cases ω_m is the maximum frequency and the system works as a low-pass filter [8].

1.2. 1D diatomic chain of particles

There are a number of ways of enhancing the lattice theories. For example, one could enhance the interaction potential by introducing nonlinearities [22]. Another way is to add more degrees of freedom into the system either by adding more particles per unit cell [3, 8] or by allowing the lattice or a particle to rotate [3, 22]. The additional degrees of freedom will be reflected in the number of dispersion branches.

The easiest example is one-dimensional NaCl that has two atoms per unit cell – one with mass m_1 and the other with m_2. The dispersion relation is then [8]

$$\omega^2 = U_1'' \left(\frac{1}{m_1} + \frac{1}{m_2} \right) \pm \left[\left(\frac{1}{m_1} + \frac{1}{m_2} \right)^2 - \frac{4 \sin^2 kd}{m_1 m_2} \right]^{1/2} \tag{4}$$

where U_1 is the interaction energy which accounts for nearest-neighbour interaction only. The dispersion curves for Eq. (4) are depicted in Fig. 3, where two dispersion branches can be seen.

In order to fully understand the meaning of the second dispersion branch, we will find the amplitude ratio for small kd. The amplitude ratio is exactly 1 for the lower branch and $-m_2/m_1$ for the upper branch.

The waves corresponding to the lower branch have equal amplitudes and phase difference equal zero; thus all the particles are displaced by the same amount and in the

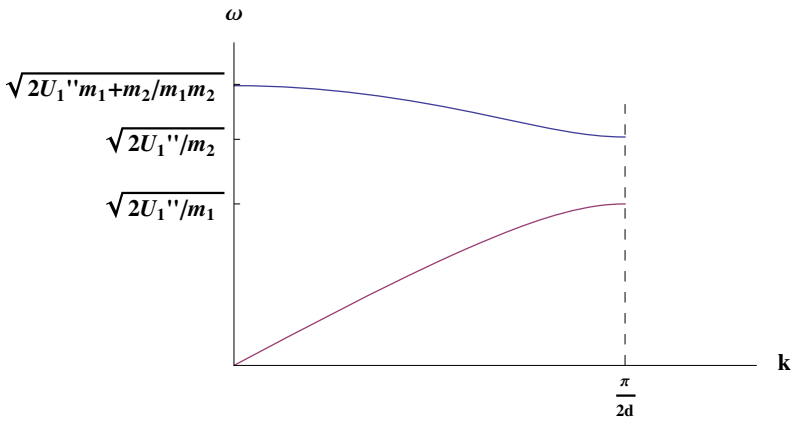

Figure 3: Dispersion curves for Eq. (4) (1D NaCl).

same direction. The wavelength of each wave is infinite and the lattice is displaced as a whole. There is no restoring force and the frequency is zero [8].

On the other hand, the waves for the upper branch are exactly out of phase, i.e., the displacement of particles of mass m_1 is opposite to that of the neighbouring particles m_2. Evidently the centre of mass of the two neighbouring particles is stationary, but restoring forces enter so that the frequencies of the waves are no longer zero. The lengths of the waves are still infinite since, each wave is regarded as propagating through just one type of particle [8].

Traditionally the lower branch is called the acoustic branch and the upper branch the optical branch. The names are due to the fact that in case of one-dimensional NaCl, the opposite movement of the charges induces photons. It is important, however, to understand that while acoustic branches are external modes where all particles move in unison, the optical branches are internal modes that reflect the effect of internal degrees of freedom.

1.3. Continualisation

In case of a discrete chain, the equation of motion of each particle is given by

$$m\frac{\partial^2 u_n(t)}{\partial t^2} = K(u_{n-1}(t) - 2u_n(t) + u_{n+1}(t)). \tag{5}$$

The main idea of continualisation is to replace discrete degrees of freedoms $u_n(t)$ and $u_{n\pm1}(t)$ by continuous field variables $u(x,t)$ and $u(x\pm l,t)$. Standard continualisation is achieved by using a Taylor series. If only the first terms in series expansion are

accounted for, we are left with the classical wave equation which is also known as the continuum limit

$$u_{tt} = d^2\omega_0^2 u_{xx}. \tag{6}$$

Dispersive continuum equations can be derived by preserving more terms in series expansion. If two terms are preserved, we get the following equation:

$$u_{tt} = d^2\omega_0^2 \left(u_{xx} + \frac{d^2}{12} u_{xxxx} \right), \tag{7}$$

where $\omega_0 = (K/m)^{1/2}$ is the natural frequency.

It is well known that for waves with $k = (12/d^2)^{1/2}$ the frequencies are imaginary and Eq. (7) becomes unstable [24]. One way of improving the model (7) would be adding more terms from the series expansion. If a third term $(d^4/360 \cdot u_{xxxxxx})$ is added, the model indeed becomes unconditionally stable. The drawback, however, is that the enhanced model allows infinitely fast propagation of energy [24].

The continualisation methods can be improved in several ways. One possibility would be enhancing the methods used for going from the discrete degree of freedom to the continuous one [24]. Another possibility is to replace the unstable term in Eq. (7) by a stable one [4, 28]. The improvement of the models is due to the fourth order mixed derivative that will appear in derived equations. The following model was derived in [23]:

$$u_{tt} = c^2 u_{xx} + d^2 A_{21} \left(u_{tt} - c^2 \frac{A_{22}}{A_{21}} u_{xx} \right)_{xx} \tag{8}$$

where $c = d\omega_0$ has the dimension of speed and A_{21} and A_{22} are dimensionless positive parameters. It is important to mention that all the aforementioned methods derive similar equations with only differences in the choice of parameters.

Although model (8) is unconditionally stable, it is not causal as it allows infinite speed of elastic energy transfer by evanescent waves [23]. Model (8) can be further improved by adding a fourth time derivative into the model [23]:

$$u_{tt} = c^2 u_{xx} + d^2 A_{21} \left(u_{tt} - c^2 \frac{A_{22}}{A_{21}} u_{xx} \right)_{xx} - \frac{d^2}{c^2} A_{23} u_{tttt} \tag{9}$$

where A_{23} is a positive constant. A similar result is also derived by Pichugin et. al., by following a different method [28].

The existence of the fourth order time derivative in Eq. (9) is reflected in the number of dispersion branches – in addition to the acoustic branch, also an optical branch is present (Fig. 4). It is due to the optical dispersion branch that the evanescent waves cannot propagate as waves with frequencies higher than cutoff frequency are now propagated at a finite speed [23].

The optical dispersion branch also brings additional degrees of freedom into the continuum model. This is expected as microstructure has degrees of freedom of its own. It will be shown in the next subsection that these additional degrees of freedom arise naturally in microcontinuum models.

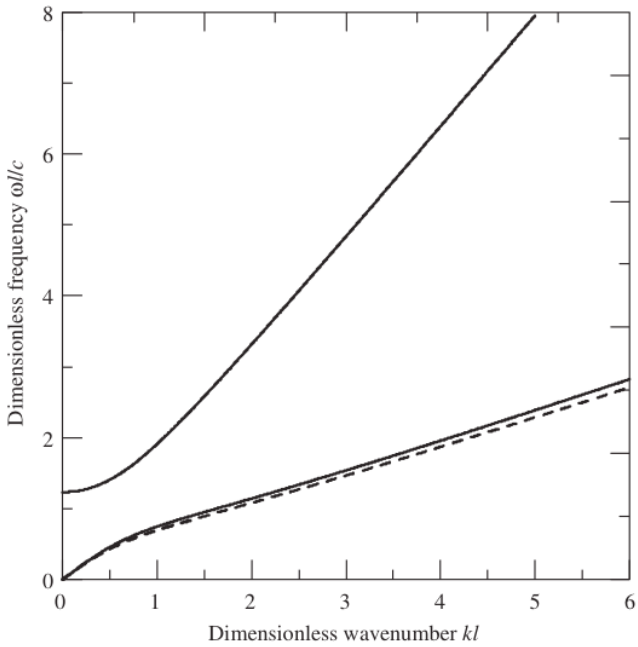

Figure 4: Dispersion curves for Eqs. (9) (solid lines) and (8) (dashed line). Reproduced from [23].

1.4. Microcontinuum theories

The main idea of microcontinuum field theories is that the matter is envisioned as a large collection of deformable cells. Each cell (or microvolume) has a finite size and an inner structure that represents its microstructure. Mathematically the inclusion of the internal scale means that each material particle is enhanced with three deformable directors that bring nine degrees of freedom over the classical theory [15]. These extra degrees of freedom are reflected in additional modes of high frequency wave propagation. These modes are seen in experiments but are not predicted by classical continuum mechanics.

The foundations of microcontinuum theories were independently laid down by Eringen and Suhubi [16] and Mindlin [25]. Although Eringen and Suhubi's approach is more general, because nonlinearities and thermoelasticity are included, the results are similar when isothermal linear wave propagation is considered.

One should also mention that simplifications of microcontinuum theories exist. When the material points are only allowed to have breathing-type microdeformations, we have reduced the model to microstretch continuum and the internal degrees of freedom are reduced to four – three microrotations and one microstretch. In micropolar continuum the material particle is only allowed to have rigid rotations. When the deformable directors are removed, the microcontinuum theory reduces to the classical continuum theory [15].

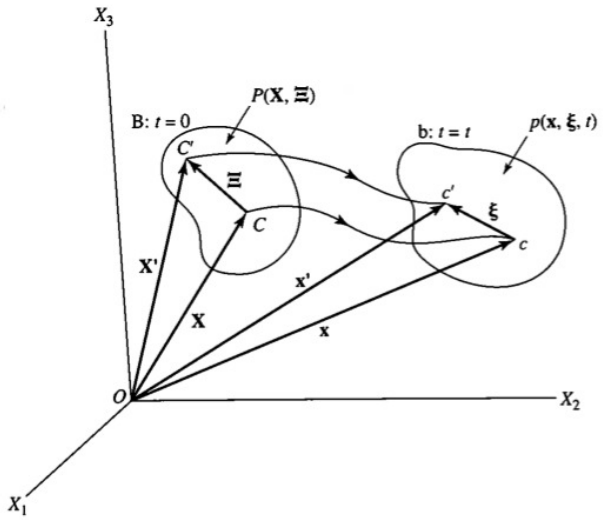

Figure 5: Deformation of the microelement. Reproduced from [15]

The motion of microstructured material is depicted in Fig. 5. The relative position of the microelement in the reference state B is defined by two vectors – the position

of the centroid C (given by the vector X_K, $K = 1,2,3$) and the relative position of the microelement in respect to the centroid C (given by the vector Ξ_K). The deformation carries $P(\boldsymbol{X}, \boldsymbol{\Xi})$ to $p(\boldsymbol{x}, \boldsymbol{\xi})$ so that

$$X_K \to x_k = \hat{x_k}(X_K, t), \tag{10}$$

$$\Xi_K \to \xi_k = \hat{\xi}_k(X_K, \Xi_K, t), \tag{11}$$

$$x'_k = x_k + \xi_k, \tag{12}$$

where $K = 1,2,3$ and $k = 1,2,3$. The mapping (10) is called macromotion and the mapping (11) is called micromotion. Since material particles considered are very small in comparison to the macroscopic scales of the body, the following linear approximation in Ξ_K is permissible for micromotion:

$$\xi_k = \chi_{kK}(X_K, t)\Xi_K. \tag{13}$$

The inverse macro- and micromotions are given by

$$X_K = \hat{X}_k(x_k, t), \tag{14}$$

$$\Xi_K = \chi_{Kk}(x_k, t)\xi_k, \tag{15}$$

The two-point tensors χ_{kK} and χ_{Kk} are called the microdeformation and the inverse microdeformation tensors, respectively.

Due to the inner structure the motion of microstructured material is characterised not only by classical macrodeformation consisting of translation, macrorotation and macrostretch, but also by microdeformation that involves translation of the particles, microrotation and microstretch that can be accompanied by further microrotations [15]. These different modes of deformation allow additional modes of wave propagation.

1.5. Mindlin's theory of microstructured materials

This subsection is based on [25].

In order to describe a microstructured medium, the following tensors have been introduced: a strain tensor (macrodeformation tensor)

$$\varepsilon_{ij} = \frac{1}{2}\left(\frac{\partial u_j}{\partial x_i} + \frac{\partial u_i}{\partial x_j}\right), \tag{16}$$

where u is the macrodisplacement, the tensor of relative deformation (the difference between the macrodisplacement gradient and the microdeformation)

$$\gamma_{ij} = \frac{\partial u_j}{\partial x_i} - \Psi_{ij}, \tag{17}$$

where Ψ_{ij} is the microdeformation tensor and the microdeformation gradient (the macrogradient of the microdeformation)

$$\varkappa_{ijk} = \frac{\partial \Psi_{jk}}{\partial x_i}. \tag{18}$$

All three tensors are independent of the microcoordinates. The internal energy is introduced as

$$U = U(\varepsilon_{ij}, \gamma_{ij}, \varkappa_{ijk}). \tag{19}$$

The strain state of the macrovolume is given by Cauchy stresses

$$\tau_{ij} = \frac{\partial U}{\partial \varepsilon_{ij}} = \tau_{ji}, \tag{20}$$

the relative stresses

$$\sigma_{ij} = \frac{\partial U}{\partial \gamma_{ij}} \tag{21}$$

and the coupled stresses

$$\mu_{ijk} = \frac{\partial U}{\partial \varkappa_{ijk}}. \tag{22}$$

The components of μ_{ijk} can be interpreted as coupled forces per unit area. The kinetic energy is given by

$$T = \frac{1}{2}\rho \dot{u}_j \dot{u}_j + \frac{1}{6}\rho' d_{kl}^2 \dot{\Psi}_{kj} \dot{\Psi}_{lj}, \tag{23}$$

where ρ' is the microdensity, ρ is the sum of macro- and microdensities and d_{kl} is related to the size of the microvolume. If external forces are absent, the wave motion is given by twelve stress-equations of motion

$$\rho \ddot{u}_j = \partial_i(\tau_{ij} + \sigma_{ij}), \tag{24}$$

$$\frac{1}{3}\rho' d_{lj}^2 \ddot{\psi}_{lk} = \partial \mu_{ijk} + \sigma_{jk}. \tag{25}$$

The derivation of the displacement equations of motion can be found in [25]. We will provide dispersion relations only. For equations describing one-dimensional wave processes, the following dispersion relations are derived (see Fig. 6):

(1) shear optical waves (SO)(twice):

$$\frac{1}{3}\rho' d^2 \omega^2 = b_2 + b_3 + (a_{10} + a_{13})k^2, \tag{26}$$

(2) rotational optical waves (RO):

$$\frac{1}{3}\rho' d^2 \omega^2 = b_2 - b_3 + (a_{10} - a_{13})k^2, \tag{27}$$

(3) longitudinal waves – acoustic (LA), optical (LO), dilatational (LDO):

$$\left\| \begin{array}{ccc} k_{11}k^2 - \rho\omega^2 & k_{12}k & k_{13}k \\ k_{21}k & k_{22}k^2 + k'_{22} - \frac{1}{2}\rho' d^2\omega^2 & k_{23}k^2 \\ k_{31}k & k_{32}k^2 & k_{33}k^2 + k'_{33} - \rho' d^2\omega^2 \end{array} \right\| = 0, \qquad (28)$$

(4) and transverse waves – acoustic (TA), optical (TO), rotational optical (TRO) (twice):

$$\left\| \begin{array}{ccc} \bar{k_{11}}k^2 - \rho\omega^2 & \bar{k_{12}}k & \bar{k_{13}}k \\ \bar{k_{21}}k & \bar{k_{22}}k^2 + \bar{k'_{22}} - \frac{1}{2}\rho' d^2\omega^2 & \bar{k_{23}}k^2 \\ \bar{k_{31}}k & \bar{k_{32}}k^2 & \bar{k_{33}}k^2 + \bar{k'_{33}} - \rho' d^2\omega^2 \end{array} \right\| = 0, \qquad (29)$$

where indexed k's are parameters connected to material parameters.

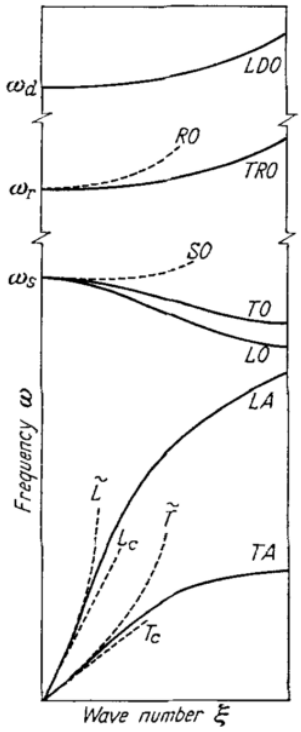

Figure 6: Sketch of the dispersion curves derived form Mindlin's model. Reproduced from [25]

While the acoustic modes are external modes where all cells move in unison, the optical dispersion curves reflect internal degrees of freedom. Nonzero frequency when $k = 0$ is due to the proper motion on the microscale.

It is also clear that while Eqs. (26), (27) are independent modes, the longitudinal and transverse systems form coupled systems of acoustic and optical modes. In the

numerical analysis part of this thesis it will be shown that when coupled modes are present, then harmonic wave propagation on the macroscale induces high frequency motion on the microscale.

In Fig. 6 dispersion curves for classical wave equation (L_c and T_c) and low frequency approximations ($\tilde{L}$ and $\tilde{T}$) are also displayed. The low frequency approximations derived by Mindlin are not perfect because these are usable only at short wavelengths. It will be shown later how to derive an approximation with the slaving principle that is usable at all wavelengths.

1.6. Dispersion of longitudinal waves in rods

Dispersion of waves in rods is an example of geometrical dispersion. Although rods are the simplest of all engineering structures, wave propagation in rods is a rather complicated problem because of the presence of the boundaries. The exact solution for wave motion in rods was derived by Pochhammer [29] in 1876. Pochhammer's theory is, however, usable in infinite rods only and is therefore not very practical for a number of engineering problems. As a result approximate theories have been constructed which, contain the essential features of the exact problem in a simplified form [1].

The simplest approximation is Bernoulli's model which provides a dispersionless model that is only usable at low frequencies and large wavelengths:

$$u_{tt} - c_R^2 u_{xx} = 0. \tag{30}$$

Here $c_R^2 = E/\rho$ is the rod wave speed, where E is the Young modulus and ρ is the density.

In order to account for dispersion of waves in circular rods, a radial degree of freedom has to be introduced. This is the basis of the Mindlin–Herrmann axial rod theory. The Mindlin–Herrmann theory is expressed mathematically by the following system [17]:

$$u_{tt} - c_l^2 u_{xx} - \aleph_2^2 \frac{2\lambda}{a\rho} w_x = 0, \tag{31}$$

$$w_{tt} - \aleph_1^2 c_\tau^2 w_{xx} + \frac{8\aleph_2^2(\lambda+\mu)}{a^2\rho} w + \frac{4\aleph_2^2\lambda}{a\rho} u_x = 0, \tag{32}$$

with the following dispersion relation:

$$(-\omega^2 + c_l^2 k^2)\left[-\omega + \aleph_1^2 c_\tau^2 k^2 + \frac{8\aleph_2^2(\lambda+\mu)}{a^2\rho}\right] - \frac{8\lambda^2\aleph_2^4}{a^2\rho^2} k^2 = 0, \tag{33}$$

where u is the longitudinal and w is the transverse displacement, λ is Lamé's first parameter, μ is the shear modulus, $c_l^2 = (\lambda+2\mu)/\rho$ is the longitudinal and $c_\tau^2 = \mu/\rho$ is the transverse wave speed, a is the radius of the rod, and $\aleph_{1,2}$ are coefficients.

By setting $\aleph_1 = \aleph_2 = 1$ and recognising that $E = \mu(3\lambda + 2\mu)/(\lambda + \mu)$ Eq. (33) can be written in the following form:

$$a^2(\omega^2 - c_l^2 k^2)(\omega^2 - c_\tau^2 k^2) - 8(c_l^2 - c_\tau^2)(\omega^2 - c_R^2 k^2) = 0. \tag{34}$$

It is seen immediately that short waves are propagated at either longitudinal (c_l) or transverse (c_τ) wave speeds. Long waves only admit one non-zero speed c_R of rod waves. Actually, short waves do not 'feel' the lateral boundary since it is far away and they propagate as in an infinite elastic body. For long waves the classical limit speed of rod waves is obtained [7].

The dispersion curve for Eq. (34) is sketched in Fig. 7. It consists of two branches – acoustic and optical. The acoustic branch starts with a slope that represents the rod wave speed c_R. In the short wave limit the branch assumes the slope of shear waves. The optical branch starts at a finite frequency $\omega_0 = 2/a((\lambda + \mu)/\rho)^{1/2}$ which represents uniform nonpropagating oscillations of the cross section. In the short wave limit the upper branch tends to longitudinal bulk waves.

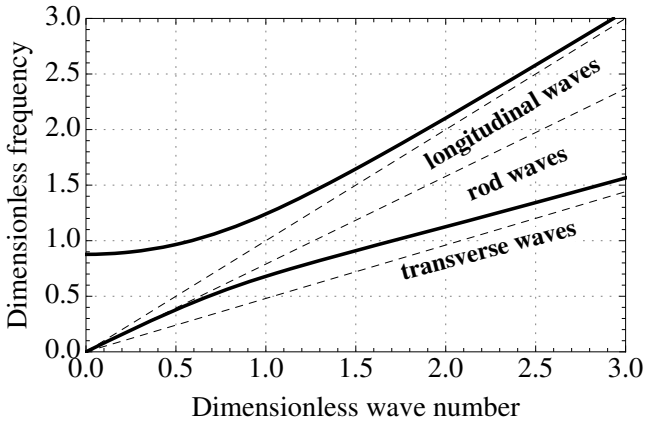

Figure 7: Dispersion curves for Eq. (34) (Mindlin-Herrmann model).

The Rayleigh–Love theory for longitudinal waves in rods provides a simpler approximation than the Mindlin–Herrmann theory. The basic assumption of the theory is that the cross-sectional strain $\bar{\varepsilon}$ is related to the longitudinal strain as in statics [7]

$$\bar{\varepsilon} = -\nu \frac{\partial u}{\partial x}, \tag{35}$$

where ν is the Poisson coefficient. The Rayleigh–Love equation for longitudinal waves is

$$u_{tt} - c_R u_{xx} - \nu^2 R^2 u_{xxtt} = 0, \tag{36}$$

with the following dispersion relation:

$$\omega = \frac{c_R}{\sqrt{1+\nu^2 R^2 k^2}}. \tag{37}$$

Here $R = (I_0/A)^{1/2}$ is the polar radius of gyration and I_0 is the polar inertial moment. The Rayleigh–Love theory only accounts for lateral inertia. If we also add the effect of the shift deformation, we derive Bishop's model for longitudinal waves in rods

$$u_{tt} - c_R^2 u_{xx} - \nu^2 R^2 (u_{tt} - c_\tau^2 u_{xx})_{xx} = 0, \tag{38}$$

with the following dispersion relation:

$$\omega = k\sqrt{\frac{c_R^2 + c_\tau^2 \nu^2 R^2 k^2}{1+\nu^2 R^2 k^2}}. \tag{39}$$

The dispersion relations (37) and (39) are depicted in Fig. 8. From Fig. 8 it is clear that Bishop's theory (39) is in good agreement with the lowest branch of the dispersion relation (33). The Rayleigh–Love theory (37) provides a good approximation in the long wave limit only as it predicts zero group speed for short waves. In a similar

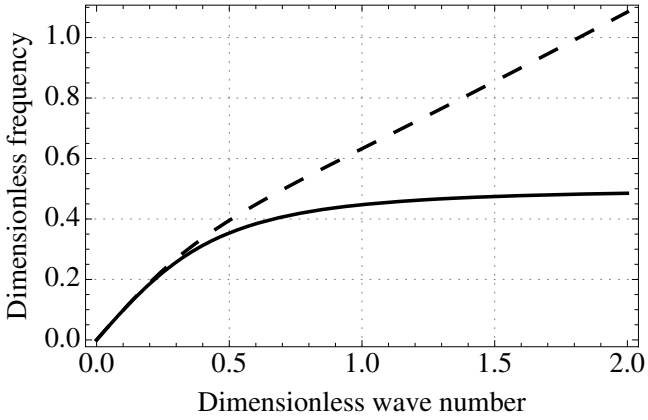

Figure 8: Dispersion curves for the Rayleigh–Love (37) (solid line) and Bishop's (39) (dashed line) models.

way it is also possible to derive approximations for flexural, torsional, and transverse waves in the rod.

1.7. Dispersion in layered media

Dispersion of waves in layered media is another example of geometrical dispersion. Layered media occur in nature and are also manufactured by bonding layers of different materials together to obtain composite materials with desired mechanical properties. A wave propagating through a layered elastic medium behaves quite differently

from a wave in a homogeneous medium, due to the effects of the interfaces between the layers [5].

The exact dispersion relation for waves in layered media in the direction of the layering is given by [5]

$$\cos kd = \cos\left(\frac{\omega d_a}{c_{la}}\right)\cos\left(\frac{\omega d_b}{c_{lb}}\right) - \frac{1}{2}\left(\frac{z_a}{z_b}+\frac{z_b}{z_a}\right)\sin\left(\frac{\omega d_a}{c_{la}}\right)\sin\left(\frac{\omega d_b}{c_{lb}}\right), \quad (40)$$

where $d = d_a + d_b$ denotes the length of the unit cell consisting of materials a and b, z_a and z_b denote the acoustic impedances and c_{la} and c_{lb} denote the longitudinal wave speeds of materials a and b, respectively.

Equation (40) yields real solutions for k only for values of frequencies within distinct bands. Between these bands the solutions are complex and amplitudes of displacement and stress decrease. For this reason these bands are called stop bands and the bands where k is real are called pass bands. Figure 9 shows a case where the ratio of acoustic impedances is $z_b/z_a = 5$ and the ratio of transit times across the layers is $d_a c_{lb}/d_b c_{la} = 10$ [5]. When $z_a = z_b$, Eq. (40) yields a simple expression for the phase

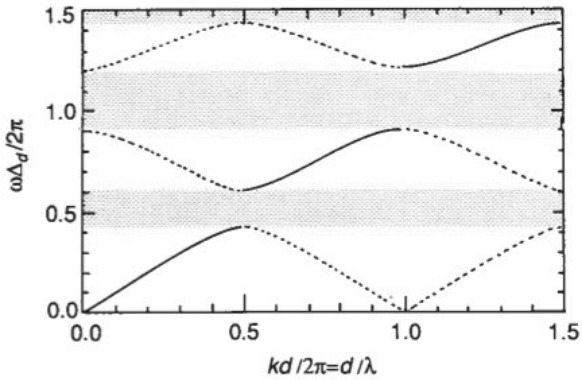

Figure 9: Dispersion in layered media. Reproduced from [5].

speed c_1 in terms of the compressional wave speeds of the two materials:

$$\frac{d}{c_1} = \frac{d_a}{c_{la}} + \frac{d_b}{c_{lb}}. \quad (41)$$

If in addition $\alpha_a = \alpha_b = \alpha$, the two materials are identical and $c_1 = \alpha$. In the limit $\omega \to 0$ the solution for the phase speed is

$$c_1 = \frac{d}{\Delta_d}, \quad (42)$$

$$\Delta_d^2 = \frac{d_a}{c_{la}}^2 + \left(\frac{z_a}{z_b}+\frac{z_b}{z_a}\right)\frac{d_a d_b}{c_{la}c_{lb}} + \frac{d_b}{c_{lb}}^2. \quad (43)$$

This is the approximate value of the phase speed if the wavelength is large in comparison with the width of the unit cell. In a special case where $c_{la} = c_{lb} = c_l$ but densities of the two materials are unequal, it yields that $c_1 < c_l$, i.e., the phase speed of the wave is smaller than the longitudinal wave speed in the two materials [5].

1.8. Summary

The modelling of wave propagation in dispersive media introduces higher order derivatives into the governing equations. Regardless of the dispersion type – geometrical or physical, the dispersion curves look very similar, which is due to the number and order of the partial derivatives. In spite of visual similarities, the role of the dispersion curves must be explained in the context of the problem. For example the optical dispersion branch in case of the waves in rods reflects the propagation of longitudinal waves, whereas in case of the micropolar model, the optical dispersion branch reflects the rotations of the microstructure.

When modelling wave dispersion in microstructured materials, a choice between the discrete and microcontinuum approach has to be made. In the discrete approach the microstructure is envisioned as a structure of rigid particles that are connected with elastic springs. The microcontinuum model is then deduced by making use of the continualisation methods. The implementation of the discrete approach is relatively simple and the effects of the microstructure emerge naturally when at least two particles per unit cell are considered and/or the particles are allowed to rotate. Important strength of the discrete approach is that the distance between the particles emerges as the inherent length scale of the material. The weakness, however, is that the particles and springs do not present a real physical picture and assumptions have to be made about the movement of the particles.

In the microcontinuum approach the continuous material is separated into the macro- and microstructure. The motion on the macroscale is then coupled to the micromotion and the microstructural effects arise naturally in microcontinuum models. This microstructure can either be envisioned as a collection of deformable cells or as the presence of internal variables. Although the mathematics is more difficult, such an approach provides a physically more sound picture and the optical dispersion branches emerge naturally. The main weakness of the microcontinuum approach is that it is very difficult to say something about the parameters associated with the microstructure. However, the inverse problems, which allow us to find the material parameters, are now intensively studied [19].

2. Mindlin–Engelbrecht–Pastrone model

2.1. Single scale

As a result of the discussion in the previous section, we will focus here on the micro-continuum approach.

The one-dimensional version of the Mindlin model, as formulated by Engelbrecht and Pastrone [12, 13], will serve as a basis for this thesis.

The Mindlin–Engelbrecht–Pastrone model is described by two scalar functions – the macrodisplacement $u(x,t)$ and the microdeformation $\varphi(x,t)$. The kinetic (23) and potential energy (19) densities will then have the following forms:

$$K = \frac{1}{2}\rho u_t^2 + \frac{1}{2} I \varphi_t^2, \quad W = W(u_x, \varphi, \varphi_t), \tag{44}$$

where u_x is the macrodeformation and φ_x is the gradient of the microdeformation, ρ and I are the density and the microinertia, respectively. By making use of the Euler–Lagrange equations for the Lagrangian $L = K - W$ and recognising that

$$\sigma = \frac{\partial W}{\partial u_x}, \quad \eta = \frac{\partial W}{\partial \varphi_x}, \quad \tau = \frac{\partial W}{\partial \varphi}, \tag{45}$$

we obtain the equation of motion

$$\rho u_{tt} = \sigma_x, \quad I\varphi_{tt} = \eta_x - \tau, \tag{46}$$

where σ is the macro- and η is the microstress and τ is the interacting force.

The simplest potential energy function describing the influence of the microstructure is a quadratic function

$$W = \frac{1}{2}\alpha u_x^2 + A u_x \varphi + B\varphi^2 + C\varphi_x^2, \tag{47}$$

where α, A, B and C are material constants. The physical meanings of these parameters are related to bulk (α) and microstress moduli (C), coupling effects (A) and the interactive force (B). The stresses (45) then take the forms

$$\sigma = \alpha u_x + A\varphi, \quad \eta = C\varphi, \quad \tau = A u_x + B\varphi, \tag{48}$$

and the equation of motion (46) becomes

$$\rho u_{tt} = \alpha u_{xx} + A\varphi_x, \quad I\varphi_{tt} = C\varphi_{xx} - A u_x - B\varphi. \tag{49}$$

it is clear that system (49) is a coupled system where macrodisplacement $u(x,t)$ is coupled to the microdeformation $\varphi(x,t)$ and vice versa. It should also be pointed

out that the coupling is controlled by the parameter A. If the parameter A is set to zero, system (49) reduces to two equations of wave motion – one for macroscale and the other for microscale. The effect of coupling is best seen in the solutions of the boundary value problem (see Section 4).

Often it is more comfortable to represent system (49) in the form of one fourth order PDE for macrodisplacement. To this end the second equation of system (49) is differentiated once with respect to x and then the first equation is plugged into the second one. This yields

$$u_{tt} = (c_0^2 - c_A^2)u_{xx} - p^2(u_{tt} - c_0^2 u_{xx})_{tt} + p^2 c_1^2 (u_{tt} - c_0^2 u_{xx})_{xx}, \tag{50}$$

where the parameters

$$c_0^2 = \frac{\alpha}{\rho}, \quad c_1^2 = \frac{C}{I}, \quad c_A^2 = \frac{A^2}{\rho B}, \quad p^2 = \frac{I}{B} \tag{51}$$

have been introduced. The parameters c_0, c_1, and c_A are velocities and the parameter p^2 is a time constant. The meaning of these parameters will become clear in the following analysis of this thesis. Although Eq. (50) represents system (49) in terms of macrodisplacement, the influence of the microstructure is fully retained.

One should also note that the Eq. (51) is similar to the 'causal' equation (9) derived by Metrikine [23].

2.2. Multiscale

Instead of including just one microstructure, the model derived in the previous subsection can be generalised to the case with two separate microstructures. The second microstructure can either be embedded in the first microstructure at a smaller scale or there exist two concurrent microstructures.

The equation of motion is derived in a similar way to the single scale model. One only needs to assume appropriate forms of the internal energies. Here we repeat the models derived by Berezovski et al. [6].

The case of two hierarchical microstructures ('the scale within the scale') was derived by Engelbrecht et al. [13]. The corresponding microstructure hierarchy is represented schematically in Fig. 10. In this case the internal energy is a function of macrodisplacement $u(x,t)$ and microdeformations $\varphi_1(x,t)$ and $\varphi_2(x,t)$ as follows:

$$\begin{aligned} W = \frac{1}{2}\alpha u_x^2 + A_1 u_x \varphi_1 + \frac{1}{2}B_1 \varphi_1^2 + \frac{1}{2}C_1 (\varphi_1)_x^2 \\ + A_{12}(\varphi_1)_x \varphi_2 + \frac{1}{2}B_2 \varphi_2^2 + \frac{1}{2}C_2 (\varphi_2)_x^2. \end{aligned} \tag{52}$$

Figure 10: Schematic representation of the hierarchical microstructure.

This leads to the stresses in the form

$$\begin{aligned}\sigma &= \frac{\partial W}{\partial u_x} = \rho c^2 u_x + A_1 \varphi_1, \\ \eta_1 &= \frac{\partial W}{\partial (\varphi_1)_x} = C_1 (\varphi_1)_x + A_{12} \varphi_2, \quad \eta_2 = \frac{\partial W}{\partial (\varphi_2)_x} = C_2 (\varphi_2)_x,\end{aligned} \tag{53}$$

and to the interactive forces

$$\tau_1 = \frac{\partial W}{\partial \varphi_1} = A_1 u_x + B_1 \varphi_1, \quad \tau_2 = \frac{\partial W}{\partial \varphi_2} = A_{12} (\varphi_1)_x + B_2 \varphi_2. \tag{54}$$

The equations of motion will now take the form

$$\rho u_{tt} = \alpha u_{xx} + A_1 (\varphi_1)_x, \tag{55}$$

$$I_1 (\varphi_1)_{tt} = C_1 (\varphi_1)_{xx} - A_1 u_x - B_1 \varphi_1 + A_{12} (\varphi_2)_x, \tag{56}$$

$$I_2 (\varphi_2)_{tt} = C_2 (\varphi_2)_{xx} - A_{12} (\varphi_1)_x - B_2 \varphi_2, \tag{57}$$

where I_1 and I_2 are appropriate inertia measures.

In system (55)–(57) the motion of the first microscale is coupled to the macromotion and the motion of the second microscale is coupled to the motion of the first scale. Another possible configuration is to couple both scales directly to the macroscale as seen in Fig. 11. The internal energy will then have the form

$$\begin{aligned}W = \frac{1}{2}\alpha u_x^2 + A_1 u_x \varphi_1 + \frac{1}{2} B_1 \varphi_1^2 + \frac{1}{2} C_1 (\varphi_1)_x^2 \\ + A_2 u_x \varphi_2 + \frac{1}{2} B_2 \varphi_2^2 + \frac{1}{2} C_2 (\varphi_2)_x^2.\end{aligned} \tag{58}$$

The stresses and interactive forces are determined as in case of hierarchical microstructure ((53) and (54)) and the equations of motion is derived:

$$\rho u_{tt} = \alpha u_{xx} + A_1 (\varphi_1)_x + A_2 (\varphi_2)_x, \tag{59}$$

$$I_1 (\varphi_1)_{tt} = C_1 (\varphi_1)_{xx} - A_1 u_x - B_1 \varphi_1, \tag{60}$$

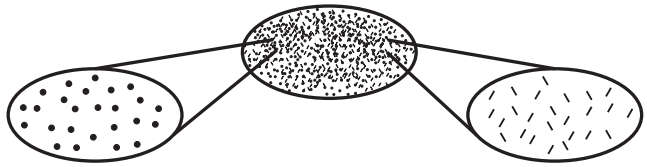

Figure 11: Schematic representation of the concurrent microstructure.

$$I_2(\varphi_2)_{tt} = C_2(\varphi_2)_{xx} - A_2 u_x - B_2 \varphi_2. \tag{61}$$

In system (59)–(61) the macroscale is directly coupled to the microscales and the microstructures are completely independent. In order to account for coupling between the microstructures, the coupling constant A_{12} is reintroduced into the internal energy

$$\begin{aligned} W = \frac{1}{2}\alpha u_x^2 + A_1 u_x \varphi_1 + \frac{1}{2} B_1 \varphi_1^2 + \frac{1}{2} C_1 (\varphi_1)_x^2 \\ + A_2 u_x \varphi_2 + \frac{1}{2} B_2 \varphi_2^2 + \frac{1}{2} C_2 (\varphi_2)_x^2 + A_{12} (\varphi_1)_x \varphi_2, \end{aligned} \tag{62}$$

and the corresponding equations of motion will be

$$\rho u_{tt} = \alpha u_{xx} + A_1 (\varphi_1)_x + A_2 (\varphi_2)_x, \tag{63}$$

$$I_1(\varphi_1)_{tt} = C_1(\varphi_1)_{xx} + A_{12}(\varphi_2)_x - A_1 u_x - B_1 \varphi_1, \tag{64}$$

$$I_2(\varphi_2)_{tt} = C_2(\varphi_2)_{xx} - A_{12}(\varphi_1)_x - A_2 u_x - B_2 \varphi_2. \tag{65}$$

2.3. Hierarchical approximation

System (49) can be approximated by making use of the slaving principle, which means that the full system is approximated in such a way that the acoustic branch of the dispersion relation is singled out and the optical dispersion branch is discarded. Mathematically the slaving principle means that the microdeformation φ is determined in terms of u_x, thus deducing a single PDE where macromotion prevails while retaining the influence of the microstructure. The underlying assumption is that the influence of the microstructure is small. A special feature of this approximation is that it can be used over the whole range of wave numbers, since it does not represent short or long wave approximation. The procedure of obtaining an approximation of system (49) is explained in detail in papers by Engelbrecht and Pastrone [12, 13].

It is supposed that the inherent length-scale l is small compared to the wavelength L of the excitation. The following dimensionless variables and parameters are introduced:

$$U = u/U_0, \quad X = x/L, \quad T = c_0 t/L, \quad \delta = (l/L)^2, \quad \varepsilon = U_0/L, \tag{66}$$

where U_0 is the amplitude of the excitation. In addition, it is assumed that $I = \rho l^2 I^*$ and $C = l^2 C^*$, where I^* is dimensionless and C^* has the dimension of stress.

Next, system (49) is rewritten in its dimensionless form and the slaving principle [9] is applied. It is supposed that

$$\varphi = \varphi_0 + \delta\varphi_1 + \delta^2\varphi_2 + \dots. \tag{67}$$

The dimensionless form of Eq. (49b) yields

$$\varphi = -\varepsilon\frac{A}{B}U_X - \frac{\delta}{B}\left(aI^*\varphi_{TT} - C^*\varphi_{XX}\right), \tag{68}$$

from which the successive terms

$$\varphi_0 = -\varepsilon\frac{A}{B}U_X, \quad \varphi_1 = \varepsilon\frac{A}{B^2}\left(aI^*U_{XTT} - C^*U_{XXX}\right), \dots \tag{69}$$

of the expansion (67) are obtained. Inserting them into Eq. (49a) in its dimensionless form, we finally get

$$U_{TT} = \left(1 - \frac{c_A^2}{c_0^2}\right)U_{XX} + \frac{c_A^2}{c_B^2}\left(U_{TT} - \frac{c_1^2}{c_0^2}U_{XX}\right)_{XX}, \tag{70}$$

where $c_B^2 = L^2/p^2 = BL^2/I$. Note that c_B involves the scales L and l and c_A includes the interaction effects through the parameter A. Equation (70) is valid up to $O(\delta)$ because higher order terms are neglected. In addition, in general $\varepsilon >> \delta^2$.

Now it is possible to restore the dimensions in order to compare the result with Eq. (50). Equation (70) yields

$$u_{tt} = \left(c_0^2 - c_A^2\right)u_{xx} + p^2c_A^2\left(u_{tt} - c_1^2u_{xx}\right)_{xx}. \tag{71}$$

This is an example of a Whitham-type [34] hierarchical equation. Note that in case of no coupling between the macro- and microstructure ($A = 0$), the classical wave equation follows.

The same reasoning can be used on system (55)–(57). To this end the slaving principle is used on the system, taking into account two independent small parameters $\delta_1 = l_1^2/L^2$ and $\delta_2 = l_2^2/L^2$. One also needs to assume the follwing parameters:

$$I_1 = \rho l_1^2 I_1^*, \quad I_2 = \rho l_2^2 I_2^*, \quad C_1 = l_1^2 C_1^*, \quad C_2 = l_2^2 C_2^*, \quad A_{12} = l_2 A_{12}^*, \tag{72}$$

where I_1^* and I_2^* are dimensionless and A_{12}^*, C_1^* and C_2^* have the dimensions of stress. The dimensionless hierarchical approximation will then be

$$\begin{aligned} U_{TT} = {} & \left(1 - \frac{A_1^2}{\alpha B_1}\right)U_{XX} + \delta_1\frac{A_1^2I_1^*}{B_1^2}\left(U_{TT} - \frac{C_1^*}{\alpha I_1^*}U_{XX}\right)_{XX} \\ & + \delta_2\frac{A_1^2\left(A_{12}^*\right)^2I_2^*}{B_1^2B_2^2}\left[\frac{B_2}{\alpha I_2^*}U_{XXXX} - \delta_2\left(U_{TT} - \frac{C_2^*}{\alpha I_2^*}U_{XX}\right)_{XXXX}\right]. \end{aligned} \tag{73}$$

After restoring the dimensions we get

$$\begin{aligned} u_{tt} = \left(c_0^2 - c_{A1}^2\right) u_{xx} + p_1^2 c_{A1}^2 \left[u_{tt} - \left(c_1^2 - c_{A12}^2\right) u_{xx}\right]_{xx} \\ - p_1^2 c_{A1}^2 p_2^2 c_{A12}^2 \left(u_{tt} - c_2^2 u_{xx}\right)_{xxxx}, \end{aligned} \tag{74}$$

where the parameters

$$c_1^2 = \frac{C_1}{I_1}, \quad c_{A1}^2 = \frac{A_1^2}{\rho B_1}, \quad p_1^2 = \frac{I_1}{B_1}, \quad c_2^2 = \frac{C_2}{I_2}, \quad c_{A12}^2 = \frac{A_2^2}{I_1 B^2}, \quad p_2^2 = \frac{I_2}{B_2} \tag{75}$$

have been introduced. The parameters c_i and c_{Ai} are speeds, while p_i denote time constants.

Systems (59)–(61) and (63)–(65) can be approximated in a similar way.

3. Dispersion analysis of the Mindlin–Engelbrecht–Pastrone model

3.1. The single scale model

The presence of higher order derivatives in Eqs. (50) and (71) indicates dispersion. In order to derive the dispersion relations, we assume the solution in the form of a wave

$$u(x,t) = \hat{u}\exp[i(kx-\omega t)], \tag{76}$$

with the wave number k, the angular frequency ω and the amplitude $\hat{u}$. Introducing this into Eqs. (50) and (71), we obtain the following dispersion relations:

$$\omega^2 = (c_0^2 - c_A^2)k^2 + p^2(\omega^2 - c_0^2k^2)(\omega^2 - c_1^2k^2) \tag{77}$$

and

$$\omega^2 = (c_0^2 - c_A^2)k^2 - p^2c_A^2(\omega^2 - c_1^2k^2)k^2. \tag{78}$$

It can be seen immediately that in the long wave limit ($pc_0k << 1$) both equations provide the same limiting speed $c_R = (c_0^2 - c_A^2)^{1/2}$, which is less than the usual speed calculated from strain-stiffness ($c_0^2 = \alpha/\rho$). This is due to the compliance of the unit cell [25]. In the short wave limit ($pc_0k >> 1$) the full dispersion relation (77) provides two modes of wave propagation – one with the speed c_1, which is related to the movement of the unit cells in unison and the other with the speed c_0, which is related to the deformation of the unit cells themselves. As the approximated model (71) does not explicitly account for the internal degrees of freedom, in the short wave region only the limiting speed c_1 appears in (78).

In the three-dimensional theory developed by Mindlin [25], the speed c_1 also emerges as the limiting speed for the shear and rotational optical branches. In the present one-dimensional setting such a movement is not possible and therefore these curves are not present. We also note that the speeds c_R and c_1 are related to the free energy (47) in the same way as in Mindlin's three-dimensional theory (Eqs. (8.15) and (8.20) in [25]).

When Eq. (77) is solved for the frequency ω, four real roots can be found:

$$\omega = \pm\frac{\sqrt{2+2(c_0^2+c_1^2)p^2k^2 \pm 2\sqrt{1+2(c_1^2-c_0^2+2c_A^2)p^2k^2+(c_0^2-c_1^2)^2p^4k^4}}}{2p}. \tag{79}$$

For any given value of the wave number k there will be two values of ω, which correspond to the acoustic ($\omega \to 0$ when $k \to 0$) and optical dispersion branches ($\omega \to 1/p$ when $k \to 0$). The existence of the optical dispersion branch is expected due to the additional degree of freedom that involves distortion of the unit cells. The internal modes are in the domain of higher frequencies.

When solving Eq. (78) for ω, the following two roots can be found:

$$\omega = \pm\sqrt{\frac{c_0^2 - c_A^2(1 - c_1^2 p^2 k^2)}{1 + c_A^2 p^2 k^2}}k. \tag{80}$$

For any value of k there exists one value of ω, which corresponds to the acoustic dispersion branch.

The characteristic dispersion curves are depicted in Figs. (12) and (13). The full

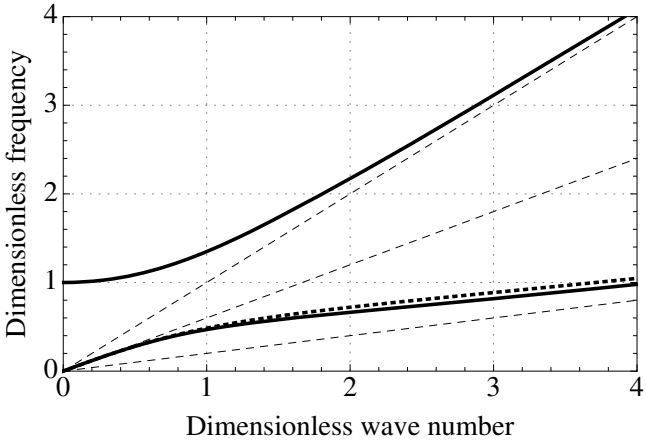

Figure 12: Dispersion curves in case of $c_R > c_1$ ($c_A = 0.8c_0$ and $c_1 = 0.2c_0$).

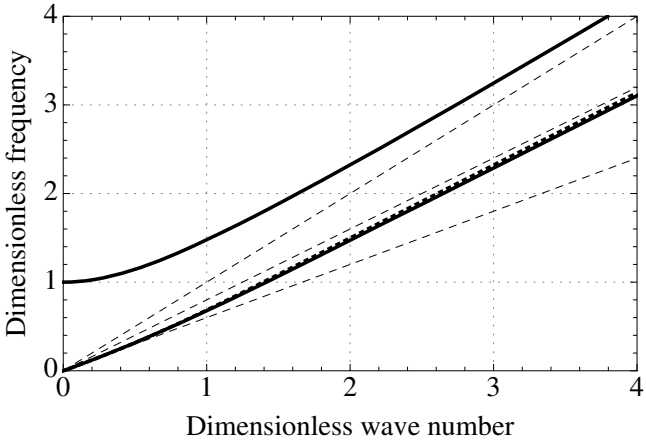

Figure 13: Dispersion curves in case of $c_R < c_1$ ($c_A = 0.8c_0$ and $c_1 = 0.8c_0$).

dispersion relation (77) is represented by solid lines and consists of two branches – acoustic and optical. Dashed lines represent the asymptotic lines $\omega = k$, $\omega = c_1/c_0 \cdot k$ and $\omega = c_R/c_0 \cdot k$.

The optical dispersion branch starts with a zero slope and then asymptotically approaches the line $\omega = k$. The acoustic dispersion branch starts with a slope $\omega = c_R/c_0 \cdot k$ and then asymptotically approaches the line $\omega = c_1/c_0 \cdot k$. The approximated dispersion relation (78) is represented by the dotted line.

In general, the dispersion type following the acoustic dispersion branch can be either normal ($c_R > c_1$, see Fig. 12) or anomalous ($c_R < c_1$, see Fig. 13). A special case is $c_R = c_1$, which represents the dispersionless case. As the phase speed related to the optical dispersion branch is always higher than the group speed related to the same dispersion branch, the dispersion type of the optical dispersion branch is always normal. The dispersion type of the acoustic dispersion branch is explicitly related to the material properties [26].

The acoustic and optical dispersion branches are for $\omega - k$ plane. The phase speed ($c_{ph} = \omega/k$) and the group speed ($c_{gr} = \partial\omega/\partial k$) are calculated following these branches. The phase (dashed lines) and group (solid lines) speed curves for the full dispersion relation (77) are depicted in Figs. 14 (against the frequency) and 15 (against the wave number). Both figures have $c_A = 0.3c_0$ and $c_1 = 0.2c_0$. Also note that Fig. 14 is plotted over a shorter range on the horizontal axis than Fig. 15. This is because the change in speed is quicker with increasing frequency (Fig. 14) than with the increasing wavelength (Fig. 15).

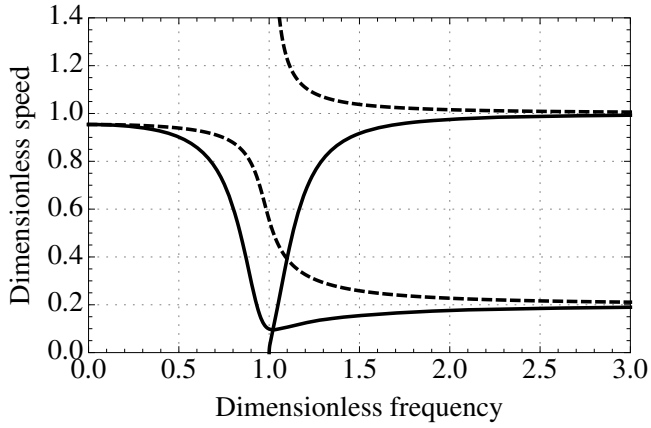

Figure 14: Group (solid line) and phase (dashed line) speed curves against the frequency. $c_A = 0.3c_0$ and $c_1 = 0.2c_0$

It can be seen from Figs. 14 and 15 that the phase speed and the group speed behave slightly differently. While the asymptotic value of the acoustic phase speed curve approaches gradually the asymptotic value c_1/c_0, the group speed curve changes more rapidly, initially assuming the value that is lower than c_1/c_0 and then approaching the asymptotic value c_1/c_0. In case of very strong normal dispersion, the group speed curve assumes a value that is very close to zero before approaching the asymptotic

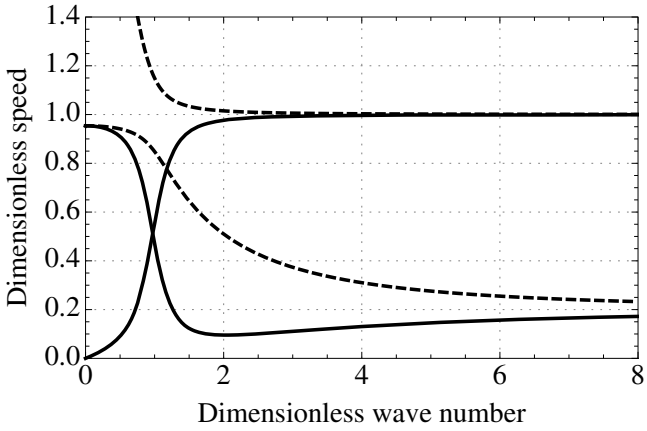

Figure 15: Group (solid line) and phase speed (dashed line) curves against the wave number. $c_A = 0.3c_0$ and $c_1 = 0.2c_0$

value c_1/c_0. The effect becomes more subtle when $c_R \approx c_1$. In case of the optical dispersion branch, the phase speed curve starts at infinity and the group speed curve at zero. In the short wave limit both curves approach the asymptotic value 1.

3.2. Applicability of the approximated model

The applicability of the approximated model from the dispersion analysis perspective has been analysed [26].

Although the hierarchical approximation (71) provides a good approximation of the full model (50), there are differences in the behaviour of the corresponding dispersion relations (78) and (77) when $k > 1/pc_0$. This is due to the parameters controlling the short wave behaviour – in the full dispersion relation (77) the short wave behaviour is controlled by the time parameter p, whereas in the approximated dispersion relation (78) it is controlled by the the time parameter p and the auxiliary speed c_A.

When $c_A/c_0 \to 1$, the dispersion relation (78) provides a good approximation of the acoustic dispersion branch of the dispersion relation (77) (Fig. 12). The approximation becomes worse when $c_A/c_0 \to 0$, which can be seen in the behaviour of the corresponding dispersion curves (Fig. 16). Since the free energy (47) must be positive definite and $c_R^2 = c_0^2 - c_A^2$, the parameter c_A is confined to have the following values:

$$0 < \frac{c_A}{c_0} < 1. \tag{81}$$

In spite of the different behaviour of the dispersion relations (77) and (78) in a region of $k > 1/pc_0$, in the very short wave limit both dispersion curves are characterised

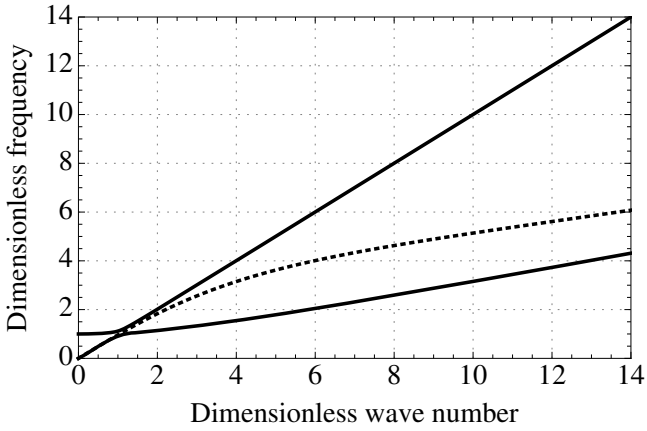

Figure 16: Dispersion curves of the full (solid line) and the approximated (dashed line) model when $c_A/c_0 = 0.2$ and $c_1/c_0 = 0.3$.

by the same limiting speed c_1. This is best seen in the behaviour of the group speed curves (Fig. 17).

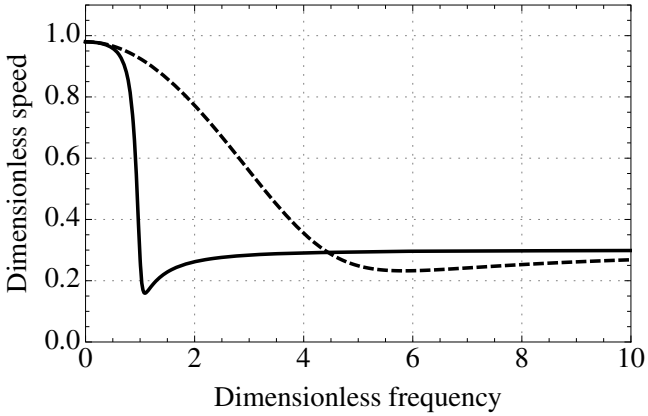

Figure 17: Behaviour of the group speed curves for Eqs. (49) (solid line) and (71) (dashed line) against the wave number when $c_A/c_0 = 0.2$ and $c_1/c_0 = 0.3$.

Figure 18 illustrates the ranges of the parameters where the values obtained from both relations agree within a 5 per cent error (the area between the dashed lines) and within a 10 per cent error (the area between the continuous lines) at the point $k = 1.5/pc_0$. The behaviour for higher values of k is similar, only the area of good agreement becomes narrower. When k becomes very large, the area of good agreement becomes larger [26].

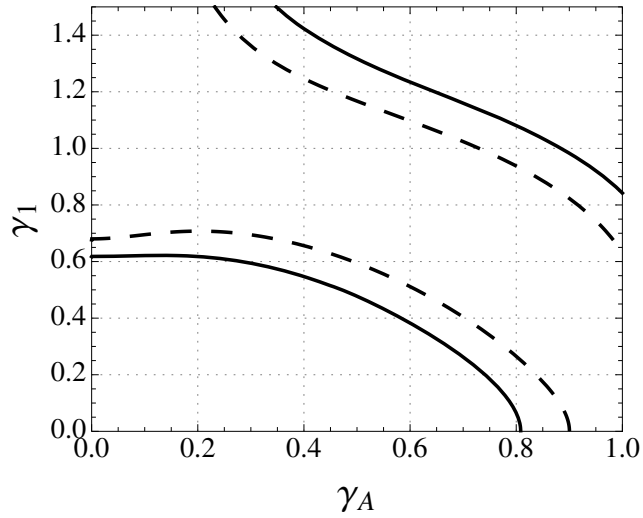

Figure 18: The ranges of parameters. See explanation in text.

3.3. Multiscale model

In order to study the dispersion of multiscale systems (55)–(57), (59)–(61) and (63)–(65), we assume the solutions in the form of harmonic waves

$$u(x,t) = \hat{u}e^{i(kx-\omega t)}, \quad \varphi_1(x,t) = \hat{\varphi}_1 e^{i(kx-\omega t)}, \quad \varphi_2(x,t) = \hat{\varphi}_2 e^{i(kx-\omega t)}, \tag{82}$$

where u is the macrodisplacement and φ_1 and φ_2 are microdeformations on two different scales.

Plugging (82) into Eqs. (55)–(57), we get

$$\begin{vmatrix} \rho_0 k^2 - \rho_0 \omega^2 & -iA_1 k & 0 \\ iA_1 k & C_1 k^2 - I_1 \omega^2 + B_1 & -iA_{12} k \\ 0 & iA_{12} k & C_2 k^2 - I_2 \omega^2 + B_2 \end{vmatrix} \begin{vmatrix} \hat{u} \\ \hat{\varphi}_1 \\ \hat{\varphi}_2 \end{vmatrix} = 0. \tag{83}$$

In order to get nontrivial solutions, the determinant of this system must vanish. This leads to the dispersion relation

$$\begin{aligned} &(c^2k^2 - \omega^2)(c_1^2k^2 - \omega^2 + \omega_1^2)(c_2^2k^2 - \omega^2 + \omega_2^2) \\ &-c_{A12}^2\omega_2^2k^2(c^2k^2 - \omega^2) - c_{A1}^2\omega_1^2k^2(c_2^2k^2 - \omega^2 + \omega_2^2) = 0, \end{aligned} \tag{84}$$

where the parameters

$$c_{A1}^2 = \frac{A_1^2}{\rho_0 B_1}, \quad c_{A12}^2 = \frac{A_{12}^2}{I_1 B_2}, \quad \omega_1^2 = \frac{B_1}{I_1}, \quad \omega_2^2 = \frac{B_2}{I_2} \tag{85}$$

have been introduced. Here the parameter c_{A1} reflects the effect of the microscale 1 on the macrostructure and is the same as c_A in the single scale model, the parameter c_{A12} reflects the coupling between the scales; ω_1 and ω_2 are the characteristic frequencies, which may also be regarded as reciprocal time parameters.

The dispersion relations for systems (59)–(61) and (53)–(65) are

$$\begin{aligned}(c^2k^2-\omega^2)(c_1^2k^2-\omega^2+\omega_1^2)(c_2^2k^2-\omega^2+\omega_2^2)-c_{A12}^2\omega_2^2k^2(-c_0^2k^2+\omega^2)\\ -c_{A1}^2\omega_1^2k^2(c_2^2k^2-\omega^2+\omega_2^2)-c_{A2}^2k^2\omega_2^2(c_1^2k^2-\omega^2+\omega_1^2)=0\end{aligned} \tag{86}$$

and

$$\begin{aligned}(c^2k^2-\omega^2)(c_1^2k^2-\omega^2+\omega_1^2)(c_2^2k^2-\omega^2+\omega_2^2)\\ -c_{A2}^2\omega_2^2k^2(c_1^2k^2-\omega^2+\omega_1^2)-c_{A1}^2\omega_1^2k^2(c_2^2k^2-\omega^2+\omega_2^2)=0.\end{aligned} \tag{87}$$

respectively. In these equations the speed $c_{A2}^2=A_2^2/(\rho_0 B_2)$ has been introduced.

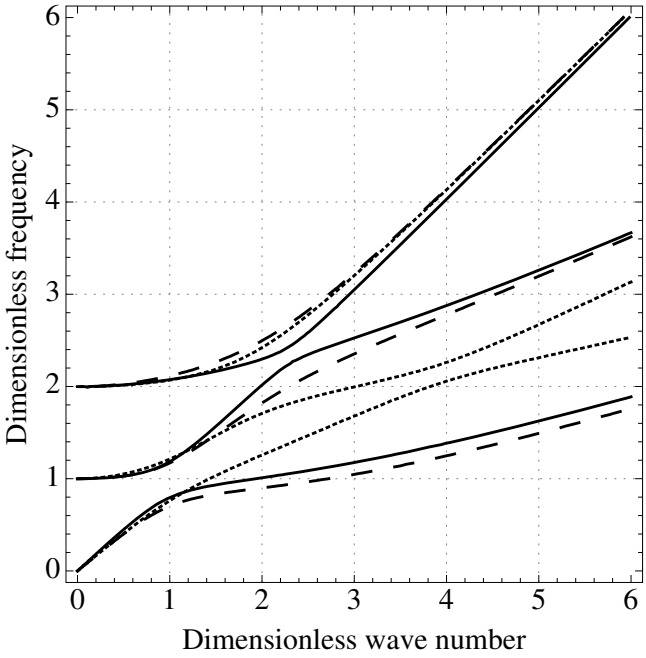

Figure 19: Comparison of the dispersion curves of Eqs. (84), (86) and (87) for $c_{A1}/c_0=c_{A2}/c_0=c_{A12}/c_0=0.4$, $c_1/c_0=0.5$ and $c_2/c_0=0.3$: solid lines – hierarchical model (87); dashed lines – concurrent model (86); dotted lines – concurrent model (87).

The dispersion relations (84) (solid lines), (86) (dashed lines) and (87) (dotted lines) are depicted in Fig. 19. It can be seen that due to addition of the second microstructure, three dispersion branches emerge – one acoustic branch and two optical

branches per model. For simplicity we will limit ourselves to the case where $\omega_1 = 1$, $\omega_2 = 2$ and $c_1/c_0 > c_2/c_0$.

It can be seen immediately that while the behaviour of the hierarchical model (84) and concurrent model (86) is quite similar, the concurrent model (87) departs drastically in the region of medium-range wavelengths. We can therefore conclude that the coupling between the microstructures has a significant effect on the dispersion in that region [6].

In the long wave limit the slope of the acoustic dispersion branch depends on the coupling between the macro- and microstructures. The hierarchical model (84), where the macrostructure only interacts with one microstructure, starts with a slope $\omega = [(c_0^2 - c_{A1}^2)/c_0^2]^{1/2}k$. The concurrent models (86) and (87) start with a slope $\omega = [(c_0^2 - c_{A1}^2 - c_{A2}^2)/c_0^2]^{1/2}k$, which is due to the interaction of the macrostructure with both microstructures.

The medium wavelength behaviour of the acoustic dispersion branch depends on the coupling between the microstructures. If there is no coupling between the microstructures as in Eq. (87), the acoustic dispersion branch approaches the asymptotic line $\omega = c_1 k$. In case of the coupling between the microstructures, the acoustic dispersion branch approaches the asymptotic line $\omega = [(c_1^2 - c_{A12}^2)/c_0^2]^{1/2}k$. In the short wave limit the acoustic dispersion branches for all three models approach the same asymptotic line $\omega = c_2 k$.

The behaviour of the optical dispersion branches is highly dependent on the coupling between the macro- and microstructures. In case of the hierarchical model (84), where there is coupling between the microstructures and between the macrostructure and one microstructure, the middle optical dispersion branch first approaches the asymptotic line $\omega = k$ and then the asymptotic line $\omega = c_1/c_0 \cdot k$. The upper optical dispersion branch approaches the same asymptotic lines, but in a different order – first the asymptotic line $\omega = c_1/c_0 \cdot k$ and then the asymptotic line $\omega = k$.

If the microstructures are only coupled to the macrostructures as in the concurrent model (87), the upper optical dispersion branch approaches the asymptotic line $\omega = k$ and the middle optical dispersion branch approaches first the asymptotic line $\omega = c_2/c_0 \cdot k$ and then the asymptotic line $\omega = c_1/c_0 \cdot k$.

In case of the concurrent model (86), where there is coupling between the microstructures and the macrostructure is coupled to both microstructures, the upper optical dispersion branch behaves similarly to the concurrent model (87). The middle optical dispersion branch behaves similarly to the concurrent model (87) in the long wave limit and similarly to the hierarchical model (84) in the short wave limit.

3.4. Summary

The dispersion analysis has shown that the inclusion of the microstructure in the continuum model brings additional degrees of freedom into the model, which manifest themselves in the emergence of optical dispersion curves. The number of optical curves depends on the number of degrees of freedom. In the 3D setting, for example, up to nine degrees of freedom can emerge. In case of the Mindlin–Engelbrecht–Pastrone model, only one optical curve appears as the model is set in the 1D setting and the underlying microstructure can only deform. If the multiscale model is considered, more than one optical curves will appear. Due to the coupling between the scales, the behaviour of the curves will become more complex.

Although the dispersion analysis has clearly shown that the optical dispersion curves emerge due to the microstructure, it cannot provide insight into the question whether the optical dispersion branches create measurable effects when wave propagation is considered. This will be studied in the next sections in the context of the boundary and initial value problems.

4. Boundary value problem

Proceeding from the dispersion analysis in the previous section, we will now focus on the simulations of wave propagation in microstructured materials. The boundary value problem is studied in the present section and the initial value problem will be studied in the next section.

It is clear from the dispersion analysis that there are different modes of wave propagation in microstructured materials. Higher frequency optical branches will only appear if the microstructure is considered. It is still unclear whether the higher frequency optical modes have significance in numerical experiments. We are therefore interested in two questions – whether the optical modes are measurable and whether these need to be considered in actual experiments. These topics will be addressed in the following sections. We will also revisit the problem of applicability of the hierarchical approximation (71).

4.1. Displacement boundary condition

In order to study the effect of the optical dispersion branch, the governing equation in a half-space is solved in the form of system (49). It is assumed that the macro- and microstructure are initially at rest and that there is a macrodisplacement at the boundary.

The dimensionless form of system (49) is

$$\begin{aligned} u_{\tau\tau} &= u_{\chi\chi} + d_1\varphi_\chi, \\ \varphi_{\tau\tau} &= \gamma_1^2\varphi_{\chi\chi} - d_2 u_\chi - \varphi, \end{aligned} \tag{88}$$

where $\tau = t/p$ and $\chi = x/(c_0 p)$ are the dimensionless time and space, respectively, and $\gamma_1^2 = c_1^2/c_0^2$ and $\gamma_A^2 = d_1 d_2 = c_A^2/c_0^2$ are the dimensionless speeds. The boundary and initial conditions in the dimensionless form are

$$\begin{aligned} &u(\chi,\tau=0) = u_\tau(\chi,\tau=0) = 0, \\ &u(\chi=0,\tau) = f(\tau), \\ &\varphi(\chi=0,\tau) = 0, \\ &\lim_{\chi\to\infty} u(\chi,\tau) = \lim_{\chi\to\infty} \varphi(\chi,\tau) = 0. \end{aligned} \tag{89}$$

The problem defined by Eqs. (88) and (89) can be solved by applying the Laplace transform over the dimensionless time τ. Defining the Laplace transform for macro-

and microdisplacement as [23]

$$\begin{aligned} U(\chi,s) &= \int_0^\infty u(\chi,\tau)\exp(-s\tau)d\tau, \\ \Phi(\chi,s) &= \int_0^\infty \varphi(\chi,\tau)\exp(-s\tau)d\tau, \end{aligned} \tag{90}$$

we obtain the following problem in the Laplace domain:

$$\begin{aligned} s^2U &= U'' + d_1\Phi', \\ s^2\Phi &= \gamma_1^2\Phi'' - d_2U' - \Phi, \end{aligned} \tag{91}$$

$$\begin{aligned} &U(\chi=0,s) = L(f(\tau)), \\ &\Phi(\chi=0,s) = 0, \\ &\lim_{\chi\to\infty} U(\chi,s) = \lim_{\chi\to\infty}\Phi(\chi,s) = 0 \quad Re(s) > 0, \end{aligned} \tag{92}$$

where L denotes the Laplace transform.

The general solution of Eqs. (91), which satisfies the boundary condition at infinity, is

$$\begin{aligned} U(\chi,s) &= C_1e^{-k_1\chi} + C_2e^{-k_2\chi}, \\ \Phi(\chi,s) &= C_1\frac{k_1(k_1^2+2\gamma_A^2-2\gamma_1^2s^2)}{2d_1(1+s^2)}e^{-k_1\chi} + C_2\frac{k_2(k_2^2+2\gamma_A^2-2\gamma_1^2s^2)}{2d_1(1+s^2)}e^{-k_2\chi}, \end{aligned} \tag{93}$$

where

$$\begin{aligned} k_{1,2} = \frac{1}{2\gamma_1}[&2+2s^2-2\gamma_q qA^2+2\gamma_1^2s^2 \\ &\pm 2(1+2s^2-2\gamma_A^2-2\gamma_1^2s^2+s^4-2s^2\gamma_A^2-2s^4\gamma_1^2+\gamma_A^4-2\gamma_A^2\gamma_1^2s^2+\gamma_1^4s^4)^{1/2}]^{1/2}. \end{aligned} \tag{94}$$

The unknown constants C_1 and C_2 are found by substituting the general solutions (93) into boundary conditions (92). These constants are

$$\begin{aligned} C_1 &= L(f(t))\cdot\frac{k_2(2\gamma_1^2s^2-2\gamma_A^2-k_2^2)}{2k_1\gamma_A^2-k_2^3+k_1^3-2k_2\gamma_A^2-2k_1\gamma_1^2s^2+2k_2\gamma_1^2s^2}, \\ C_2 &= L(f(t))\cdot\frac{k_1(2\gamma_1^2s^2-2\gamma_A^2-k_1^2)}{2k_2\gamma_A^2-k_1^3+k_2^3-2k_1\gamma_A^2-2k_2\gamma_1^2s^2+2k_1\gamma_1^2s^2}. \end{aligned} \tag{95}$$

Equations (93)–(95) give the solution in the Laplace domain. In order to return to the time domain, the following inverse transform is applied:

$$u(\chi,\tau) = \frac{1}{2\pi i}\int_{c-i\infty}^{c+i\infty} e^{s\tau}U(\chi,s)ds, \tag{96}$$

where c is real and positive and greater than the real part of all singularities of $U(\chi,s)$. The inverse transform is accomplished numerically by evaluating the following integral [10, 11, 18, 23]:

$$u(\chi,\tau) = \frac{1}{2\pi} e^{c\tau} \cdot \Re \left[\int_{-w_0}^{w_0} U(\chi, s = c + iw) e^{iw\tau} dw \right]. \tag{97}$$

4.2. Results – displacement boundary condition

The main goal of the present subsection is to show that the optical dispersion branch has a measurable effect in the wave processes in microstructured solids. To this end the time-dependent sine function is used as a boundary condition for macrodisplacement. The use of the harmonic sine function allows exact control over the frequency at the boundary. The results are depicted in Figs. 20–23 which can be found in Appendix A.

In addition to the solutions of the boundary value problem (parts b of Figs. 20–23), the corresponding phase and group speed curves are provided (parts a of Figs. 20–23). Here we have preferred the use of the phase and group speed curves over the dispersion curves, as they provide a clearer understanding of what to expect in experiments. As the phase and group speed curves are calculated following the dispersion curves (79), the usage of phase and group speed curves in the analysis is equivalent to the usage of dispersion curves. The acoustic phase and group speed curves correspond to the acoustic dispersion branch and the optical phase and group speed curves correspond to the optical dispersion branch.

Although the frequency of the disturbance can be any positive real number, we will limit the dimensionless frequency $\eta = p\omega$ to the values $0 < \eta < 1$. This is the frequency range where only the acoustic dispersion branch exists, which is represented by the phase (dashed line) and group (solid line) speed curves that exist over the full range of frequencies (see Fig. 20a). The phase and group speed curves that only exist when $\eta > 1$ represent the optical dispersion branch. The case $\eta = 1$ can be considered as a high frequency limit, where the effects of the optical dispersion branch start prevailing. Note that the high frequency limit is defined by the time constant p which is related to the microinertia of the microstructure.

Figure 20b shows the result of the simulation when $\gamma_A = 0.6$, $\gamma_1 = 0.5$ and $\eta = 0.8$ at dimensionless time $\tau = 60$. The wave profile in Fig. 20b can roughly be divided into two parts – acoustic, which is the wave profile up to the acoustic front (denoted by 'front acu.' in Fig. 20b), and optical, which is a low amplitude part between the acoustic and optical fronts (denoted by 'opt.' in Fig. 20b). 'Front acu.' and 'opt.' are related to the maximum asymptotic speeds of the acoustic and optical dispersion

curves, respectively. For convenience we also divide the acoustic part into the main part, which has the amplitude almost equal to unity, and the medium amplitude part.

The main acoustic part travels at the group speed $\gamma_g = 0.53$, which corresponds to the frequency of the harmonic boundary condition (see Fig. 20a), and travels the dimensionless distance $\chi = 31.62$ (denoted by 'main group' in Fig. 20b). The approximate dimensionless wavelength can be estimated from Fig. 20b by measuring the distance between the two adjacent wave crests. In case of the main acoustic part the dimensionless wavelength is $\Lambda \approx 5.4$, which correlates well with the dimensionless wave number $\xi = pc_0k \approx 1.15$ given by the dispersion analysis (see Eq. (79)).

The medium amplitude part of the acoustic part travels at the highest group speed $\gamma_g = 0.8$ given by the acoustic dispersion branch, hence travelling the dimensionless distance $\chi = 48$ (denoted by 'front acu.' in Fig. 20b). It can be seen that the medium amplitude part is slightly out of phase. The coordinate where the medium amplitude part gets out of phase coincides reasonably well with the distance $\chi \approx 41.6$ travelled at the phase speed ($\gamma_p \approx 0.69$) of the given boundary condition.

The optical part of the wave profile is a low amplitude part that travels at the asymptotic speed of the optical dispersion branch, which is equal to the unity and therefore travels the dimensionless distance $\chi = 60$. This high frequency and low amplitude optical part reflects the effect of the optical dispersion branch. The amplitude of the optical part is not completely independent but depends on the frequency of the boundary condition. This effect will be revisited in the next subsection.

Another example is given by Fig. 21. As the maximum group speed related to the acoustic dispersion branch ($\gamma_g \approx 0.44$) is much lower than the maximum group speed related to the optical dispersion branch ($\gamma_g = 1$), the effect of the optical dispersion branch is seen very clearly in the emergence of the low amplitude optical part (see Fig. 21b). We also note that due to weak dispersion ($0.3 \leq \gamma_p \leq 0.44$), the medium amplitude part is much closer to the main acoustic part and it becomes difficult to divide the acoustic part in to two. The distances travelled by the acoustic front ($\chi = 21.8$) and the optical front ($\chi = 50$) are denoted in Fig. 21b. In addition, the distances travelled at the group speed ($\chi = 14.4$) and the phase speed ($\chi \approx 17.8$) of the boundary condition have been marked. The dimensionless wavelength of the main acoustic part ($\Lambda \approx 4.5$) corresponds well to the dimensionless wave $\xi \approx 1.4$ number given by the dispersion analysis.

In case of anomalous dispersion (see Fig. 22) the medium amplitude part is merged with the main acoustic part. The optical front travels at the speed $\gamma_g = 1$ and therefore reaches the distance $\chi = 65$. The acoustic front travels at the maximum speed given by the acoustic dispersion branch ($\gamma_g = 0.6$) and travels the distance $\chi = 39$. It can also be seen that in case of anomalous dispersion a negative tail appears in front of the acoustic part. This effect is better seen in case of the impulse boundary condition.

In case of strong anomalous dispersion (see Fig. 23a) the main acoustic part of the

wave profile becomes distorted (see Fig. 23b). This is due to the interaction between the fast moving short wavelengths and the low speed large wavelengths.

4.3. Results – amplitude of the optical part

The amplitude of the optical part is not completely independent but depends on the frequency of the boundary condition. In order to illustrate this dependence, we will turn to the dispersionless case, which means that there is no dispersion following the acoustic dispersion branch. In this case any dispersive effects are only due to the optical dispersion branch. The amplitude of the optical part is compared at different frequencies of the boundary condition. As an example we will use the system with parameters $\gamma_A = 0.6$ and $\gamma_1 = 0.8$.

The wave profiles at two different frequencies of the boundary condition ($\eta_1 = 0.1$ and $\eta_2 = 0.5$) and the magnifications of the optical parts are depicted in Fig. 24 in Appendix A. It can be clearly seen that the lower frequencies of the boundary condition induce lower amplitude optical parts than higher frequencies do. In case of dimensionless frequency $\eta_1 = 0.1$, the dimensionless amplitude of the optical part is $A \approx 0.002$, whereas in case of dimensionless frequency $\eta_2 = 0.5$ the dimensionless amplitude of the optical part is $A \approx 0.02$, thus ten times larger.

This result was expected as the low frequency corresponds to the large wavelength. It is intuitively clear that large wavelengths do not 'feel' the microstructure as much as short wavelengths do.

4.4. Impulse boundary condition

In oder to compare the full system (49) to the hierarchical approximation (71), the impulse boundary condition derived by Metrikine et al. [24] is used.

In case of hierarchical approximation (71), the impulse boundary value problem in dimensionless form is

$$u_{\tau\tau} - u_{\chi\chi} - \frac{c_A^2}{\tilde{c}^2} u_{\chi\chi\tau\tau} + \frac{c_1^2 c_A^2}{\tilde{c}^4} u_{\chi\chi\chi\chi} = 0, \tag{98}$$

$$\begin{aligned} u(\chi, \tau = 0) = u_\tau(\chi, \tau = 0) = 0, \\ \left(u_\chi + \frac{c_A^2}{\tilde{c}^2} u_{\chi\tau\tau} - \frac{c_1^2 c_A^2}{\tilde{c}^4} u_{\chi\chi\chi} \right)_{\chi=0} = P\delta\tau, \\ \lim_{\chi\to\infty} u(\chi, \tau) = 0, \end{aligned} \tag{99}$$

where $\delta(\tau)$ is the Dirac delta function, P is related to the intensity of the pulse and $\tilde{c}^2 = c_0^2 - c_A^2$ has been introduced for convenience. Note also that dimensionless space is now defined as $\chi = x/(\tilde{c}p)$.

The full system (49) will be solved in the form of one fourth order PDE for displacement (50). For the present problem Eq. (50) is rewritten in the form

$$u_{\tau\tau} - u_{\chi\chi} - \frac{c_0^2 + c_1^2}{\tilde{c}^2} u_{\chi\chi\tau\tau} + \frac{c_0^2 c_1^2}{\tilde{c}^4} u_{\chi\chi\chi\chi} + u_{\tau\tau\tau\tau} = 0. \tag{100}$$

The boundary condition for Eqs. (100) is similar to Eq. (99):

$$\begin{gathered} u(\chi, \tau = 0) = u_\tau(\chi, \tau = 0) = 0, \\ \left(u_\chi + \frac{c_0^2 + c_1^2}{\tilde{c}^2} u_{\chi\tau\tau} - \frac{c_0^2 c_1^2}{\tilde{c}^4} u_{\chi\chi\chi} \right)_{\chi=0} = P\delta\tau, \\ \lim_{\chi\to\infty} u(\chi, \tau) = 0. \end{gathered} \tag{101}$$

The boundary problems given by Eqs. (98)–(99) and (100)–(101) are solved by making use of the Laplace transform. The solving process is exactly the same as in case of the displacement boundary condition in Subsection 4.1.

4.5. Results – impulse boundary condition

The objective of the present subsection is to compare the behaviour of the hierarchical approximation (98) to the full system (100). To this end the impulse boundary conditions (99) and (101) are used and the wave profiles given by both models are compared at equal instances of dimensionless time. In addition, the group speed curves of both models are compared. For convenience the phase speed curves have been omitted. The results are depicted in Figs. 25–30 which can be found in Appendix A.

The first example is given in Fig. 25. Here the parameters are chosen so that the hierarchical approximation (98) provides an excellent approximation of the full model (100) – the group speed curve of Eq. (98) (dashed line) coincides with the group speed curve of the acoustic dispersion branch of Eq. (100) (solid line) (see Fig. 25a). As the hierarchical approximation provides an approximation of the acoustic dispersion curve only, the quality of the approximation is defined by the acoustic dispersion branch of the full model.

The wave profiles at the dimensionless time $\tau = 40$ are shown in Fig. 25b. It can be seen that the hierarchical approximation (98) (dashed line) provides a very good approximation of the impulse given by the full model (100) (solid line). However, while the full model (100) has an oscillating part in front of the main pulse travelling

at the speed $\gamma_g = 1/(1-\gamma_A^2)^{1/2} \approx 2.29$, the hierarchical model (98) has no sharp front and the elastic field decays exponentially in front of the impulse. The oscillating part in front of the impulse in case of the full model is due to the optical dispersion branch and is similar to the optical part discussed in Subsection 4.2.

Another example is given in Fig. 26. From the group speed curves (Fig. 26a) it can be seen that although the hierarchical approximation (98) provides a good approximation over a wide range of frequencies, there exists a frequency region ($0.4 \lesssim \eta \lesssim 1.1$) where the approximate model departs from the full model (100). The influence of that region can be seen in Fig. 26b: the main impulse is well approximated, but differences occur in the tail part of the impulse. Nevertheless, it can be said that the approximation is good. However, attention should be paid if a considerable part of the energy is in the frequency range where the dispersion curve of the hierarchical approximation departs from the acoustic dispersion branch given by the full model. We also note that dispersion is stronger in the present example (compare Figs. 26a and 25a) and therefore the tail in Fig. 26b is longer than in Fig. 25b. Here also the full model has an oscillating part in front of the impulse, which is due to the optical dispersion branch.

In the third example, given in Fig. 27, the agreement between the hierarchical approximation and the full model is not good over a wide range of frequencies (see Fig. 27a). The hierarchical approximation provides good results only when $\eta < 1$ or $\eta > 8$, which makes the approximation virtually unusable. This is also evident in Fig. 27b where the wave profiles at dimensionless time $\tau = 40$ are depicted. It can be seen that although the example in Fig. 27b represents a case of strong dispersion (see Fig. 27a), the hierarchical approximation only accounts for dispersion at very high frequencies.

As the maximum group speed given by the optical dispersion branch ($\gamma_g \approx 1.005$) is almost equal to the maximum group speed given by the acoustic dispersion branch ($\gamma_g = 1$), the oscillating part in front of the impulse is hardly noticeable (see Fig. 28). Nevertheless, it can be seen that in case of full the model the wave profile has a sharp front and travels the distance $\chi = 40.2$, which corresponds exactly to the asymptotic group speed given by the dispersion analysis (see Fig. 27a). The hierarchical approximation on the other hand has a decaying front and the elastic field is also disturbed in the region which is farther to the distance travelled at the maximum speed given by the dispersion analysis. This is in accordance with the idea that the optical dispersion branches are needed in order to make the model causal [23].

The fourth example is a case of anomalous dispersion (see Fig. 29a). As expected, there is now a negative tail in front of the impulse (see Fig. 29b). The impulse is well approximated by the hierarchical approximation (98). In case of the full equation (100), an oscillation occurs both in front of and behind the impulse.

The last example is a dispersionless case (i.e., no dispersion related to the acoustic dispersion branch) (see Fig. 30a). It can be seen immediately in Fig. 30b that in case of hierarchical approximation, which provides the acoustic dispersion branch only, the impulse does not disperse and travels at constant speed. In case of the full model, the impulse disperses. Whereas in case of the full model, the main impulse travels a shorter distance than in case of the approximation. This is due to the frequencies in the range $1 < \eta \lesssim 1.6$ that travel at the speeds $0 < \gamma_g < 1$

4.6. Summary

The solutions to the boundary value problem clearly show that the optical dispersion branch has a measurable effect in numerical experiments – the high frequency oscillations due to the optical dispersion branch appear both in case of harmonic displacement and impulse boundary conditions. The speeds at which different parts of the wave profile travel are in good accordance with the values given by the dispersion analysis.

The boundary value problem also provides a different insight into the question of the applicability of the hierarchical approximation. This approximation is usable over a wide range of parameters and can simplify the analysis significantly. However, the results match the full system better when most of the harmonics are in the range $0 < \eta < 1$. The higher harmonics can alter the wave profiles significantly.

Here we have used the boundary conditions that encompass a wide range of frequencies and therefore one may ask whether the optical dispersion branch is important if most of the wave energy is concentrated in a low frequency area. This problem will be studied in the next section.

5. Initial value problem

While the dispersion analysis has shown that in case of the internal scale the high frequency optical dispersion branches emerge, the solutions to the boundary value problem clearly show that the influence of these branches creates measurable effects in the wave processes. As the hierarchical equation (71) does not account for the optical dispersion branch, special attention has to be paid to the results when utilising the hierarchical approximation.

When making use of the numerical methods, then will always be a possibility that the high frequency oscillations are not physical but rather caused by numerical procedures. In the present section it will be shown that high frequency oscillations also appear in case of the initial value problem [27]. It will also be shown that the effect is considerably less pronounced at low frequencies.

5.1. Numerical method

The pseudospectral method is used to solve the initial value problem under localised initial and periodic boundary conditions. In the present analysis the pseudospectral method based on the discrete Fourier transform is applied (see [30, 32, 33] and references therein).

The hierarchical approximation in dimensionless form (70) can be rewritten as

$$U_{TT} - bU_{XX} = \delta\left(\beta U_{TT} - \gamma U_{XX}\right)_{XX}, \tag{102}$$

where

$$\gamma_A^2 = 1 - b, \quad \gamma_1^2 = \frac{\gamma}{\beta}, \quad \delta = \frac{l^2}{L^2}. \tag{103}$$

By making use of change of variables the full system (49) is rewritten in the form

$$\begin{aligned} U_{TT} &= \frac{AL}{\alpha U_o}\varphi_X + U_{XX}, \\ \varphi_{TT} &= \frac{C\rho}{\alpha I}\varphi_{XX} - \frac{B\rho L^2}{\alpha I}\varphi - \frac{A\rho U_o L}{\alpha I}U_X. \end{aligned} \tag{104}$$

The initial condition and the requirement of periodicity are as follows:

$$U(X,0) = U_o \operatorname{sech}^2 B_o X, \quad U(X,T) = U(X + 2km\pi, T),\ m = 1,2,\ldots, \tag{105}$$

where $k = 64$, i.e., the total length of the spatial period is 128π. For the amplitude and the width of the initial pulse we use the values $U_o = 1$ and $B_o = \pi/2$. Initial

phase speed is taken to be zero, and can be interpreted as starting from the peak of the interaction of two waves propagating in opposite directions.

For the full system (49) two more initial conditions are needed for the microdeformation. We assume that at $T = 0$ the microdeformation and the corresponding speeds are zero, i.e., $\varphi(X,0) = 0$ and $\varphi_T(X,0) = 0$. The integration interval is from zero to $T_f = 180$. We uses an initial condition which leads to the emergence of two solitary waves that propagate in opposite directions. Nevertheless, the spatial period is long enough and the time interval short enough to avoid interactions regardless of periodic boundary conditions.

5.2. Results

The characteristic solution of Eqs. (102) and (104) is depicted in Fig. 31. It can be seen that under used initial and boundary conditions (105) the initial pulse at $X = 64\pi$ splits in to two waves propagating in the opposite directions. Previous studies have shown that in case of nonlinearity these waves evolve differently [30, 31, 32, 33]. In the present analysis the nonlinearities are excluded and therefore only the pulse travelling to the right is depicted (see Fig. 32). The corresponding group speed curves can be found in Fig. 33.

It can be seen immediately in Fig. 32 that the hierarchical approximation (102) provides a good approximation for the full system (104): there are differences in the tails, but the main pulses given by both models are in excellent agreement. The measured speed of the main pulse is $\gamma_R = 0.6063$, which correlates well with the theoretical value $\gamma_R = (1-\gamma_A^2)^{1/2} = 0.6164$ given by the dispersion analysis. Tamm et al. [31, 32] have shown that the hierarchical approximation (102) provides a good approximation for the full system (104), the measured speeds agree with the theoretical values and the effect of the nonlinearities on speeds is small.

The effect of the optical dispersion branch can be seen in the behaviour of the full system (104) (solid line in Fig. 32) where oscillations emerge in front of the main pulse and the tail of the full system is longer than in case of the hierarchical approximation (102) (dashed line in Fig. 32). This result is in very good agreement with the group speed curves depicted in Fig. 33. It can be seen that in case of the hierarchical approximation, which provides an approximation of the acoustic dispersion branch only, the dispersion is relatively weak and the speeds are bounded between the values $0.6164 < \gamma_g < 0.3162$. The full system is also influenced by the optical dispersion branch and there are also harmonics that can have speeds between the values $0 < \gamma_g < 1$, whose effect can be seen in the emergence of a faster front and a slower tail.

The effect of the optical dispersion branch is best understood if the dispersion due to the acoustic dispersion branch is excluded. This can be achieved in the dispersionless

case, which means that there is no dispersion following the acoustic dispersion branch and consequently in the hierarchical approximation. In this case any dispersion effects are only due to the optical dispersion branch. The wave solutions travelling to the right and the corresponding group speed curves are depicted in Figs. 34 and 35 at four different sets of parameters. The wave profiles in Fig. 34 are arranged from left to right in the decreasing order of the parameter γ_A^2. As in the case of zero dispersion the group speed curve of the hierarchical approximation (71) coincides with the acoustic dispersion branch of the full system (49), only the group speed curves of the full system are depicted in Fig. 35. The optical dispersion branch is the same in all four cases and is represented by the solid line. The acoustic dispersion branches are represented by dashed lines. The corresponding parameters $1-\gamma_A^2=\gamma_1^2$ are marked in the vertical axis.

As seen in Fig. 34 the optical dispersion branch has a measurable effect in the wave processes. This effect depends on the value of the parameter γ_A: large values of γ_A induce large amplitude oscillations (see top left in Fig. 34), but the effect becomes negligible at small values of γ_A (see bottom right in Fig. 34). Note that the parameter γ_A also controls the speed of the main pulse.

The results can be explained by comparing the group speed curves in case of $\gamma_A^2=0.9$ (See Fig. 35) with the corresponding wave profile (top left in Fig. 34). At high values of γ_A^2 (which correspond to the small values in the vertical axis in Fig. 35) the speed of the main pulse is relatively small and a number of frequencies travel faster than the main pulse; therefore a relatively high amplitude oscillations will appear in front and behind of the main pulse. The maximum amplitude of these oscillations correlate well with the amplitude decrease of the main pulse. In case of hierarchical approximation, which experiences no dispersion, the amplitude does not change.

In the top right and bottom left parts of Fig. 34 it can be seen that as the speed of the main pulse increases, the effect of the optical dispersion branch decreases. If there still are frequencies that can travel faster than the main pulse, the oscillations due to the optical dispersion branch will appear.

The last example is given in the bottom right part of Fig. 34 (which corresponds to the topmost acoustic dispersion branch in Fig. 35). We can see that the effect of the optical dispersion branch becomes negligible in case of $\gamma_A^2=0.1$. The effect is still there, but extreme magnifications are needed to see it. By inspecting the group speed curves it can be seen that there are virtually no frequencies that can travel faster and the high frequency oscillations do not spring from the main pulse. This result was expected as the parameter γ_A is related to the coupling between the macro- and microstructure.

5.3. Summary

The analysis of the initial value problem has clearly shown that the high frequency oscillations arise due to the optical dispersion branch. The effect is best seen if the dispersionless case is considered – while the hierarchical approximation gives no dispersion, the low amplitude high frequency oscillations appear in case of the full system. Moreover, it has been shown that the effect is small if the parameter γ_A is small, which corresponds to weak interaction between the macro- and microstructure.

The main difference between the solutions of the boundary condition problem and the initial value problem is that the effect of the optical dispersion branch tends to be larger in case of the boundary value problem with the impulse boundary condition. This is due to the choice of the boundary condition, where the energy is equally distributed between all frequencies. In case of the initial condition, analysed in Section 5, a significant part of energy is concentrated in low frequency components.

6. Conclusions

This thesis focuses on the dispersion analysis of wave motion in microstructured solids. The analysis is based on the one-dimensional Mindlin-type equation derived by Engelbrecht et al. [12] and its hierarchical approximation.

In case of both models, the influence of the microstructure is revealed in the behaviour of the acoustic dispersion curve: in classical homogeneous models the acoustic dispersion curve is linear, but in the presence of the microstructure the speeds corresponding to the acoustic dispersion branch depend on the wave number. This is due to the inherent length scale introduced by the underlying microstructure.

In addition, the influence of the microstructure is also displayed in the emergence of the so-called optical dispersion branches, which are related to the steady state motion of the microstructure. Due to the mathematical procedures involved in deriving the hierarchical approximation, the optical dispersion branches are excluded in the approximated equation.

As shown in the thesis, the dispersion effects are significant for waves in microstructured solids. The physical background of a mathematical model must be understood in details like it is done for the Mindlin–Engelbrecht–Pastrone model. Although simplified models are attractive, the ranges of their applicability must be determined.

Main attention is paid to the physical microstructure, but the mathematical models of rods where geometrical dispersion is of importance are also briefly described. The analysis of dispersive effects in microstructured solids shows that the models of rods must be studied with the same accuracy, especially the applicability of the Mindlin–Hermann and Bishop models which bear straight resemblance to models in microstructured solids.

More specifically it is possible to highlight the following results:

Dispersion relations

- Two types of mathematical models, the full model (50) and and a simplified hierarchical equation (71) are studied in detail.
- Full dispersion analysis is presented for the full model (50) and its hierarchical approximation (71).
- It is shown how the dispersive effects are directly related to the microstructure.
- The applicability of the hierarchical approximation is analysed from the perspective of the dispersion analysis. It is found that the hierarchical equation provides a good approximation to the full system.

- Traditional single scale model is generalised to a multiscale model which permits us to analyse hierarchical and concurrent microstructures.

- While the single scale model is characterised by two dispersion branches, acoustic and optical, the multiscale model has three dispersion branches – one acoustic branch and two optical branches. The behaviour of the second optical dispersion branch depends on the type of the multiscale model (concurrent or hierarchical).

Boundary value problem

- The influence of dispersion is demonstrated for the boundary value problem.

- It is shown how the differences in phase and group speeds of various models lead to significant differences in wave profiles.

- The influence of the coupling of the macro- and microstructure in terms of wave motion is characterised by the behaviour of the optical dispersion curve, which stems from the stationary motion of the microstructure.

- It is shown that the amplitude predicted by the optical front depends on the frequency of the boundary condition: lower frequencies induce lower amplitude at optical fronts.

- The most interesting case is the existence of a medium range of the wavelengths where significant differences appear in wave profiles calculated from two models.

- It is shown that additional high frequency oscillations appear in case of the full model (88). These oscillations are related to the optical dispersion branch and are especially seen in high frequency oscillations in front of the main pulse. In the hierarchical model the pulse has a decaying front.

- The ranges of the good approximation of the full system by the hierarchical one are established.

Initial value problem

- The influence of the optical dispersion branch is demonstrated for the initial value problem.

- It is shown that if there is no dispersion in the acoustic dispersion branch (i.e. dispersion effects are only due to the optical dispersion branch), in case of the full model (104) a low amplitude wave packet appears, reflecting the effect of the optical dispersion branch.
- The amplitude of the low amplitude wave packet depends on the parameter γ_A which reflects the coupling between the scales. At small values of γ_A the dispersive effects due to the optical dispersion branch tend to be negligible.

Further studies will be focusing on the inclusion of nonlinearities in the boundary value problem and in the analysis of the multiscale models.

Abstract

The focus of the thesis is on the dispersion analysis of wave motion in microstructured solids. The basis of the analysis is the 1D Mindlin-type model derived by Engelbrecht et al. [12] and its hierarchical approximation. This model has a clear physical background and reflects well the influence of the microstructure on the macrostructure. Full dispersion analysis is presented for both models and the influence of the dispersion is demonstrated for boundary and initial value problems. The behaviour of the hierarchical approximation is compared with the full Mindlin–Engelbrecht–Pastone model and its applicability is analysed. Special attention is paid to the clarification of effects caused by the optical dispersion branches, which are clearly seen in wave profiles generated either by boundary or initial excitations. In addition, a single scale model is generalised to a multiscale model and the corresponding dispersion analysis is carried out.

The results of the thesis have been presented in two international conferences and published in three scientific papers indexed by the ISI Web of Science.

Kokkuvõte

Käesolevas töös on uurimise all lainelevi dispersioon mikrostruktuuriga materjalides. Analüüsi aluseks on Engelbrechti ja Pastrone poolt [12] tuletatud Mindlini tüüpi võrrand ning selle hierarhiline aproksimatsioon, mis kirjeldavad ühemõõtmelist lainelevi mikrostruktuuriga materjalides. Mõlema mudeli puhul on analüüsitud dispersiooniseoseid ning dispersiooni mõju on näidatud nii raja- kui ka algväärtus ülesande korral. Hierarhilise aproksimatsiooni käitumist on võrreldud täisvõrrandiga ning aproksimatsiooni kasutatavust on analüüsitud. Erilist tähelepanu on pööratud efektidele, mida põhjustavad optilised dispersioonikõverad, mis on selgelt nähtavad raja- ja algväärtus ülesannete lahendites. Traditsiooniline makro-mikro süsteem on seotud ühe mastaabi-teguriga; see on üldistatud mitme mastaabiga juhule ning vastavaid dispersiooni omadusi on analüüsitud.

Käesoleva töö tulemused on esitatud kahel rahvusvahelisel konverentsil ja avaldatud kolmes teadusartiklis tunnustatud erialaajakirjades ja konverentsikogumikus, mis on indekseeritud andmebaasis ISI Web of Science.

References

[1] H. Abramson, H. Plass, and E. Ripperger. Stress Wave Propagation in Rods and Beams. In H. Dryden and T. von Karman, editors, *Advances in Applied Mechanics*, volume 5, pages 111–194, New York, 1958. Academic Press INC., Publishers.

[2] I. V. Andrianov, J. Awrejcewicz, and D. Weichert. Improved Continuous Models for Discrete Media. *Mathematical Problems in Engineering*, 2010:1–36, 2010.

[3] A. Askar. *Lattice Dynamical Foundations of Continuum Theories*. World Scientific, Singapore, 1985.

[4] H. Askes, A. Metrikine, A. Pichugin, and T. Bennett. Four simplified gradient elasticity models for the simulation of dispersive wave propagation. *Philosophical Magazine*, 88(28):3415–3443, 2008.

[5] A. Bedford and D. Drumheller. *Introduction to Elastic Wave Propagation*. John Wiley & Sons, 1994.

[6] A. Berezovski, J. Engelbrecht, and T. Peets. Multiscale modeling of microstructured solids. *Mechanics Research Communications*, 37(6):531–534, 2010.

[7] M. Braun. *Wave Propagation in an Elastic Rod*. Unpublished note, 2003.

[8] L. Brillouin. *Wave Propagation in Periodic Structures*. Dover Publications, INC, NY, 1953.

[9] P. L. Christiansen, V. Muto, and S. Rionero. Solitary wave solutions to a system of Boussinesq-like equations. *Chaos, Solitons & Fractals*, 2(1):45–50, Jan. 1992.

[10] A. M. Cohen. *Numerical Methods for Laplace Transform Inversion*. Springer Verlag, 2007.

[11] D. G. Duffy. *Transform Methods for Solving Partial Differential Equations*. Chapman & Hall /CRC, 2004.

[12] J. Engelbrecht, A. Berezovski, F. Pastrone, and M. Braun. Waves in microstructured materials and dispersion. *Philosophical Magazine*, 85(33–35):4127–4141, 2005.

[13] J. Engelbrecht, F. Pastrone, M. Braun, and A. Berezovski. Hierarchies of waves in nonclassical materials. In P. P. Delsanto, editor, *The Universality of Nonclassical Nonlinearity: Applications to Non-destructive Evaluations and Ultrasonics*, pages 29–48. Springer, 2006.

[14] A. C. Eringen. Linear theory of micropolar elasticity. *Journal of Mathematics and Mechanics*, 15:909–923, 1966.

[15] A. C. Eringen. *Microcontinuum Field Theories. I Foundations and Solids*. Springer, New York, 1999.

[16] A. C. Eringen and E. S. Suhubi. Nonlinear Theory of Simple Micro-elastic Solids - I. *International Journal of Engineering Science*, 2:189–203, 1964.

[17] V. I. Erofeyev, V. Kazhaev, and N. Semerikova. *Waves in Rods. Dispersion, Dissipation, Nonlinearity.* Fizmatlit, Moscow, 2002.

[18] K. Hollenbeck. INVLAP.M: A matlab function for numerical inversion of Laplace transforms by the de Hoog algorithm, http://www.isva.dtu.dk/staff/karl/invlap.htm, 1998.

[19] J. Janno and J. Engelbrecht. *Microstructured Solids: Inverse Problems.* Springer, Heidelberg et al., 2011.

[20] C. Kittel. *Introduction to Solid State Physics*. John Wiley & Sons, Inc., 1966.

[21] I. A. Kunin. *Elastic Media with Microstructure I: One-Dimensional Models*. Springer, 1982.

[22] G. A. Maugin. *Nonlinear Waves in Elastic Crystals*. Oxford University Press, 1999.

[23] A. V. Metrikine. On causality of the gradient elasticity models. *Journal of Sound and Vibration*, 297(3–5):727–742, 2006.

[24] A. V. Metrikine and H. Askes. One-dimensional dynamically consistent gradient elasticity models derived from a discrete microstructure:: Part 1: Generic formulation. *European Journal of Mechanics-A/Solids*, 21(4):555–572, 2002.

[25] R. Mindlin. Microstructure in linear elasticity. *Archive for Rational Mechanics and Analysis*, 16(1), 1964.

[26] T. Peets, M. Randrüüt, and J. Engelbrecht. On modelling dispersion in microstructured solids. *Wave Motion*, 45:471–480, 2008.

[27] T. Peets and K. Tamm. Dispersion analysis of wave motion in microstructured solids. In T.-T. Wu and C.-C. Ma, editors, *IUTAM Symposium on Recent Advances of Acoustic Waves in Solids: Proceedings, Taipei, Taiwan, May 25-28, 2009*, volume 26 of *IUTAM Bookseries*, pages 349–354. Springer, Dordrecht, 2010.

[28] A. V. Pichugin, H. Askes, and A. Tyas. Asymptotic equivalence of homogenisation procedures and fine-tuning of continuum theories. *Journal of Sound and Vibration*, 313:858–874, 2008.

[29] L. A. Pochhammer. Biegung des Kreiscylinders-Fortpflanzungs-Geschwindigkeit kleiner Schwingungen in einem Kreiscylinder. *Journal für die reine und angewandte Mathematik*, 81, 1876.

[30] A. Salupere, K. Tamm, and J. Engelbrecht. Numerical simulation of interaction of solitary deformation waves in microstructured solids. *International Journal of Non-Linear Mechanics*, 43(3):201–208, 2008.

[31] K. Tamm. *Wave Propagation and Interaction in Mindlin-Type Microstructured Solids: Numerical Simulation*. PhD thesis, Tallinn University of Technology, 2011.

[32] K. Tamm and A. Salupere. On the propagation of 1D solitary waves in Mindlin-type microstructured solids. *Mathematics and Computers in Simulation*, (in press).

[33] K. Tamm and A. Salupere. On the propagation of solitary waves in Mindlin-type microstructured solids. *Proceedings of the Estonian Academy of Sciences*, 59(2):118–125, 2010.

[34] G. B. Whitham. *Linear and Nonlinear Waves*. J. Wiley, New York, 1974.

Appendix A: Figures

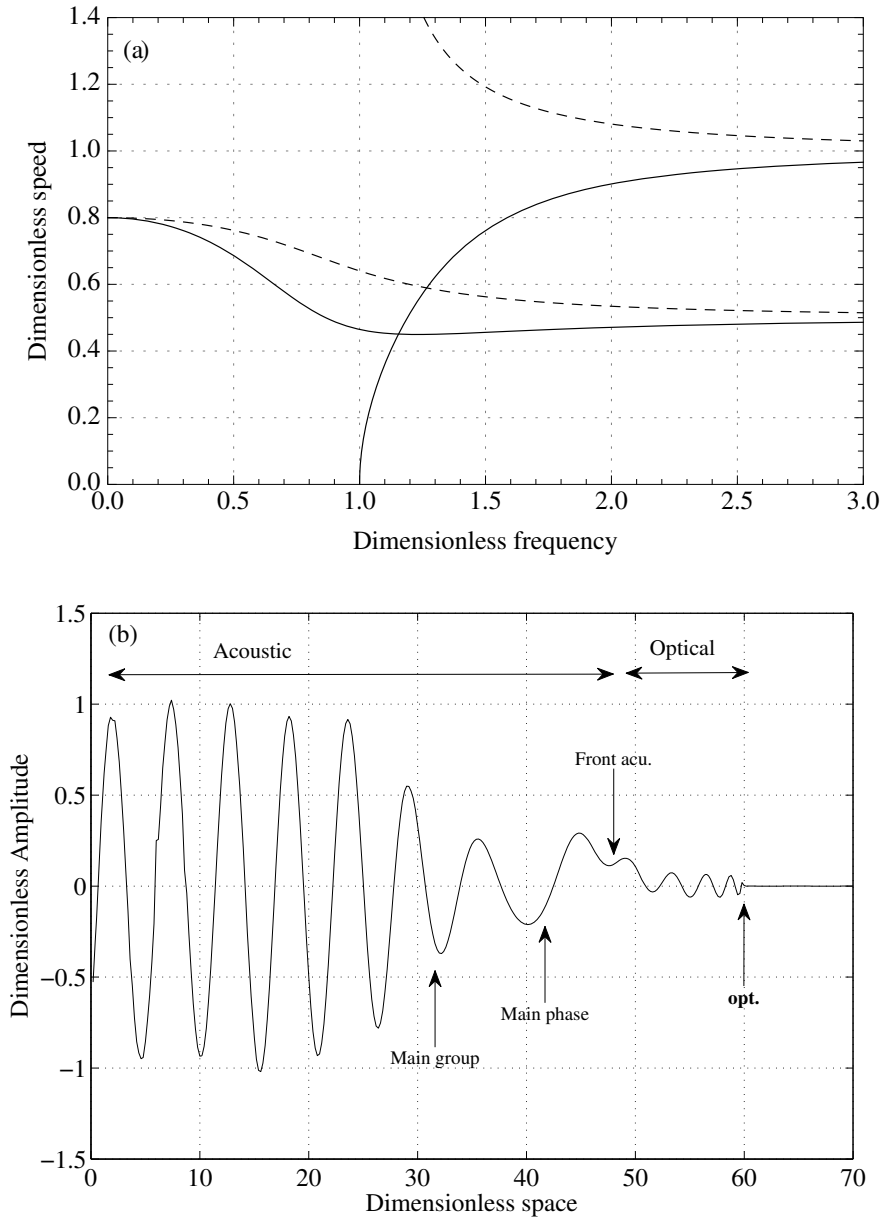

Figure 20: (a) Phase (dotted lines) and group (solid lines) speed curves for the full model in case of $\gamma_A = 0.6$ and $\gamma_1 = 0.5$ and (b) the wave profile at $\tau = 60$ in case of harmonic displacement BC ($\eta = 0.8$).

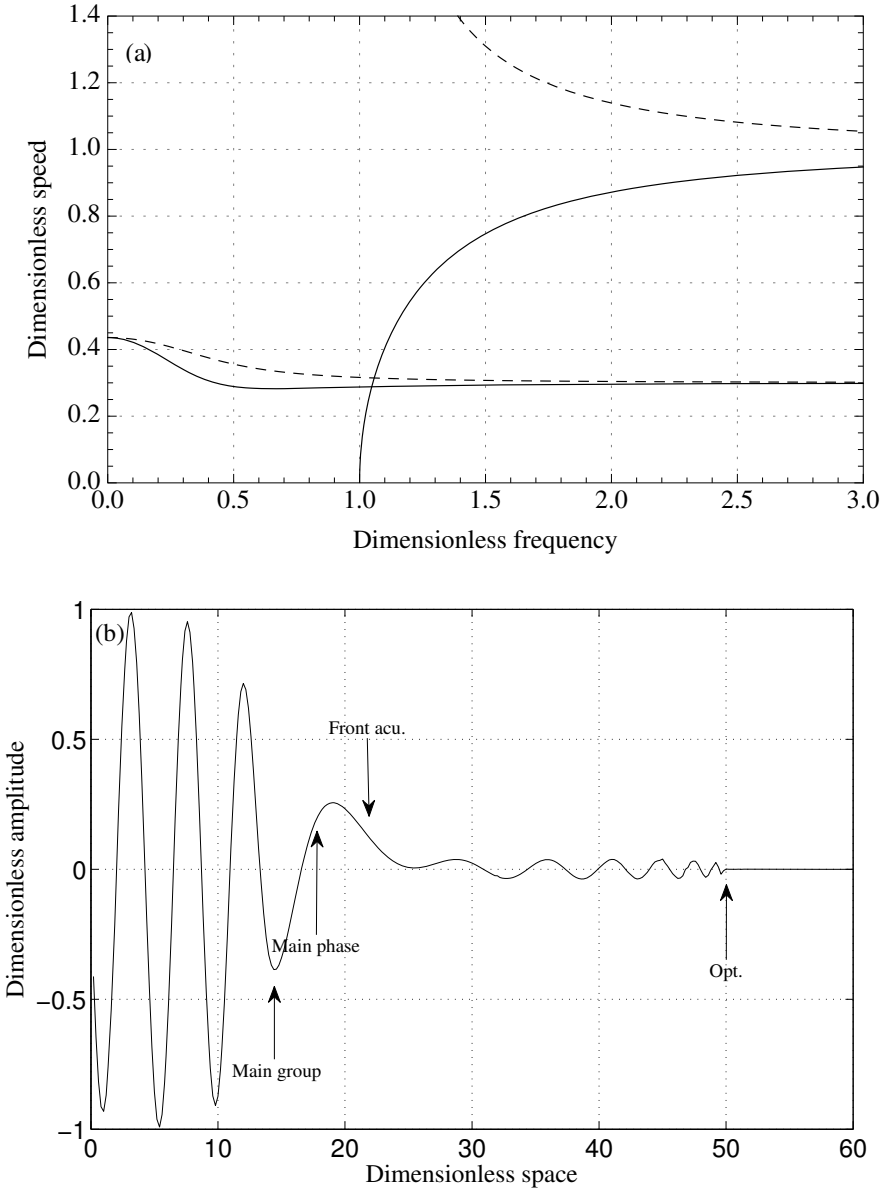

Figure 21: (a) Phase (dotted lines) and group (solid lines) speed curves for the full model in case of $\gamma_A = 0.9$, $\gamma_1 = 0.3$ and (b) the wave profile at $\tau = 50$ in case of harmonic displacement BC ($\eta = 0.5$).

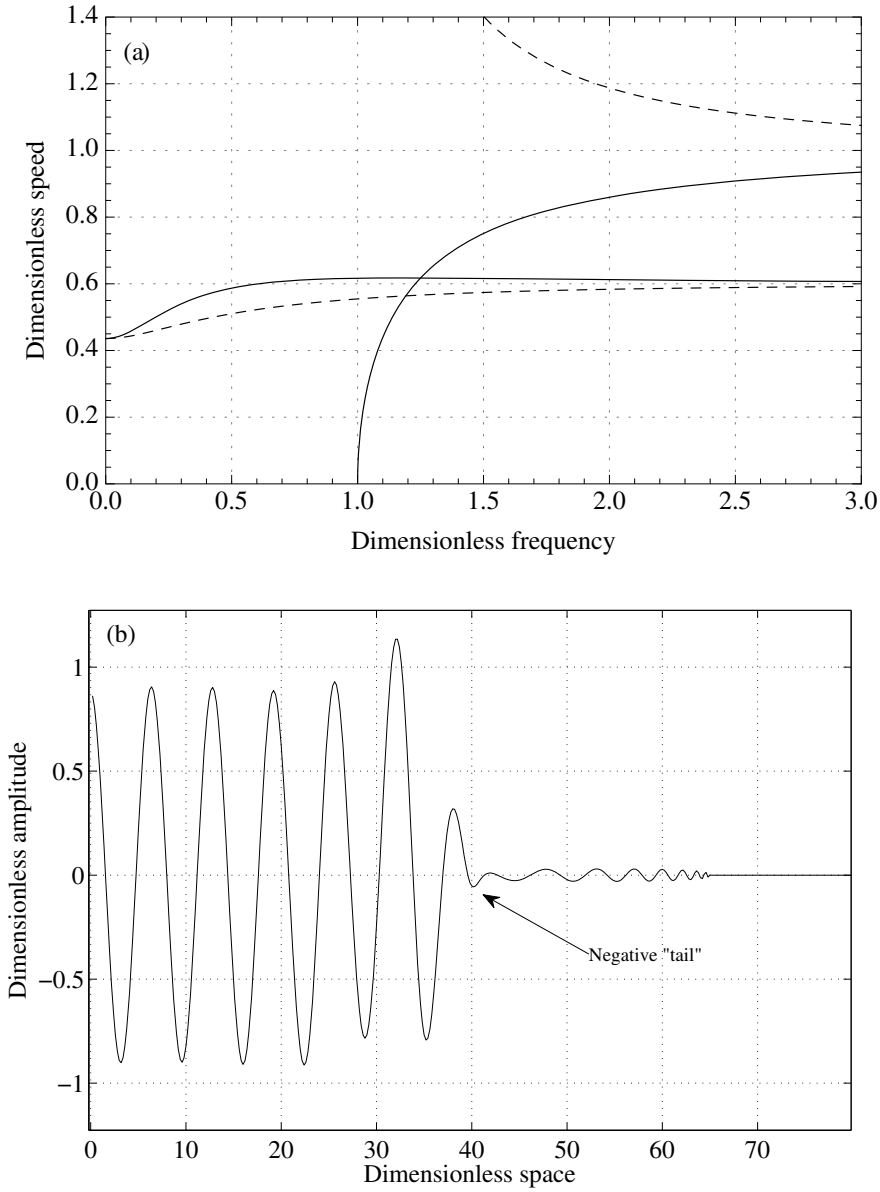

Figure 22: (a) Phase (dotted lines) and group (solid lines) speed curves for the full model in case of $\gamma_A = 0.9$, $\gamma_1 = 0.6$ and (b) the wave profile at $\tau = 65$ in case of harmonic displacement BC ($\eta = 0.5$).

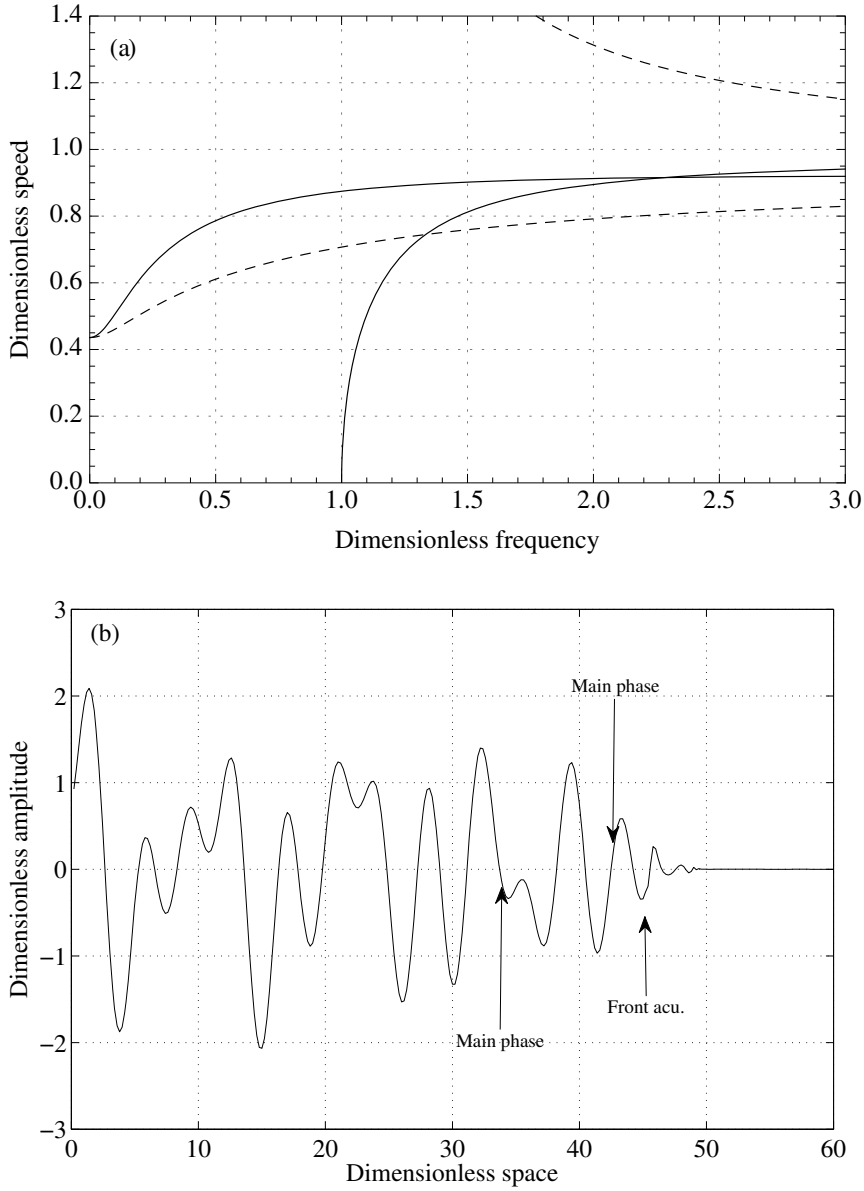

Figure 23: (a) Phase (dotted lines) and group (solid lines) speed curves for (b) the full model in case of $\gamma_A = 0.9$, $\gamma_1 = 0.9$ and the wave profile at $\tau = 50$ in case of harmonic displacement BC ($\eta = 0.8$).

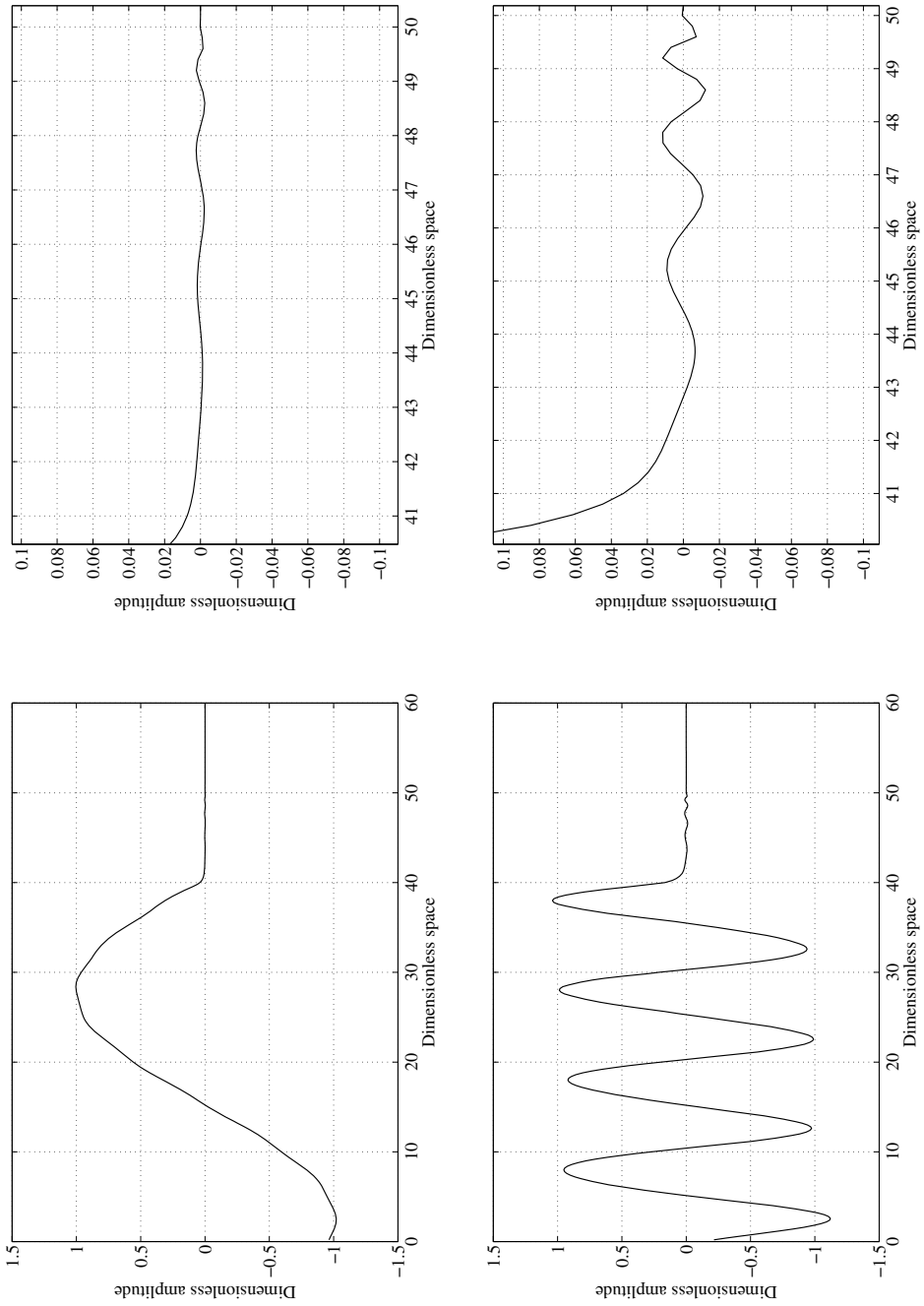

Figure 24: Wave profiles (left column) and corresponding magnifications of the optical parts (right column) for the full model at $\tau = 50$ in case of $\gamma_A = 0.6$, $\gamma_1 = 0.8$ when $\eta = 0.1$ (top panels) and $\eta = 0.5$ (bottom panels).

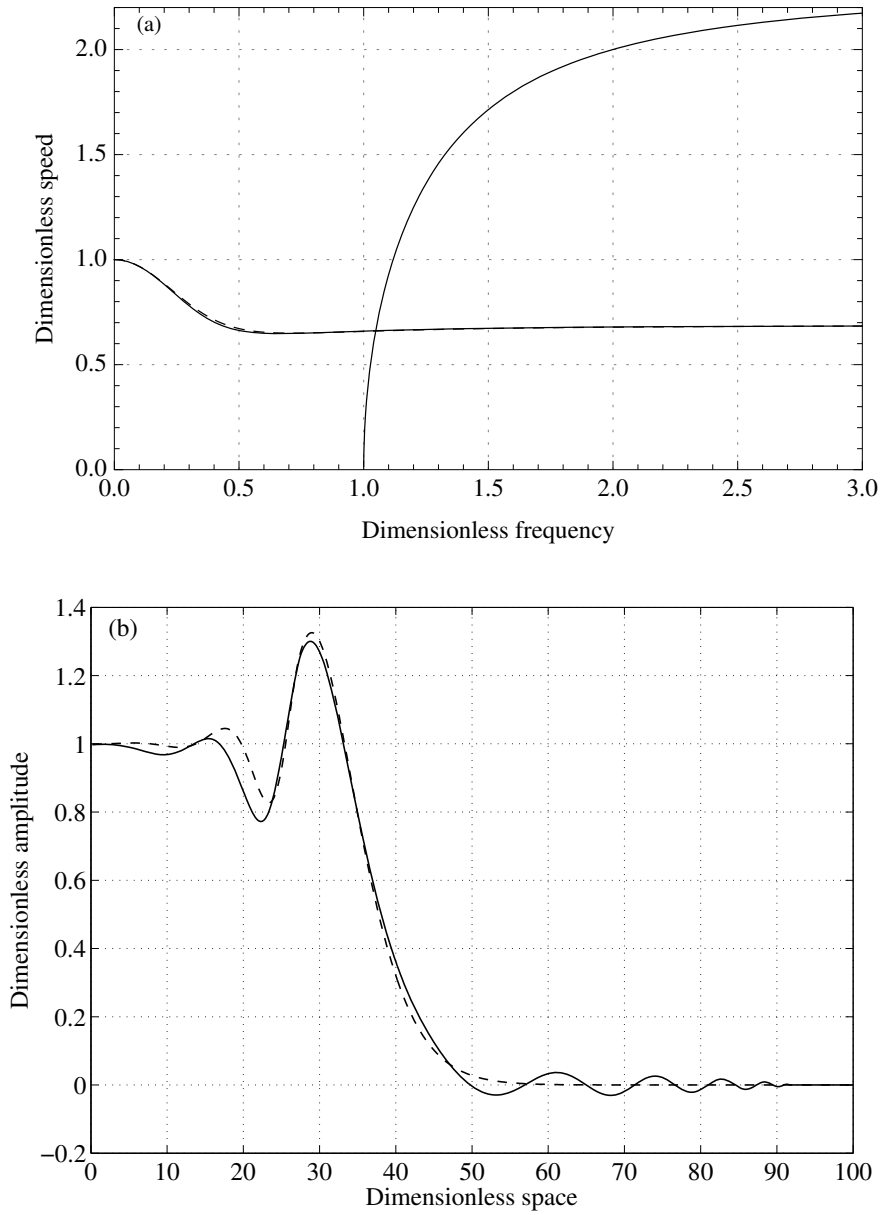

Figure 25: (a) Group speed curves of the full (solid line) and hierarchical (dashed line) models in case of $\gamma_A = 0.9$, $\gamma_1 = 0.3$ and (b) the corresponding wave profiles at $\tau = 40$ in case of impulse BC.

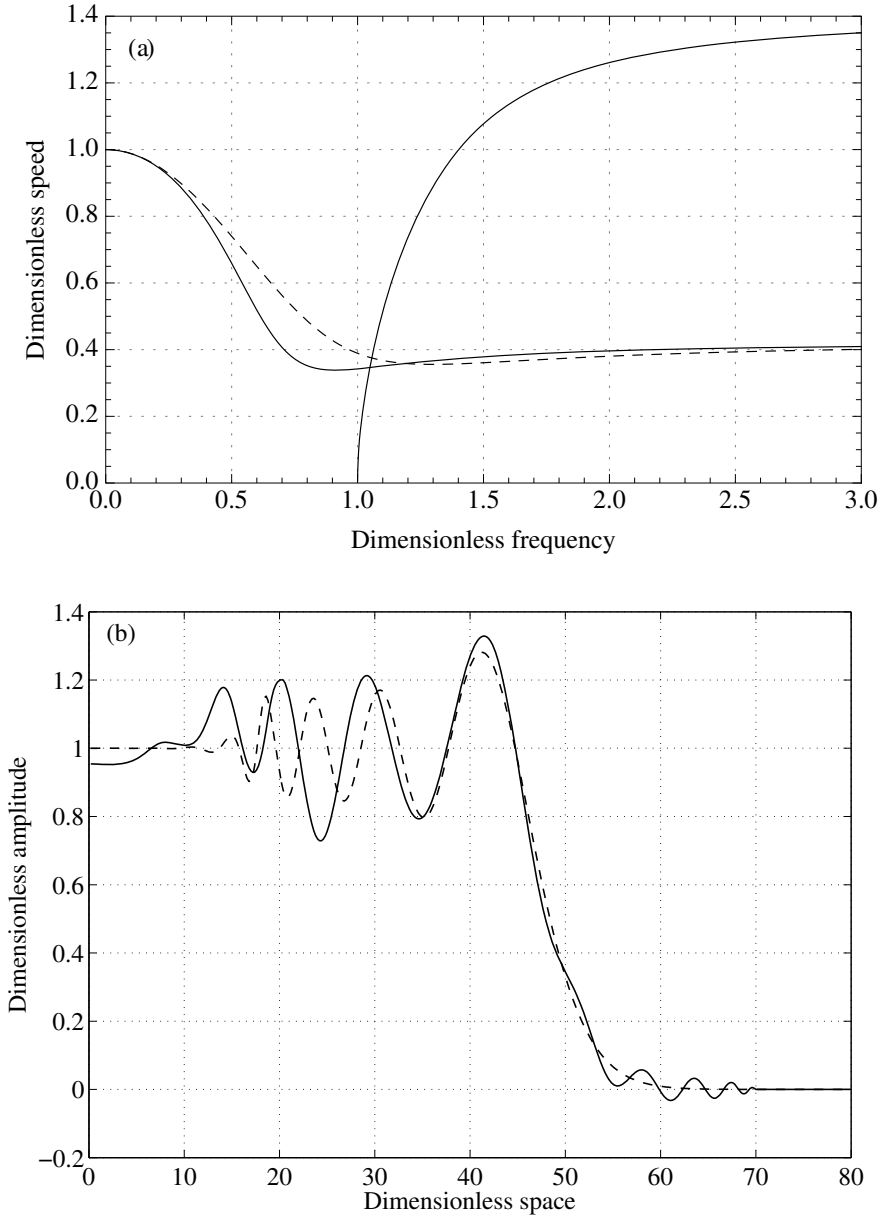

Figure 26: (a) Group speed curves of the full (solid line) and hierarchical (dashed line) models in case of $\gamma_A = 0.7$, $\gamma_1 = 0.3$ and (b) the corresponding wave profiles at $\tau = 50$ in case of impulse BC.

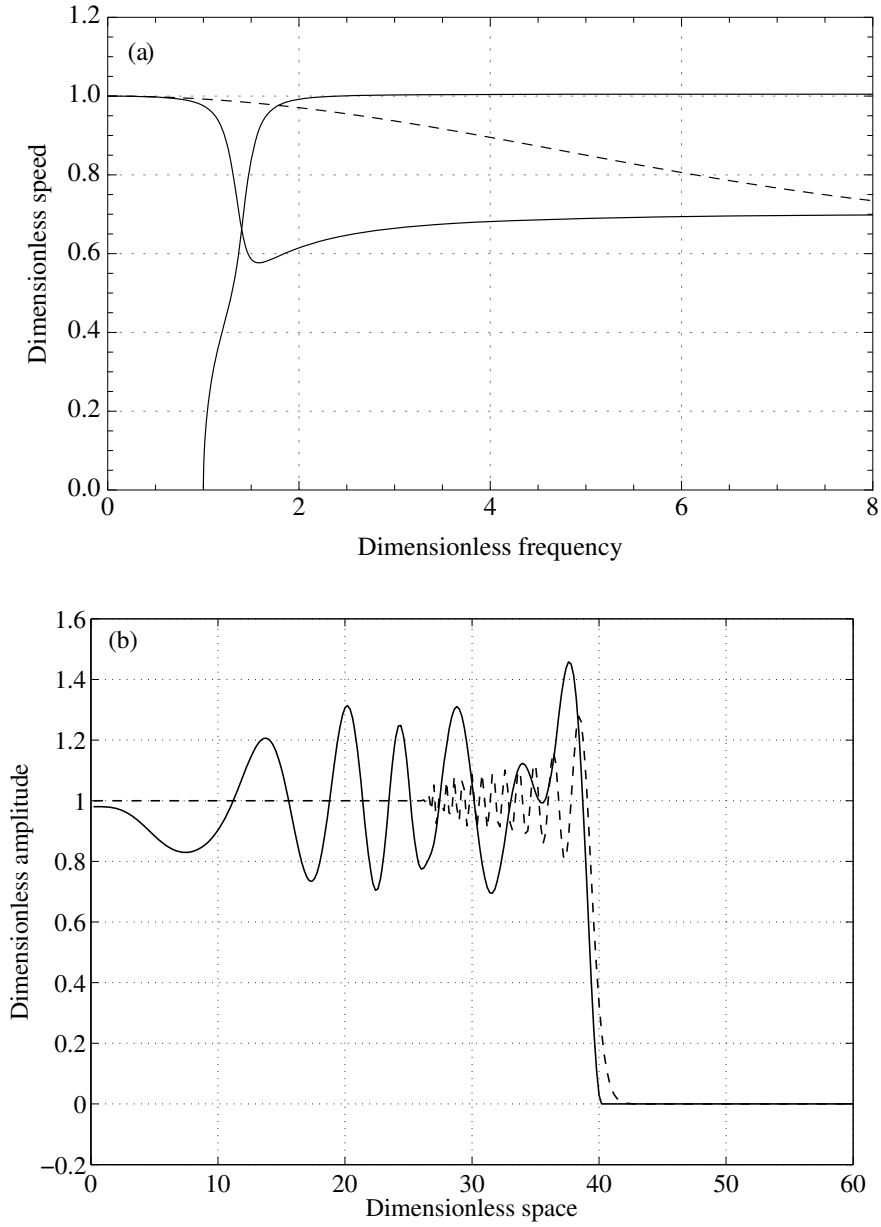

Figure 27: (a) Group speed curves of the full (solid line) and hierarchical (dashed line) models in case of $\gamma_A = 0.1$, $\gamma_1 = 0.7$ and (b) the corresponding wave profiles at $\tau = 40$ in case of impulse BC.

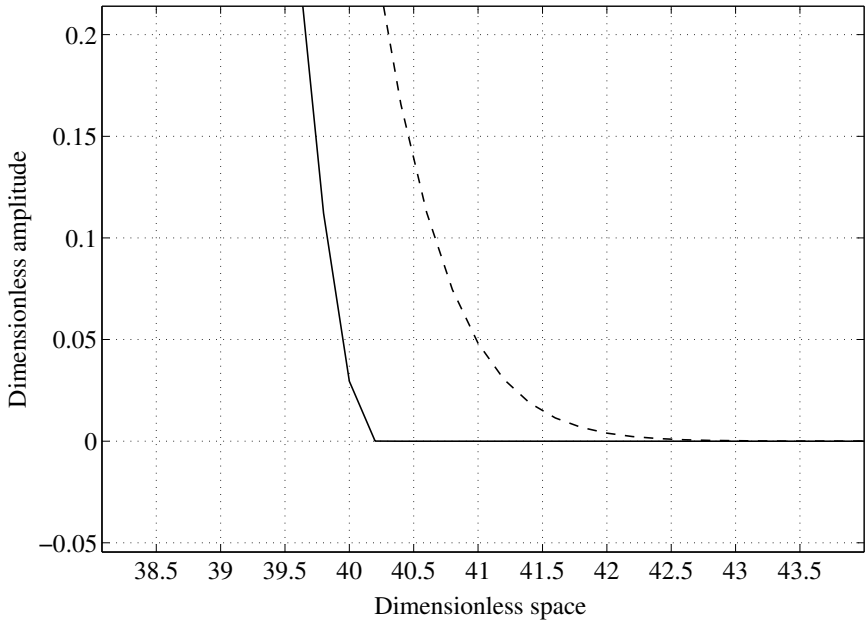

Figure 28: Magnification of the wave front in Fig. 27.

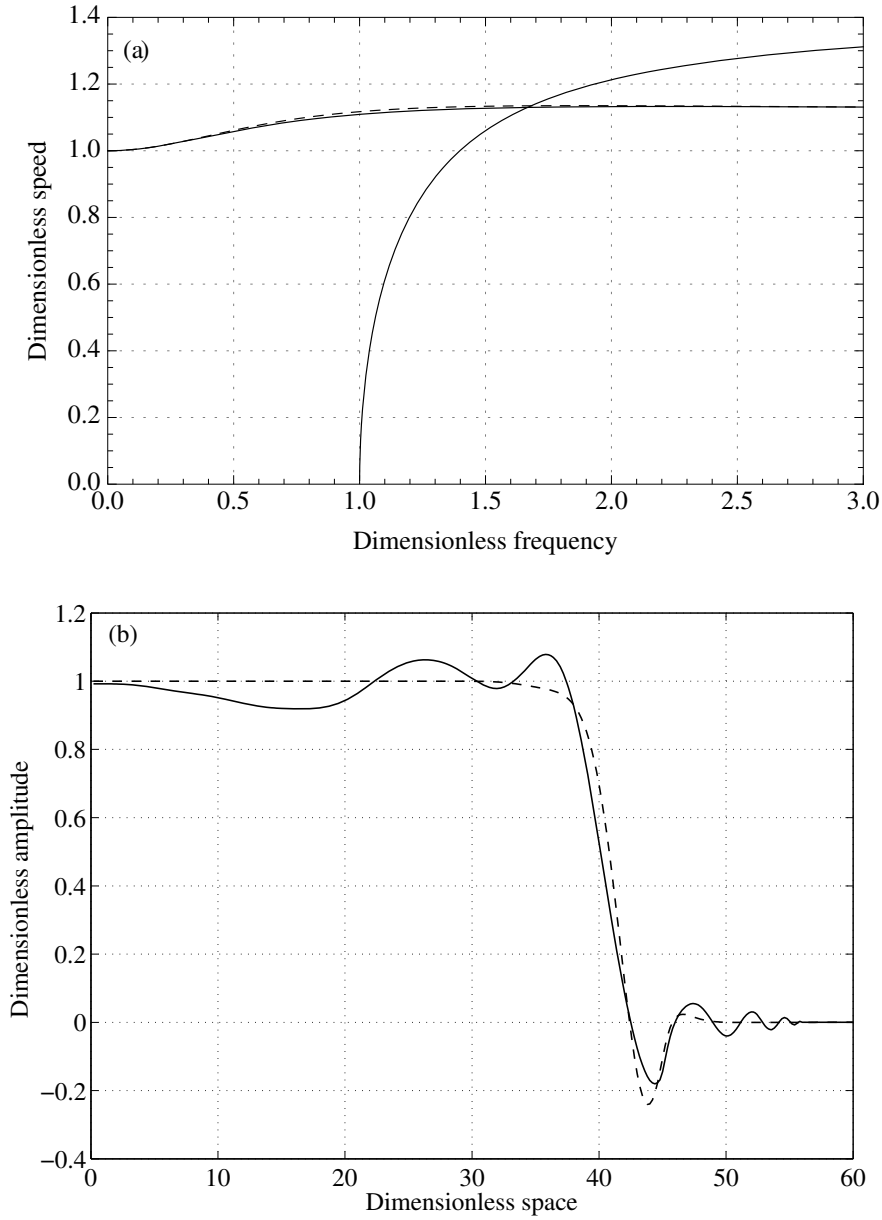

Figure 29: (a) Group speed curves of the full (solid line) and hierarchical (dashed line) models in case of $\gamma_A = 0.7$, $\gamma_1 = 0.8$ and (b) the corresponding wave profiles at $\tau = 40$ in case of impulse BC.

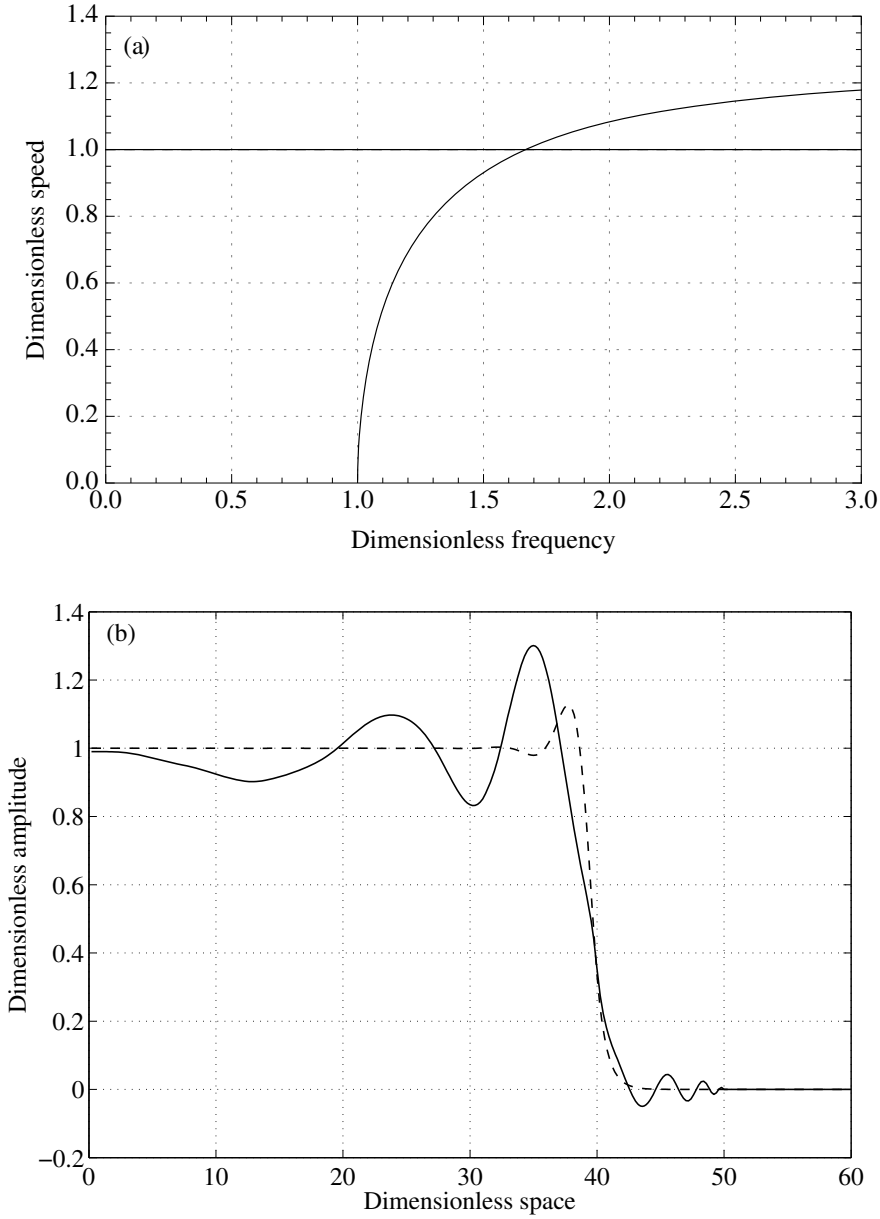

Figure 30: (a) Group speed curves of the full (solid line) and hierarchical (dashed line) models in case of $\gamma_A = 0.6$, $\gamma_1 = 0.8$ and (b) the corresponding wave profiles at $\tau = 40$ in case of impulse BC.

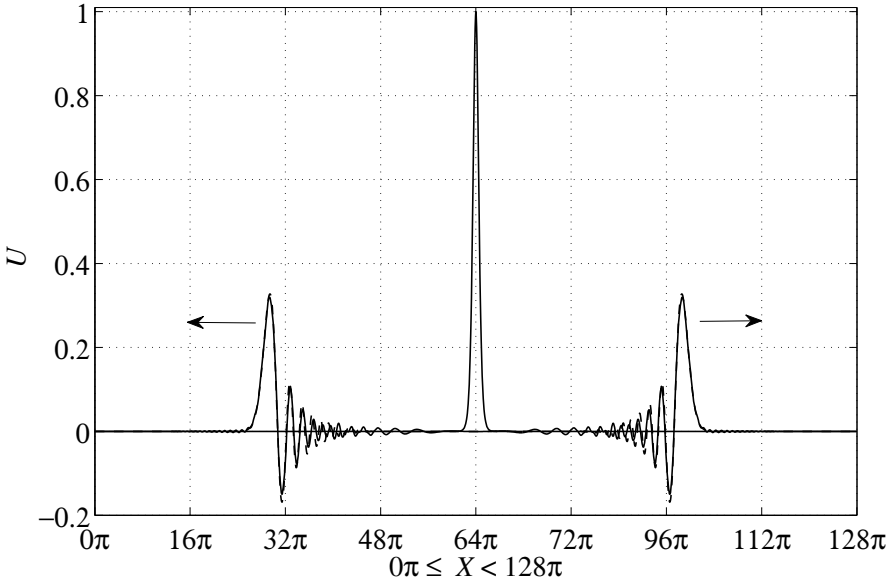

Figure 31: Solutions for Eqs. (102) (dashed line) and (104) (solid line). The pulse at $X = 64\pi$ represents the initial condition. $\gamma_A^2 = 0.62$, $\gamma_1^2 = 0.1$.

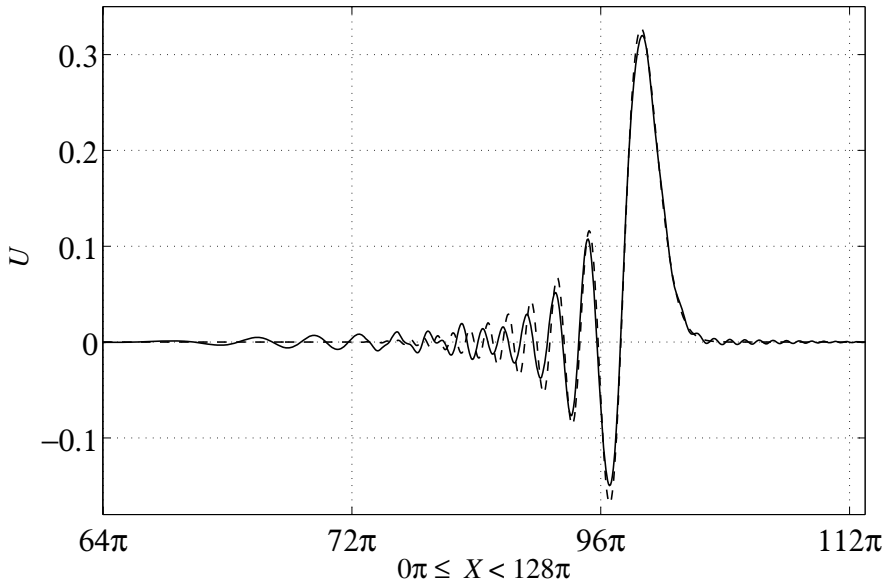

Figure 32: Solution travelling to the right for Eqs. (102) (dashed line) and (104) (solid line). $\gamma_A^2 = 0.62$, $\gamma_1^2 = 0.1$.

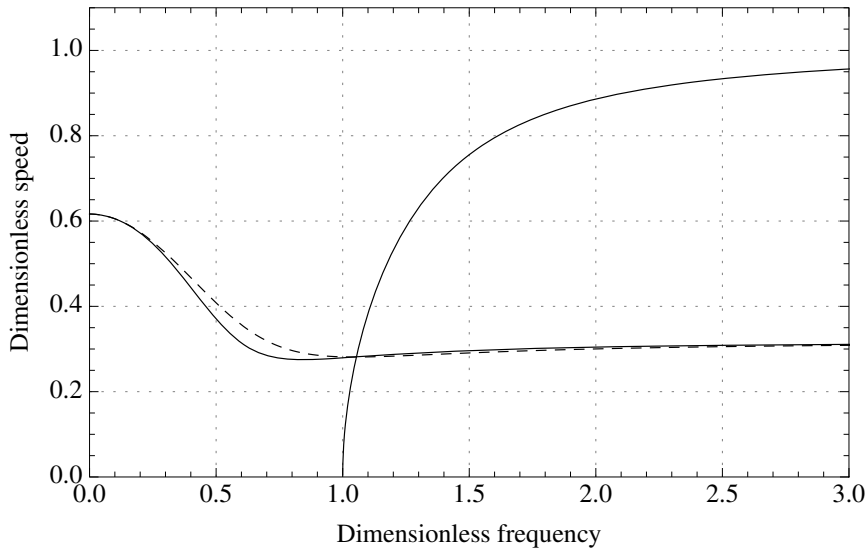

Figure 33: Group speed curves of Eqs. (50) (solid line) and (71) (dashed line). $\gamma_A^2 = 0.62$, $\gamma_1^2 = 0.1$.

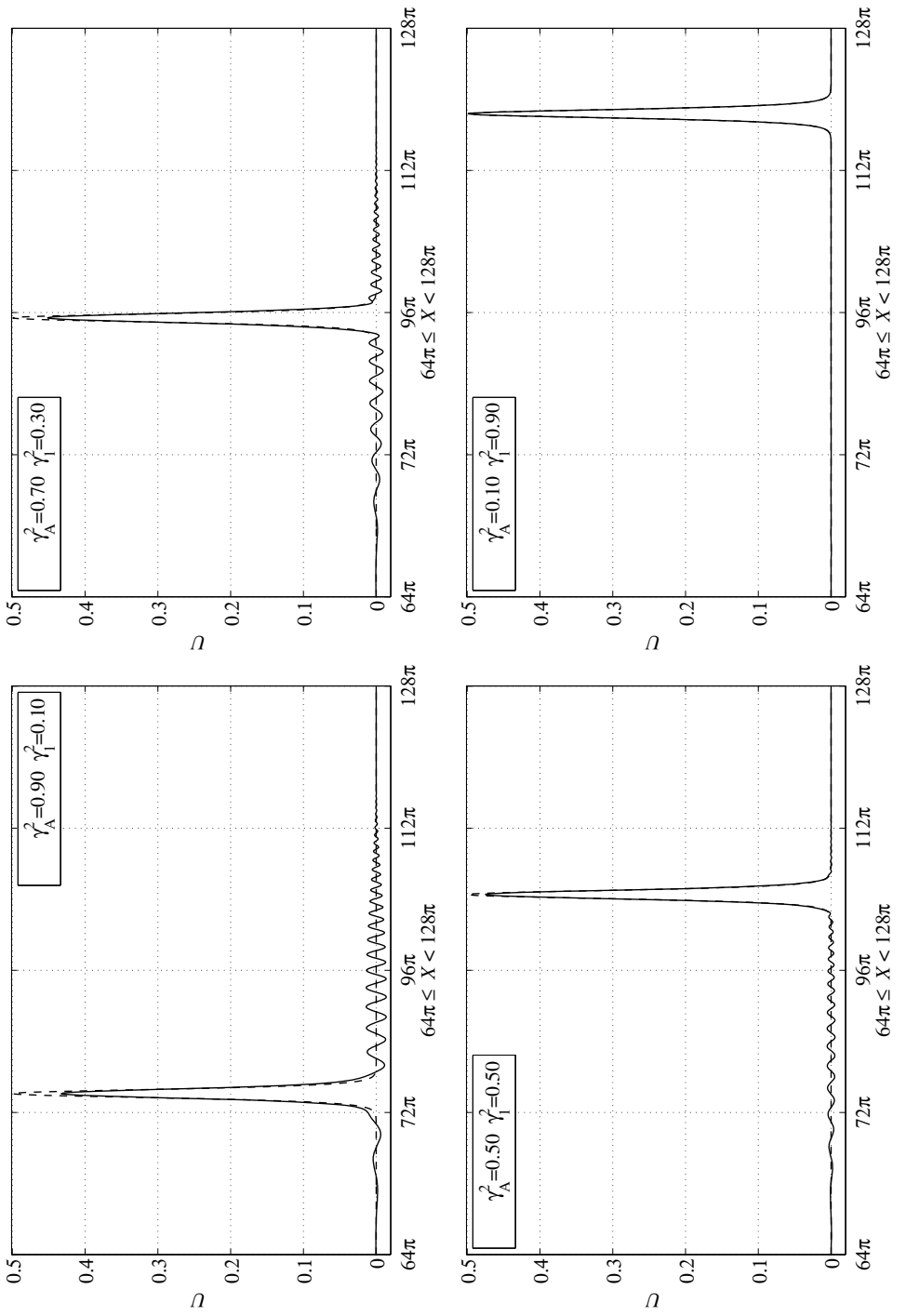

Figure 34: Right travelling solution for Eqs. (102) (dashed line) and (104) (solid line) at four different sets of parameters.

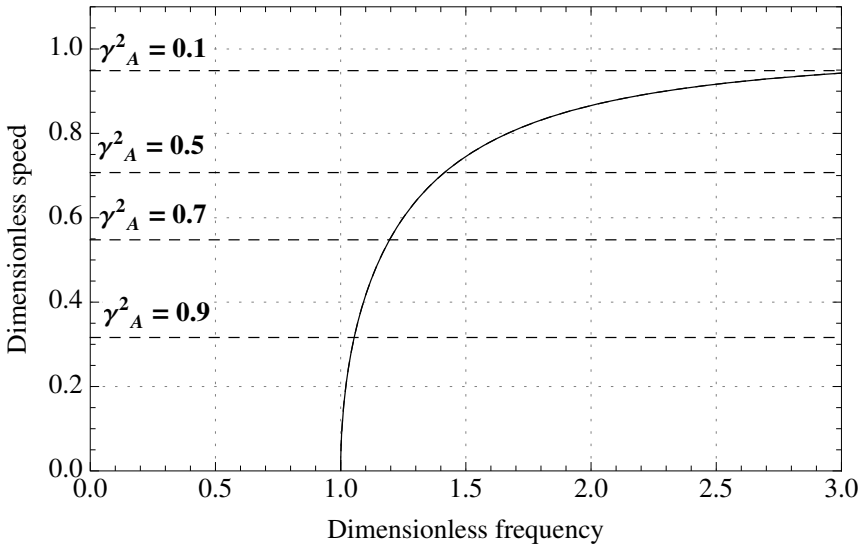

Figure 35: Group speed curves of Eq. (50) at four different sets of parameters. Here $1-\gamma_A^2=\gamma_1^2$. See explanation in text.

Appendix B: Publications

Publication I

Tanel Peets, Merle Randrüüt, and Jüri Engelbrecht.
On modelling dispersion in microstructured solids.
Wave Motion, **45**(4): 471–480, 2008.

Available online at www.sciencedirect.com
ScienceDirect
Wave Motion 45 (2008) 471–480
WAVE MOTION
www.elsevier.com/locate/wavemoti

On modelling dispersion in microstructured solids

T. Peets [*,1], M. Randrüüt [1], J. Engelbrecht

Centre for Nonlinear Studies, Institute of Cybernetics at Tallinn University of Technology, Akadeemia tee 21, 12618 Tallinn, Estonia

Received 13 April 2007; received in revised form 21 September 2007; accepted 27 September 2007
Available online 6 October 2007

Abstract

The Mindlin-type model is used for describing the longitudinal deformation waves in microstructured solids. A simplified hierarchical model is derived in one-dimensional setting which is a two-wave equation. In addition, the evolution equations (one-wave equations) are derived for both the full and simplified models. It is shown that the simplified model as well as evolution equations grasp main effects of dispersion in a wide range of physical parameters.

Keywords: Dispersion; Microstructure; Hierarchy of waves

1. Introduction

In contemporary materials science and structural mechanics much attention is given to microstructured materials possessing internal scales. Microstructured materials like alloys, crystallites, ceramics, functionally graded materials, etc have gained wide application in modern technology because combining the mechanical properties of different constituencies as in functionally graded materials or composites yields better (optimal) properties of solids. Very often they are used in severe loading conditions including impact, which means generation of stress/deformation waves. The modelling of wave propagation in such materials should be able to account for various scales of microstructure. The scale dependence involves dispersive effects and if in addition the material behaves nonlinearly then dispersive and nonlinear effects may be balanced. As widely known, in this case solitary waves may emerge as a result of such a balance.

Clearly the classical theory of continuous media is not able to describe the influence of microstructure which is needed for explain dispersive and dissipative effects. There are many studies in this field, starting from the papers of Mindlin [1] and Eringen [2] several decades ago. Now we have a solid theoretical background, see for example [3,4], but another problem has arisen: the governing equations tend to be rather complicated and the number of material parameters needed to describe the stress field, is rather high. Therefore there is an

* Corresponding author. Tel.: +372 6204169; fax: +372 6204151.
E-mail addresses: tanelp@cens.ioc.ee (T. Peets), merler@cens.ioc.ee (M. Randrüüt), je@ioc.ee (J. Engelbrecht).
[1] These authors contributed equally to this work.

0165-2125/$ - see front matter
doi:10.1016/j.wavemoti.2007.09.006

urgent need to find simplified governing equations but the physical effects should still be described with the needed accuracy.

The problem is not only in the mathematical complexity of governing equations but also in the number of waves. If in the linear theory, for example, longitudinal and shear waves can be easily separated then in the nonlinear theory the coupling can affect both waves considerably. In a general case of a complicated system of equations the main question is to understand to which wave which physical effects are related both quantitatively and qualitatively.

One of the possibilities to overcome such difficulties in contemporary mathematical physics is to introduce the notion of evolution equations governing just one single wave. Physically it means the separation (if possible) of a multi-wave process into separate waves. The waves are then governed by the so-called evolution equations every one of which describe the distortion of a single wave along a properly chosen characteristics (ray).

In this paper the attention is focused to the analysis of dispersion described by Mindlin-type models [1]. Engelbrecht et al. [5,6] have derived the one-dimensional mathematical model for longitudinal waves in microstructured materials. Based on the separation of macro- and microstructure of a material, this model is characterised by a clear physical structure of the governing equation. The analysis of the full-dispersion relation of this model compared with others is briefly presented in [5] (see also references therein). Our question here is the following: if we use asymptotic methods to simplify the model then can we describe still the physics with acceptable accuracy? We shall use two asymptotic approaches: (i) the slaving principle [7] in order to get a hierarchical asymptotic Whitham-type model from the basic one and (ii) the perturbative reduction method [8,9] in order to get evolution equations. Although nonlinearity is an important factor, here we deal only with dispersive effects and nonlinear waves will be analysed in our further publications.

The paper is organized as follows: the basic model following [5,6] is presented in Section 2. In Section 3, the asymptotic models are derived following two approaches resulting in a hierarchical simplified equation and in evolution equations. Section 4 is devoted to the dispersion analysis of the basic and the simplified models. In Section 5, final remarks are presented. It has been shown that the simplified model as well as evolution equations grasp main effects of dispersion in a wide range of physical parameters.

2. Basic model

The basic model is that of Mindlin [1] and we follow the presentation of that in [5,6]. The main idea is to distinguish between macro- and microdisplacements $u_i(x_i,t)$ and $u'_j(x'_i,t)$, respectively. Assuming that microdisplacement is defined in coordinates x'_k moving with microvolume, we define

$$u'_j = x'_k \varphi_{kj}(x_i,t), \tag{1}$$

where φ_{kj} is an arbitrary function. It is clear that actually it is microdeformation while

$$\partial u'_j/\partial x'_i = \partial'_i u'_j = \varphi_{ij}. \tag{2}$$

Further we consider the simplest 1D case and drop the indices i and j.

Now the fundamental balance laws can be formulated separately for macroscopic and microscopic scales. Introducing the Lagrangian $L = K - W$, formed from the kinetic and potential energies

$$\begin{cases} K = \frac{1}{2}\rho u_t^2 + \frac{1}{2} I \varphi_t^2 \\ W = W(u_x, \varphi, \varphi_x), \end{cases} \tag{3}$$

where ρ and I denote the macroscopic density and the microinertia, respectively, we can derive the corresponding Euler–Lagrange equations:

$$\begin{cases} \left(\frac{\partial L}{\partial u_t}\right)_t + \left(\frac{\partial L}{\partial u_x}\right)_x - \left(\frac{\partial L}{\partial u}\right) = 0 \\ \left(\frac{\partial L}{\partial \varphi_t}\right)_t + \left(\frac{\partial L}{\partial \varphi_x}\right)_x - \left(\frac{\partial L}{\partial \varphi}\right) = 0. \end{cases} \tag{4}$$

Here and further, the indices x and t denote differentiation.

The partial derivatives

$$\sigma = \partial W/\partial u_x, \quad \eta = \partial W/\partial \varphi_x, \quad F = \partial W/\partial \varphi \tag{5}$$

are recognized as the macrostress, the microstress and the interactive force, respectively.

The equations of motion are now

$$\rho u_{tt} = \sigma_x, \quad I\varphi_{tt} = \eta_x - F. \tag{6}$$

The simplest potential energy function describing the influence of a microstructure is a quadratic function

$$W = \frac{1}{2}au_x^2 + A\varphi u_x + \frac{1}{2}B\varphi^2 + \frac{1}{2}C\varphi_x^2, \tag{7}$$

where a, A, B, C denote material constants. Introducing Eq. (7) into Eq. (5) we get finally

$$\begin{cases} \rho u_{tt} = au_{xx} + A\varphi_x \\ I\varphi_{tt} = C\varphi_{xx} - Au_x - B\varphi. \end{cases} \tag{8}$$

This is the governing system of two second-order equations that can also be represented in the form of one fourth-order equation

$$u_{tt} = (c_0^2 - c_A^2)u_{xx} - p^2(u_{tt} - c_0^2 u_{xx})_{tt} + p^2 c_1^2 (u_{tt} - c_0^2 u_{xx})_{xx}, \tag{9}$$

where material parameters

$$c_0^2 = a/\rho, \quad c_1^2 = C/I, \quad c_A^2 = A^2/\rho B, \quad p^2 = I/B \tag{10}$$

are introduced. The parameters c_0, c_1, c_A are velocities while p is a time parameter. This is the basic linear equation governing 1D longitudinal waves in microstructured solids.

3. Approximations

3.1. Slaving principle

This idea (see [7]) is used in [5,9] for deriving a hierarchical asymptotic model starting from Eq. (9). It is supposed that the inherent length-scale l is small compared with the wavelength L of the excitation. The following dimensionless variables and parameters are introduced

$$U = u/U_0, \quad X = x/L, \quad T = c_0 t/L, \quad \delta = (l/L)^2, \quad \varepsilon = U_0/L, \tag{11}$$

where U_0 is the amplitude of the excitation. In addition, it is assumed that $I = \rho l^2 I^*$ and $C = l^2 C^*$, where I^* is dimensionless and C^* has the dimension of stress.

Next, the system Eq. (8) is rewritten in its dimensionless form and the slaving principle [7] is applied. It is supposed that

$$\varphi = \varphi_0 + \delta\varphi_1 + \delta^2\varphi_2 + \cdots. \tag{12}$$

The dimensionless form of Eq. (8b) yields

$$\varphi = -\varepsilon\frac{A}{B}U_X - \frac{\delta}{B}(aI^*\varphi_{TT} - C^*\varphi_{XX}) \tag{13}$$

from which the successive terms

$$\varphi_0 = -\varepsilon\frac{A}{B}U_X, \quad \varphi_1 = \varepsilon\frac{A}{B^2}(aI^*U_{XTT} - C^*U_{XXX}), \ldots \tag{14}$$

of the expansion Eq. (12) are obtained. Inserting them into Eq. (8a) in its dimensionless form, we finally get

$$U_{TT} = \left(1 - \frac{c_A^2}{c_0^2}\right)U_{XX} + \frac{c_A^2}{c_B^2}\left(U_{TT} - \frac{c_1^2}{c_0^2}U_{XX}\right)_{XX}, \tag{15}$$

where $c_B^2 = L^2/p^2 = BL^2/I$. Note that c_B involves the scales L and l and c_A includes the interaction effects through the parameter A. Eq. (15) is valid up to O(δ) because higher order terms are neglected. In addition, in general $\varepsilon \gg \delta^2$.

Now it is possible to restore the dimensions in order to compare the result with Eq. (9). Eq. (15) yields

$$u_{tt} = (c_0^2 - c_A^2)u_{xx} + p^2 c_A^2 (u_{tt} - c_1^2 u_{xx})_{xx}. \tag{16}$$

This is an example of the Whitham-type [10] hierarchical equation.

The dimensionless form of the basic linear Eq. (9) is

$$U_{TT} = \left(1 - \frac{c_A^2}{c_0^2}\right) U_{XX} - \frac{c_0^2}{c_A^2}\delta\beta U_{TTTT} + \left(\frac{c_0^2}{c_A^2} + \frac{c_1^2}{c_A^2}\right)\delta\beta U_{XXTT} - \frac{c_1^2}{c_A^2}\delta\beta U_{XXXX}, \tag{17}$$

where $\delta\beta = c_A^2/c_B^2$.

3.2. Evolution equations

Another idea to simplify the model is to use instead of the two-wave equation (16) an evolution equation that describes just one wave [8,9].

Here we follow [9] and apply the asymptotic (reductive perturbation) method. We can represent Eq. (15) in the matrix form

$$I\frac{\partial \mathbf{V}}{\partial T} + \widetilde{A}\frac{\partial \mathbf{V}}{\partial X} + \widetilde{B}\frac{\partial^3 \mathbf{V}}{\partial T \partial X^2} + \widetilde{C}\frac{\partial^3 \mathbf{V}}{\partial X^3} = 0, \tag{18}$$

where

$$\mathbf{V} = \begin{pmatrix} \partial U/\partial T \\ \partial U/\partial X \end{pmatrix} \tag{19}$$

and $I, \widetilde{A}, \widetilde{B}$ and $\widetilde{C}$ are following matrices

$$I = \begin{pmatrix} 1 & 0 \\ 0 & 1 \end{pmatrix}, \qquad \widetilde{A} = \begin{pmatrix} 0 & -(1-n^2) \\ -1 & 0 \end{pmatrix},$$
$$\widetilde{B} = \begin{pmatrix} -\delta\beta & 0 \\ 0 & -1 \end{pmatrix}, \qquad \widetilde{C} = \begin{pmatrix} 0 & \delta\beta m^2 \\ 1 & 0 \end{pmatrix},$$

where

$$n^2 = c_A^2/c_0^2 \neq 1, \qquad m^2 = c_1^2/c_0^2. \tag{20}$$

It is possible to develop vector $\mathbf{V}$ into the power series in a small parameter

$$\mathbf{V} = \mathbf{V}_0 + \varepsilon\mathbf{V}_1 + \varepsilon^2\mathbf{V}_2 + \cdots = \sum_{i=0} \varepsilon^i \mathbf{V}_i. \tag{21}$$

The space-space transformation is used:

$$\begin{cases} \xi = cT - X \\ \tau = \varepsilon X, \end{cases} \tag{22}$$

i.e.

$$\{X, T\} \rightarrow \{\xi, \tau\}, \tag{23}$$

where $c = \left(1 - \frac{A^2}{aB}\right)^{1/2} = \left(1 - \frac{c_A^2}{c_0^2}\right)^{1/2}$.

According to the asymptotic method [9] we get the sequence of equations of various powers in ε. Assuming that ε and δ are small parameters of the same order, we get finally the approximate linear evolution equation in the form

$$\frac{\partial \alpha}{\partial \tau} + \frac{\delta(\gamma - \beta c^2)}{2\varepsilon c^2} \frac{\partial^3 \alpha}{\partial \xi^3} = 0, \tag{24}$$

where $\beta = \frac{A^2 I^*}{B^2}, \gamma = \frac{A^2 C^*}{aB^2}$ and $\alpha = \frac{\partial U}{\partial T} = -c\frac{\partial U}{\partial X}$ is the unknown amplitude factor.

Similarly, applying the asymptotic method [9] for the basic linear Eq. (17) we first represent it in the matrix form

$$I\frac{\partial \mathbf{V}}{\partial T} + \widetilde{A}\frac{\partial \mathbf{V}}{\partial X} + \widetilde{D}\frac{\partial^3 \mathbf{V}}{\partial T^3} + \widetilde{E}\frac{\partial^3 \mathbf{V}}{\partial T \partial X^2} + \widetilde{F}\frac{\partial^3 \mathbf{V}}{\partial X^3} = 0, \tag{25}$$

where $I, \widetilde{A}, \widetilde{D}, \widetilde{E}$ and $\widetilde{F}$ are following matrices

$$I = \begin{pmatrix} 1 & 0 \\ 0 & 1 \end{pmatrix}, \quad \widetilde{A} = \begin{pmatrix} 0 & -(1-n^2) \\ -1 & 0 \end{pmatrix},$$
$$\widetilde{D} = \begin{pmatrix} \frac{1}{n^2}\delta\beta & 0 \\ 0 & 0 \end{pmatrix}, \quad \widetilde{E} = \begin{pmatrix} -\left(\frac{1}{n^2}\delta\beta + n_1^2\delta\beta\right) & 0 \\ 0 & -1 \end{pmatrix},$$
$$\widetilde{F} = \begin{pmatrix} 0 & n_1^2\delta\beta \\ 1 & 0 \end{pmatrix},$$

where

$$n_1^2 = c_1^2/c_A^2, \tag{26}$$

and write the evolution equation in the form

$$\frac{\partial \alpha}{\partial \tau} + \frac{\delta(\gamma - \beta c^2)}{2\varepsilon c^2} \frac{\partial^3 \alpha}{\partial \xi^3} = 0. \tag{27}$$

This means, that the approximate Eq. (15) and the basic Eq. (17) yield the evolution equations in the same form, see Eqs. (24) and (27). Consequently, using the idea of evolution equations there is no difference whether we begin the derivation from the basic Eq. (17) with the addition term U_{TTTT} or from the approximate Eq. (15) with terms U_{XXTT} and U_{XXXX}. However, note that the parameters of Eqs. (15) and (16) are different.

The character of dispersion in the case of microstructured materials is analysed in [5] on the basis of the approximate Eq. (15). It has been shown that both of the effects – inertia of the microstructure (described by term U_{TTXX}) and elasticity of the microstructure (described by term U_{XXXX}) have influence on dispersive relations and corresponding dispersion curves. If only inertia of the microstructure (term U_{TTXX}) is taken into account then the dispersion curve is concave, if only elasticity of the microstructure (term U_{XXXX}) is taken into account then the dispersion curve is convex. With both terms (double dispersion) the curve tends from one asymptote to another.

In the case of the evolution equation these two effects are described by a single term (term $\alpha_{\xi\xi\xi}$) but the sign of this term (the sign of its coefficient) depends on the ratio of the double dispersion effects.

It is possible to conclude that in case of $\gamma > \beta c^2$ (elastic effects prevailing) the dispersion curve is convex and in case of $\gamma < \beta c^2$ (inertial effects prevailing) the dispersion curve is concave. So the evolution equation keeps the main characteristics of the process. In case of $\gamma - \beta c^2 = 0$ there is no microstructure and the dispersion curve is linear, as expected.

4. Dispersion analysis

4.1. Dispersion relations

Internal scales of microstructured solids lead to dispersive effects. This is also quite clear from the governing equations derived in previous sections. The presence of higher-order derivatives in the governing equations indicates dispersion.

In order to derive dispersion relations, we assume the solution in the form of a wave

$$u(x,t) = \hat{u}\exp[\mathrm{i}(kx - \omega t)], \tag{28}$$

with wave number k, frequency ω and amplitude û.

Introducing Eq. (28) into Eq. (9) the dispersion relation

$$\omega^2 = (c_0^2 - c_A^2)k^2 + p^2(\omega^2 - c_0^2k^2)(\omega^2 - c_1^2k^2) \tag{29}$$

is obtained.The parameters involved are a time constant p and three characteristic velocities c_0,c_1,c_A. Instead of c_A the velocity $c_R^2 = c_0^2 - c_A^2$ could be introduced as a parameter, since it has an obvious meaning for the given wave process. Waves of very low frequencies ($\omega \ll p^{-1}$) propagate at the velocity c_R. The auxiliary velocity c_A does not occur explicitly as a limit velocity. The phase speed of the wave is defined as $c_p = \omega/k$ and can be obtained directly from the dispersion relation.

In order to reduce the number of independent variables we normalise the wave number, the frequency and the relative propagation speeds defining

$$\kappa = pc_0k, \quad \eta = p\omega, \quad n = c_A/c_0, \quad m = c_1/c_0. \tag{30}$$

Using these new quantities the full-dispersion relation (29) assumes the form

$$\eta^2 = (1 - n^2)\kappa^2 + (\eta^2 - \kappa^2)(\eta^2 - m^2\kappa^2). \tag{31}$$

The dimensionless phase speed is defined as $\gamma_p = c_p/c_0 = \eta/\kappa$.

For convenience we also use the parameter $c = c_R/c_0 = (1 - n^2)^{1/2}$ (see Eq. (22)).

In the same way, the approximate differential equation (16) yields the dispersion relation

$$\omega^2 = (c_0^2 - c_A^2) - p^2c_A^2(\omega^2 - c_1^2k^2)k^2. \tag{32}$$

Introducing Eq. (30) into Eq. (32) we obtain

$$\eta^2 = (1 - n^2)\kappa^2 - n^2(\eta^2 - m^2\kappa^2)\kappa^2. \tag{33}$$

4.2. The range of parameters

The numerical simulation is done with the dimensionless Eqs. (31) and (33) and with the dimensionless parameters n and m. Since $c^2 = 1 - n^2$ then $n < 1$, which makes physically sense because the velocity c_0 is interpreted as the maximum possible velocity. Therefore also $m < 1$.

We also assume that $n \neq m \neq 0$. If $n = 0$ then also $A = 0$ and then the governing Eq. (8) will have the form where there is no interaction between the macro- and the microstructure.

Therefore we will consider the parameters in the following ranges

$$0 < n < 1, \qquad 0 < m < 1. \tag{34}$$

4.3. The results

The characteristic dispersion curves are shown in Fig. 1 from which the following can be concluded. The full-dispersion relation (31), which is represented by the continuous lines, represents two branches which in general are distinct. The upper, or 'optical' branch starts at $\eta = 1$ with zero slope and in the short wave limit the branch asymptotically approaches to the line $\eta = \kappa$. Lower, or 'acoustical', branch starts at the origin with a slope $\eta = c\kappa$ and in the short wave limit the branch approaches to the asymptotic line $\eta = m\kappa$. Here the dotted lines show asymptotic values.

The approximate dispersion relation (33), which is represented by the dashed line, provides an approximation of the acoustical branch only.

It is clear that the dispersion relations (31) and (33) differ and our intention is to analyse the ranges of parameters where the results coincide. This is dictated by the values of parameters n and m. Fig. 2 illustrates the ranges of the parameters where the values obtained from the both relations agree within 5% error (the area between the dashed lines) and within 10% error (the area between the continuous lines) at the point $\kappa = 1.5$.

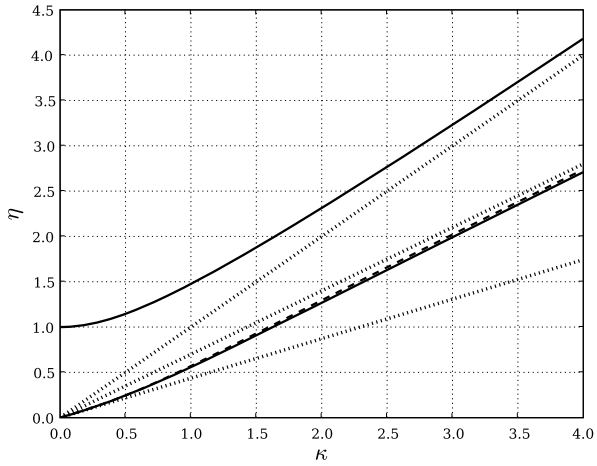

Fig. 1. The characteristic dispersion curves ($n = 0.9$, $m = 0.7$). See explanation in the text.

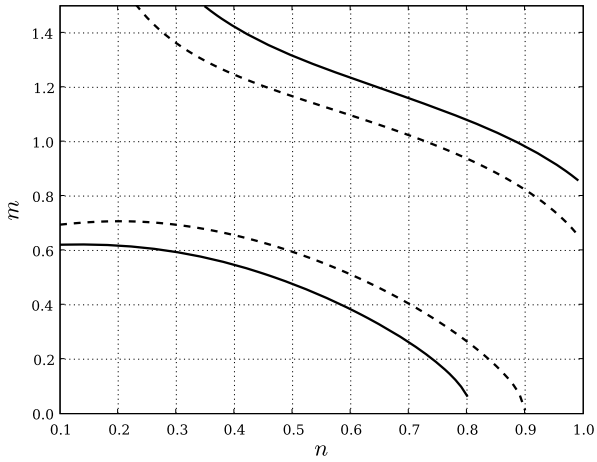

Fig. 2. The ranges of parameters. See explanation in the text.

The ranges for other values of κ behave similarly , only for $\kappa > 1.5$ the area of good agreement is narrower and for $\kappa < 1.5$ the area is wider.

Fig. 3 shows an example where the approximate dispersion relation (33) agrees very well with the full-dispersion relation (31). In Fig. 3a, $c_R < c_1$ and in Fig. 3b, $c_R > c_1$. The continuous lines correspond to the full and the dashed lines to the approximate dispersion relation.

Figs. 4 and 5 are examples of the combination of the parameters where the approximate Eq. (33) and the full-dispersion relation (31) do not coincide well. Fig. 4 is an example of $m < 1$, but not in a good approximation range (see Fig. 2). The continuous line corresponds again to the full and the dashed line to the approximate dispersion relation.

This result can be understood by examining the approximate dispersion relation (33). The strength of the second term in the approximate dispersion relation depends on the parameter n and if parameter n is close to 0 then the influence of the second term is diminished.

Fig. 5 is an example of the situation when c_1 becomes larger than c_0 ($m > 1$). Now the behaviour of the dispersion curves is changed. The full-dispersion relation (31) (represented by the continuous lines) still represents

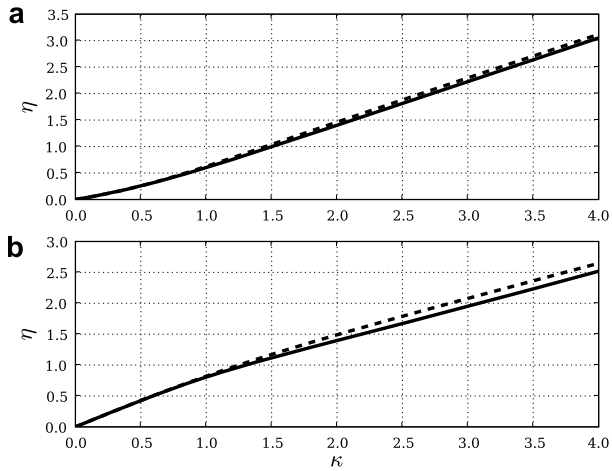

Fig. 3. The behaviour of the acoustic branches (a) $n = 0.9$, $m = 0.8$, (b) $n = 0.5$, $m = 0.6$. See explanation in the text.

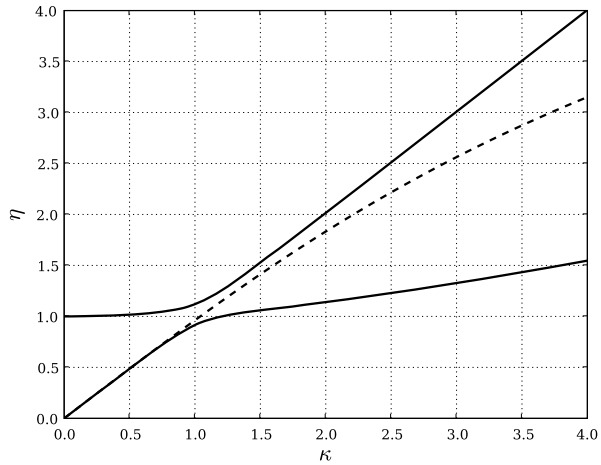

Fig. 4. The behaviour of the dispersion curves ($n = 0.2$, $m = 0.3$). See explanation in the text.

two branches but now the upper branch approaches to the asymptotic line $\eta = m\kappa$. Lower branch starts with a slope $\eta = c\kappa$ and in the short wave limit it approaches to the asymptotic line $\eta = \kappa$.

The approximate relation (33) (represented by the dashed line) also starts with a slope $\eta = c\kappa$, but in the short wave limit it approaches the asymptotic line $\eta = m\kappa$ and does not approach the acoustical branch.

5. Final remarks

Mindlin [1] has derived the dispersion relations for long wave-length (and very long wave-length) approximation and shown a similarity of dispersive effects with those in plates. While Mindlin [1] has used a concept of unit cells embedded in a surrounding medium, then many materials, especially composites, have clearly a defined layered structure. Sun et al. [12,13] have shown that an effective stiffness theory can be derived for describing waves in layered media. Actually, their result is a continuum [13] that bears clear resemblance to Mindlin's material, especially in a 1D case. It has also been shown that gradient elasticity theories [14] need both elastic and inertial effects to be taken into account. This shows again validity of the Mindlin idea. In addi-

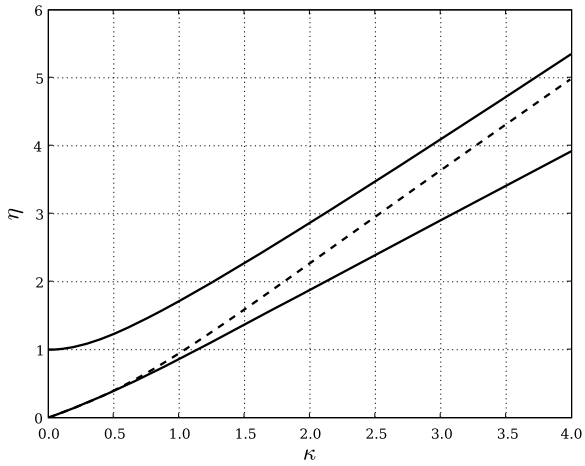

Fig. 5. The behaviour of the dispersion curves ($n = 0.7$, $m = 1.3$). See explanation in the text.

tion, the functionally graded materials (FGMs) which are widely used in contemporary technology [15], can be described by the Mindlin theory and the corresponding models presented above. The straight-forward numerical calculation of wave fields in FGMs [16] has shown explicitly the influence of microstructure for velocities as predicted by Mindlin-type models.

Here, we have derived hierarchical Mindlin-type models (Eqs. (9) and (16)) which describe well dispersive effects. In the wide range of parameters (see Fig. 2), the hierarchical asymptotic model is sufficient for grasping the real behaviour. The hierarchical model itself is certainly simpler and well-grounded physically. In addition, its similarity to discrete models [11] permits to bridge both types (continuous and discrete) models although some deeper analysis is needed in order to clarify the relations of model parameters. The full model (Eq. (9)) and its approximation (Eq. (16)) yield the same type of the evolution equation (cf. Eqs. (24) and (27)). This is not surprising because the proper scaling should lead to a result where the leading properties are accounted for. Even more, the evolution equation obtained in such a way shows clearly that for a homogeneous material (no microstructure) the dispersive effects disappear (here $\gamma = \beta c^2$, i.e. $c_1 = c$). In addition the convexity or concavity of the dispersion curve derived for cases $\gamma \neq \beta c^2$ depends clearly upon the influence of the material parameters. When in the microstructure elastic effects are stronger then $\gamma > \beta c^2$ and the dispersion curve is convex. When however the inertial effects in the microstructure are prevailing then $\gamma < \beta c^2$ and the dispersion curve is concave. The same effect follows from the analysis of full models.

This result is important even qualitatively for Nondestructive Testing (NDT). The concavity/convexity of the dispersion curve shows explicitly the influence of the basic material properties.

The main results of this paper shows that the asymptotic models, both hierarchical two-wave equation (15) (or (17)) and evolution equation (24) (or (27)) are able to grasp dispersive effects in microstructured solids within the wide range of parameters. As said in Section 1, the further studies should introduce nonlinearities like Pastrone [17].

Acknowledgements

Support of the Estonian Science Foundation under Contract Nos. 7037 (T.P.) and 7035 (M.R.) is gratefully acknowledged. The authors acknowledge the referees' valuable comments.

References

[1] R.D. Mindlin, Microstructure in linear elasticity, Arch. Rat. Mech. Anal. 16 (1964) 51–78.
[2] A.C. Eringen, Linear theory of micropolar elasticity, J. Math. Mech. 15 (1966) 909–923.

[3] G.A. Maugin, Material Inhomogeneities in Elasticity, Chapman and Hall, London, 1993.
[4] A.C. Eringen, Microcontinuum Field Theories. I. Foundations and Solids, Springer, New York, 1999.
[5] J. Engelbrecht, A. Berezovski, F. Pastrone, M. Braun, Waves in microstructured materials and dispersion, Philos. Mag. 85 (33–35) (2005) 4127–4141.
[6] J. Engelbrecht, F. Pastrone, M. Braun, A. Berezovski, Hierarchies of waves in nonclassical materials, in: P.-P. Delsanto (Ed.), The Universality of Nonclassical Nonlinearity: Applications to Non-Destructive Evalutations and Ultrasonics, Springer, Berlin, 2006, pp. 29–48.
[7] P.L. Christiansen, V. Muto, S. Rionero, Solitary wave solution to a system of Boussinesq-like equations, Chaos Solitons Fractals 2 (1992) 45–50.
[8] T. Taniuti, K. Nishihara, Nonlinear Waves, Pitman, London, 1983, in Japanese, 1977.
[9] J. Engelbrecht, Nonlinear Wave Processes of Deformation in Solids, Pitman, Boston, London, Melbourne, 1983.
[10] G.B. Whitham, Linear and Nonlinear Waves, J. Wiley, New York, 1974.
[11] G.A. Maugin, Nonlinear Waves in Elastic Crystals, Oxford University Press, Oxford, 1999.
[12] C.-T. Sun, J.D. Achenbach, G. Herrmann, Time-harmonic waves in a stratified medium propagating in the direction of the layering, J. Appl. Mech. Trans. ASME 35 (1968) 408–411, June.
[13] C.-T. Sun, J.D. Achenbach, G. Herrmann, Continuum theory for a laminated medium, J. Appl. Mech. Trans. ASME 35 (3) (1968) 467–475.
[14] H. Askes, E.C. Aifantis, Gradient elasticity theories in statics and dynamics – a unification of approaches, Int. J. Fract. 139 (2006) 297–304.
[15] S. Suresh, A. Mortensen, Fundamentals of Functionally Graded Materials, The Institute of materials, London, 1998.
[16] A. Berezovski, J. Engelbrecht, G.A. Maugin, Numerical simulation of two-dimensional wave propagation in functionally graded materials, Eur. J. Mech. A-Solids 22 (2003) 257–265.
[17] F. Pastrone, Wave propagation in microstructured solids, Math. Mech. Solids 10 (2005) 349–357.

Publication II

Tanel Peets and K. Tamm.
Dispersion analysis of wave motion in microstructured solids.
In T.-T. Wu and C.-C. Ma, editors, *IUTAM Symposium on Recent Advances of Acoustic Waves in Solids: Proceedings, Taipei, Taiwan, May 25–28, 2009*, volume 26 of IUTAM Bookseries, pages 349–354. Springer, Dordrecht, 2010.

Dispersion Analysis of Wave Motion in Microstructured Solids

Tanel Peets and Kert Tamm

Centre for Nonlinear Studies, Institute of Cybernetics at Tallinn University of Technology, Akadeemia tee 21, 12618 Tallinn, Estonia

tanelp@cens.ioc.ee

Abstract. The Mindlin-type model is used for describing longitudinal waves in microstructured solids. This model involves explicitly the internal parameters and therefore tends to be rather complicated. An hierarchical approximation is derived, which is able to grasp the main effects of dispersion with wide variety of parameters. Attention is paid to the internal degrees of freedom of the microstructure and their influence on the dispersion effects. It is shown how the internal degrees of freedom can change the effects of dispersion.

1. Introduction

It is well recognized by modern science, that matter is not continuous but has an internal structure. Clearly this microstructure plays a significant role when modelling wave propagation – waves that have a wavelength shorter than a certain threshold value, "feel" the microstructure.

There are two approaches in modelling the microstructure - one group of models are based on lattice theory [1-3], another on continuum theory [4-6].

In the discrete approach the volume elements of the matter are treated as point masses with a defined distribution and some interaction between the discrete masses. The governing equations are then deduced following the Newton's law.

In the microcontinuum theory, the macro- and microstructure of the continua are separated. Then the conservation laws for both structures should either be separately formulated [4,5], or the microstructural quantities (cells) are separately taken into account in one set of conservation laws. Engelbrecht *et al.* [6] have derived the one-dimensional model for longitudinal waves in microstructured materials based on Mindlin model [5]. This model will be the basis of our analysis. These governing equations of wave motion tend to be rather complicated and therefore there is a need for simplification. A slaving principle is used in order to derive a hierarchical asymptotic Whitham-type model.

T.-T. Wu and C.-C. Ma (eds.), *IUTAM Symposium on Recent Advances of Acoustic Waves in Solids*, IUTAM Bookseries 26, DOI 10.1007/978-90-481-9893-1_33,

An important effect caused by microstructure is dispersion. A wave packet can be viewed as a collection of harmonic waves. If such a wave travels through a microstructured material, then different harmonics "feel" the microstructure according to their wavelength and travel with different speeds. The variation of phase velocity with wavenumber is the hallmark of dispersion [7,8].

Generally if there is N particles per unit cell in discrete model, then N dispersion curves appear (3N in case of 3D model). The lower curve is called an acoustic branch, the upper curves are called optical branches and they only appear when there are at least 2 particles per unit cell. Optical branches are said to reflect the internal degrees of freedom [1,9].

Because of the inclusion of the microstructure, the dispersion curves derived from the 1D microcontinuum model, also give two distinct curves [4,6,9]. As in discrete model these curves are acoustical and optical modes where an optical modes are interpreted as internal degrees of freedom or "internal modes"[5,9]. The dispersion curve derived from the Whitham-type approximate model has only an acoustical branch. It means that the approximate model does not account directly for internal degrees of freedom. The authors have shown that this approximation is acceptable with wide variety of parameters. However the question that remains is when the internal modes can be ignored.

2. The Basic Model

The basic model is that of Mindlin [5] and we follow the presentation of its ideas in [6]. The main idea is to distinguish between macro- and microdisplacements $u_i\left(x_i,t\right)$ and $u_j'\left(x_i',t\right)$, respectively. Assuming that microdisplacement is defined in coordinates x_k', moving with a microvolume (cell), we define $u_j' = x_k'\varphi_{kj}\left(x_i,t\right)$, where φ_{kj} is an arbitrary function. It is clear that actually it is the microdeformation while $\partial u_j^{\mathrm{n}} / \partial u_i^{\mathrm{n}} = \partial_i^{\mathrm{n}} u_j^{\mathrm{n}} = \varphi_{ij}$. Further we consider the simplest 1D case and drop the indices *i* and *j*.

Now the fundamental balance laws can be formulated separately for macroscopic and microscopic scales. Introducing the Lagrangian $L = K - W$, formed from the kinetic and potential energies

$$K = \frac{1}{2}\rho u_t^2 + \frac{1}{2} I \varphi_t^2, \quad W = W(u_x, \varphi, \varphi_x), \tag{2.1}$$

where ρ and I denote the macroscopic density and the microinertia, respectively, we can use the corresponding Euler-Lagrange equations:

$$\left(\frac{\partial L}{\partial u_t}\right)_t + \left(\frac{\partial L}{\partial u_x}\right)_x - \left(\frac{\partial L}{\partial u}\right) = 0, \quad \left(\frac{\partial L}{\partial \varphi_t}\right)_t + \left(\frac{\partial L}{\partial \varphi_x}\right)_x - \left(\frac{\partial L}{\partial \varphi}\right) = 0. \tag{2.2}$$

Here and further, the indices x and t denote differentiation.

The partial derivatives

$$\sigma = \partial W / \partial u_x, \quad \eta = \partial W / \partial \varphi_x, \quad F = \partial W / \partial \varphi, \tag{2.3}$$

are recognized as the macrostress, the microstress and the interactive force, respectively.

The simplest potential energy function describing the influence of a microstructure is a quadratic function

$$W = \frac{1}{2} a u_x^2 + A \varphi u_x + \frac{1}{2} B \varphi^2 + \frac{1}{2} C \varphi_x^2, \tag{2.4}$$

where a,A,B,C denote material constants. Introducing Eq. (2.4) into Eq. (2.3) we get finally

$$\rho u_{tt} = a u_{xx} + A \varphi_x, \quad I \varphi_{tt} = C \varphi_{xx} - A u_x - B \varphi. \tag{2.5}$$

This is the governing system of two second-order equations that can also be represented in the form of one fourth-order equation

$$u_{tt} = \left(c_0^2 - c_A^2\right) u_{xx} - p^2 \left(u_{tt} - c_0^2 u_{xx}\right)_{tt} + p^2 c_1^2 \left(u_{tt} - c_0^2 u_{xx}\right)_{xx}, \tag{2.6}$$

where material parameters $c_0^2 = a / \rho, \quad c_1^2 = C / I, \quad c_A^2 = A^2 / \rho B, \quad p^2 = I / B,$ are introduced. The parameters c_0, c_1,c_A are velocities while p is a time parameter. This is the basic linear equation governing 1D longitudinal waves in microstructured solids. It has been shown by Sun *et al.* that Mindlin type model can also be used for modeling wave dispersion in layered media [10].

An approximation of Eq. (2.6) can be obtained by using the slaving principle. It is supposed that the inherent length-scale l is small compared with the wavelength L of the excitation. The following dimensionless variables and parameters are introduced $U=u/U_0$, $X=x/L$, $T=c_0t/L$, $\delta=(l/L)^2$, $\varepsilon=U_0/L$, where U_0 is the amplitude of the excitation. In addition it is assumed that $I=\rho l^2 I^*$ and $C=l^2 C^*$, where I^* is dimensionless and C^* has the dimensions of stress.

Next the system (2.5) is rewritten in its dimensionless form and the slaving principle [11] is applied. Then we get finally

$$U_{TT} = \left(1 - \frac{c_A^2}{c_0^2}\right) U_{XX} + \frac{c_A^2}{c_B^2} \left(U_{TT} - \frac{c_1^2}{c_0^2} U_{XX}\right)_{XX}, \tag{2.7}$$

where $c_B^2 = L^2/p^2 = BL^2/I$. Note that c_B involves the scales L and l and c_A includes the interaction effects through parameter A. Restoring dimensions, Eq. (2.7) yields

$$u_{tt} = \left(c_0^2 - c_A^2\right) u_{xx} + p^2 c_A^2 \left(u_{tt} - c_1^2 u_{xx}\right)_{xx}. \tag{2.8}$$

This is an example of the Whitham-type hierarchical equation.

3. Dispersion Analysis

The dispersion relations for Eqs. (2.6) and (2.8) are

$$\begin{aligned}\omega^2 &= \left(c_0^2 - c_A^2\right)k^2 + p^2\left(\omega^2 - c_0^2k^2\right)\left(\omega^2 - c_1^2k^2\right),\\ \omega^2 &= \left(c_0^2 - c_A^2\right)k^2 - p^2c_A^2\left(\omega^2 - c_1^2k^2\right)k^2.\end{aligned} \tag{3.1}$$

In order to reduce the number of independent variables, the wave number, the frequency and the propagation speeds are normalized defining $\xi = pc_0k$, $\eta = p\omega$, $\gamma_A = c_A/c_0$, $\gamma_1 = c_1/c_0$. Using these new quantities the dispersion relations (3.1) assume the forms

$$\begin{aligned}\eta^2 &= \left(1 - \gamma_A^2\right)\xi^2 + \left(\eta^2 - \xi^2\right)\left(\eta^2 - \gamma_1^2\xi^2\right),\\ \eta^2 &= \left(1 - \gamma_A^2\right)\xi^2 - \gamma_A^2\left(\eta^2 - \gamma_1^2\xi^2\right)\xi^2,\end{aligned} \tag{3.2}$$

where the parameters γ_A and γ_1 have the values $0 < \gamma_A < 1$ and $0 < \gamma_1 < 1$ respectively.

The characteristic dispersion curves are shown in Fig. 3.1. The full dispersion relation (3.2a), which is represented by the continuous line, represents two distinct branches – acoustical and optical. The acoustical branch is analogous to the case of elastic vibrations where all the cells move in unison. These are external modes. The optical branch reflects the role of the internal modes, which involve the distortion of the cells [5,9].

The optical branch is always concave, the acoustical branch can be either concave or convex or linear, which represents anomalous, normal or no dispersion respectively. This concavity and convexity of the acoustic dispersion curve shows explicitly the influence of basic material properties [12].

The full model (2.6) and approximate model (2.7) can be compared using numerical analysis. The initial value problem in dimensionless form under periodic boundary conditions is solved using the pseudospectral method [13]. The initial profile is chosen $U(X,0) = sech^2(\kappa X/2)$, where κ is the width of the profile.

Figures 3.2 and 3.3 show the results of the numerical analysis. Figure 3.2 represents the case when acoustical branch is concave (anomalous dispersion). It is clear from the numerical experiment that although there are small differences between the full model (2.6) and approximation (2.7), the approximation is able to display the main effects of dispersion i.e. the type of the dispersion.

Figure 3.3 shows a numerical experiment in case when there is no dispersion in approximate dispersion relation (3.2b) and in the acoustic branch of the full dispersion relation (3.2a). The approximate model indeed shows no dispersion effects – the initial

profile moves with constant speed and shape. The full model (2.6) however displays a small effect of dispersion, which is due to the optical bra nch or internal modes. The dispersion effects do not appear immediately, but may take some time to appear.

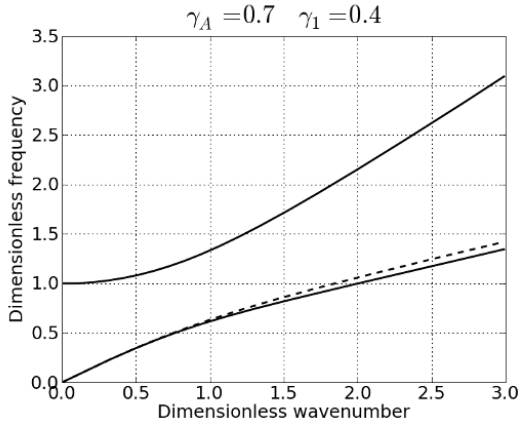

Fig. 3.1 The characteristic dispersion curves. Solid lines represent full dispersion relation, dashed line represents approximate dispersion relation.

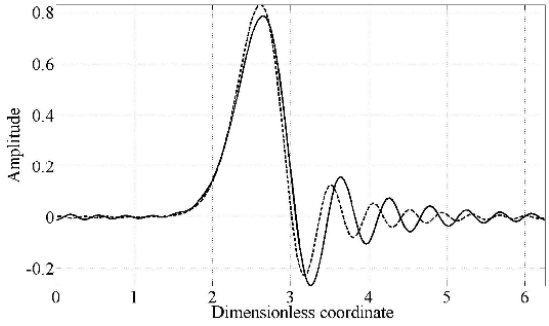

Fig. 3.2 The solutions of full model (solid line) and approximation (dashed line), in case of γ_A=0.9 and γ_1=0.7.

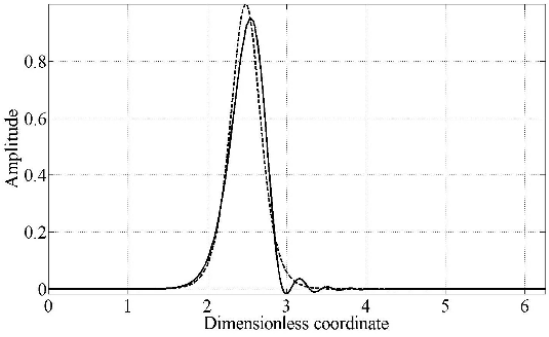

Fig. 3.3 The solutions of full model (solid line) and approximation (dashed line), in case of γ_A=0.9 and γ_1=0.7.

4. Final Remarks

The numerical analysis demonstrates that the full and approximate models give in most cases similar results. There are however conditions when approximate dispersion curve (3.2b) coincides well with the acoustic branch of the full dispersion curve (3.2a), but the numerical experiment gives different types of dispersion for the full model (2.6) and for the approximation (2.7). This is likely to be present when acoustic curve displays normal dispersion.

These effects need further investigations and will be presented in further publications.

Acknowledgements: The authors gratefully acknowledge the financial support from Estonian Science Foundation.

References

[1] Brillouin, L.: *Wave Propagation in Periodic Structures. Dover Publications*, INC, NY (1953).
[2] Metrikine, A.V., Askes, H.: One-dimensional dynamically consistent gradient elasticity models derived from a discrete microstructure. Part 1: Generic formulation. *Eur. J. Mech. A. Solids* **21** (2002) 555-572.
[3] Maugin, G.A.: *Nonlinear Waves in Elastic Crystals.* Oxford University Press (1999).
[4] Eringen, A.C.: Linear theory of micropolar elasticity. *J. Math. Mech.* **15** 909-923 (1966).
[5] Mindlin, R.D.: Microstructure in linear elasticity. *Arch. Rat. Mech. Anal.* **16** 51-78 (1964).
[6] Engelbrecht, J., Berezovski, A., Pastrone, F., Braun, M.: Waves in microstructured materials and dispersion. *Philos. Mag.* **85**(33-35) 4127-4141(2005).
[7] Nettel, S.: *Wave physics. Oscillations - Solitons - Chaos.* New York: Springer (1995).
[8] Main, I.G.: *Vibrations and Waves in Physics.* Cambridge University Press (1984).
[9] Chen, Y., Lee, J.D.: Analysis of photon dispersion relations from atomic model to continuum theory. *Nanotech* **1** 396-399 (2002).
[10] Sun, C.-T., Achenbach, J.D., Herrmann, G.: Continuum theory for a laminated medium. *J. Appl. Mech. Trans. ASME* **35**(3) 467-475 (1968).
[11] Christiansen, P.L., Muto, V., Rionero, S.: Solitary wave solution to a system of Boussinesq-like equations. *Chaos Solitons Fractals* **2** 45-50 (1992).
[12] Peets, T., Randrüüt, M., Engelbrecht, J.: On modelling dispersion in microstructured solids. *Wave Motion* **45** 471-480 (2008).
[13] Salupere, A., Tamm, K., Engelbrecht, J.: Numerical simulation of interaction of solitary deformation waves in microstructured solids. *Int. J. Non Linear Mech.* **43** 201-208 (2008).

Publication III

Arkadi Berezovski, Jüri Engelbrecht, and **Tanel Peets**.
Multiscale modelling of microstructured solids.
Mechanics Research Communications, **37** (6): 531–534, 2010.

Mechanics Research Communications 37 (2010) 531–534

Contents lists available at ScienceDirect

Mechanics Research Communications

journal homepage: www.elsevier.com/locate/mechrescom

Multiscale modeling of microstructured solids

Arkadi Berezovski*, Jüri Engelbrecht, Tanel Peets*

Centre for Nonlinear Studies, Institute of Cybernetics at Tallinn University of Technology, Akadeemia tee 21, 12618 Tallinn, Estonia

ARTICLE INFO

Article history:
Received 23 March 2010
Received in revised form 25 May 2010
Available online 3 August 2010

Keywords:
Wave propagation
Microstructure
Wave hierarchy
Dispersion

ABSTRACT

Wave propagation in solids with microstructures characterized by different internal length scales are considered in the framework of a Mindlin-type microstructure model. The corresponding dispersion relations display essential differences for medium-range wavelengths.

1. Introduction

Wave propagation in microstructured materials is strongly affected by processes at internal space scales (Kunin, 1982, 1983; Capriz, 1989; Erofeeyev, 2003). Usually, only one length scale is introduced in models of microstructured solids (Mindlin, 1964; Eringen and Suhubi, 1964; Santosa and Symes, 1991; Chen and Fish, 2001; Metrikine and Askes, 2002; Engelbrecht et al., 2005; Metrikine, 2006). However, the complexity of a microstructure must sometimes be characterized by multiple scales (Engelbrecht et al., 2006). In this paper, several possible mathematical models describing two-scale microstructures are described and their dispersive properties are analyzed in 1D settings.

One of the possible models to describe the microstructure has been proposed by Mindlin (1964) and later generalized in Engelbrecht et al. (2005). The main idea of this model is to formulate balance laws separately for macroscopic and microscopic scales. In the one-dimensional case, the derivation of governing equations can be briefly described as follows. In terms of displacement u and microdeformation φ, the simplest free energy function W is a quadratic function

$$W = \frac{\rho_0 c^2}{2} u_x^2 + A\varphi u_x + \frac{1}{2} B\varphi^2 + \frac{1}{2} C\varphi_x^2, \tag{1}$$

where ρ_0 is the density and c is the wave velocity in the macrostructure; A,B, and C are additional material parameters. The physical meaning of these parameters is related to coupling effects (A), microstress modulus (C), and the interactive force (B), see below the corresponding expressions (cf. also Mindlin, 1964). Here and further, the indices denote differentiation with respect to indicated variables.

The balance laws can be derived from the Euler–Lagrange equations (Engelbrecht et al., 1999):

$$\rho_0 u_{tt} = \sigma_x, \qquad I\varphi_{tt} = -\eta_x + \tau. \tag{2}$$

Here I is an internal inertia measure for the microstructure, σ and η are macro- and microstress, respectively, τ is the interactive internal force.

The stresses (note that σ is the Cauchy stress) are determined (cf. Mindlin, 1964; Engelbrecht et al., 2005) by

$$\sigma = \frac{\partial W}{\partial u_x} = \rho_0 c^2 u_x + A\varphi, \qquad \eta = -\frac{\partial W}{\partial \varphi_x} = -C\varphi_x, \tag{3}$$

while the interactive internal force τ is

$$\tau = -\frac{\partial W}{\partial \varphi} = -Au_x - B\varphi. \tag{4}$$

As a result, equations of motion (2) can be represented in the form

$$\rho_0 u_{tt} = \rho_0 c^2 u_{xx} + A\varphi_x, \qquad I\varphi_{tt} = C\varphi_{xx} - Au_x - B\varphi, \tag{5}$$

which must be solved with proper initial and boundary conditions.

It must be stressed that the same result can be achieved by using the formalism of internal variables. Indeed, by introducing thermodynamically consistent dual internal variables (Ván et al., 2008), the same governing equations (5) can be derived (Berezovski et al., 2009). The system of equations (5) actually describes the hierarchy of waves, because by using a slaving principle (Engelbrecht et al., 2005) it is possible to rewrite this system as the higher order

* Corresponding authors.
E-mail address: Arkadi.Berezovski@cs.ioc.ee (A. Berezovski).

0093-6413/$ – see front matter © 2010 Elsevier Ltd. All rights reserved.
doi:10.1016/j.mechrescom.2010.07.020

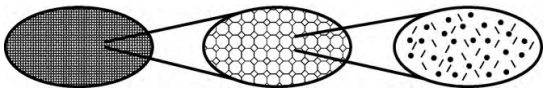

Fig. 1. Schematic representation of the microstructure hierarchy.

equation

$$u_{tt} = \left(c^2 - c_A^2\right) u_{xx} + p^2 c_A^2 \left(u_{tt} - c_1^2 u_{xx}\right)_{xx}, \tag{6}$$

which clearly shows two wave operators ordered hierarchically. Here $c_A^2 = A^2/\rho_0 B$, $c_1^2 = C/I$, and $p^2 = I/B$. The model described above takes into account a single microstructure. As it was noted by Srolovitz and Chen (2005) "disparate microstructural features often interact in significant and surprising ways". It follows that the multiscale modeling is necessary for the description of the microstructure evolution. It may happen that (i) a microstructure includes another microstructure at a smaller scale or (ii) there are two concurrent microstructures. In this paper we briefly describe case (i) which is known earlier (Engelbrecht et al., 2006) and elaborate models corresponding to case (ii). The microstructures are described by internal variables providing the corresponding fields of integral microstructural effects at each material point.

2. Hierarchical microstructures

The case of two hierarchical microstructures ("the scale within the scale") is analyzed by Engelbrecht et al. (2006). The corresponding microstructure hierarchy is represented schematically in Fig. 1.

In this case, the free energy is dependent on two internal variables φ_1 and φ_2 as follows:

$$W = \frac{\rho_0 c^2}{2} u_x^2 + A_1 \varphi_1 u_x + \frac{1}{2} B_1 \varphi_1^2 + \frac{1}{2} C_1 (\varphi_1)_x^2 + + A_{12} (\varphi_1)_x \varphi_2 + \frac{1}{2} B_2 \varphi_2^2 + \frac{1}{2} C_2 (\varphi_2)_x^2. \tag{7}$$

This leads to expressions of stresses in the form

$$\sigma = \frac{\partial W}{\partial u_x} = \rho_0 c^2 u_x + A_1 \varphi_1,$$
$$\eta_1 = -\frac{\partial W}{\partial (\varphi_1)_x} = -C_1 (\varphi_1)_x - A_{12} \varphi_2, \qquad \eta_2 = -\frac{\partial W}{\partial (\varphi_2)_x} = -C_2 (\varphi_2)_x, \tag{8}$$

and to interactive internal forces

$$\tau_1 = -\frac{\partial W}{\partial \varphi_1} = -A_1 u_x - B_1 \varphi_1, \qquad \tau_2 = -\frac{\partial W}{\partial \varphi_2} = -A_{12} (\varphi_1)_x - B_2 \varphi_2. \tag{9}$$

Accordingly, the equations of motion take the form

$$\rho_0 u_{tt} = \sigma_x = \rho_0 c^2 u_{xx} + A_1 (\varphi_1)_x, \tag{10}$$
$$I_1 (\varphi_1)_{tt} = \tau_1 - (\eta_1)_x = C_1 (\varphi_1)_{xx} - A_1 u_x - B_1 \varphi_1, \tag{11}$$
$$I_2 (\varphi_2)_{tt} = \tau_2 - (\eta_2)_x = C_2 (\varphi_2)_{xx} - A_{12} (\varphi_1)_x - B_2 \varphi_2, \tag{12}$$

where I_1 and I_2 are appropriate internal inertia measures.

In the hierarchical case, only the motion of the first microstructure is coupled with the macromotion, and the motion of the second microstructure is coupled with that of the first one.

3. Concurrent microstructures

Another example of possible coupling of macromotion and microstructures is illustrated in Fig. 2. In this case the macrodisplacement is directly connected also to the second internal variable

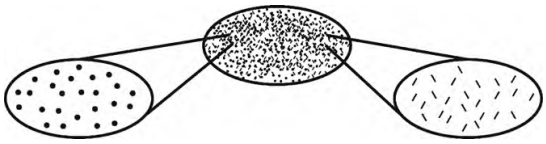

Fig. 2. Schematic representation of concurrent microstructures.

and the free energy dependence (7) is therefore modified by adding an additional term

$$W = \frac{\rho_0 c^2}{2} u_x^2 + A_1 \varphi_1 u_x + \frac{1}{2} B_1 \varphi_1^2 + \frac{1}{2} C_1 (\varphi_1)_x^2 + A_{12} (\varphi_1)_x \varphi_2 + \frac{1}{2} B_2 \varphi_2^2 + \frac{1}{2} C_2 (\varphi_2)_x^2 + A_2 \varphi_2 u_x. \tag{13}$$

Here both internal variables describe the corresponding fields of deformation induced by microstructures. In this case the equations of motion look more symmetrical

$$\rho_0 u_{tt} = \rho_0 c^2 u_{xx} + A_1 (\varphi_1)_x + A_2 (\varphi_2)_x, \tag{14}$$
$$I_1 (\varphi_1)_{tt} = C_1 (\varphi_1)_{xx} + A_{12} (\varphi_2)_x - A_1 u_x - B_1 \varphi_1, \tag{15}$$
$$I_2 (\varphi_2)_{tt} = C_2 (\varphi_2)_{xx} - A_{12} (\varphi_1)_x - A_2 u_x - B_2 \varphi_2. \tag{16}$$

In the considered case, equations of motion for microstructures are coupled with the balance of linear momentum for the macromotion and with each other.

Even a more symmetric case corresponds to completely independent microstructures. The free energy function is constructed here as the sum of two similar contributions

$$W = \frac{\rho_0 c^2}{2} u_x^2 + A_1 \varphi_1 u_x + \frac{1}{2} B_1 \varphi_1^2 + \frac{1}{2} C_1 (\varphi_1)_x^2 + A_2 \varphi_2 u_x + \frac{1}{2} B_2 \varphi_2^2 + \frac{1}{2} C_2 (\varphi_2)_x^2. \tag{17}$$

The corresponding stresses are determined as previously

$$\sigma = \frac{\partial W}{\partial u_x} = \rho_0 c^2 u_x + A_1 \varphi_1 + A_2 \varphi_2,$$
$$\eta_1 = -\frac{\partial W}{\partial (\varphi_1)_x} = -C (\varphi_1)_x, \qquad \eta_2 = -\frac{\partial \bar{W}}{\partial (\varphi_2)_x} = -C (\varphi_2)_x, \tag{18}$$

as well as the interactive internal forces

$$\tau_1 = -\frac{\partial W}{\partial \varphi_1} = -A_1 u_x - B_1 \varphi_1, \qquad \tau_2 = -\frac{\partial W}{\partial \varphi_2} = -A_2 u_x - B_2 \varphi_2. \tag{19}$$

The equations of motion here are similar to those in Eq. (5)

$$\rho_0 u_{tt} = \rho_0 c^2 u_{xx} + A_1 (\varphi_1)_x + A_2 (\varphi_2)_x, \tag{20}$$

$$I_1 (\varphi_1)_{tt} = C_1 (\varphi_1)_{xx} - A_1 u_x - B_1 \varphi_1,$$
$$I_2 (\varphi_2)_{tt} = C_2 (\varphi_2)_{xx} - A_2 u_x - B_2 \varphi_2. \tag{21}$$

In the latter case, equations of motion for microstructures are coupled with the balance of linear momentum for the macromotion, but not coupled with each other.

4. Scale separation

To demonstrate the scale separation explicitly, the dimensionless variables should be introduced as follows:

$$U = \frac{u}{U_0}, \qquad X = \frac{x}{L}, \qquad T = \frac{ct}{L}, \tag{22}$$

where U_0 and L are certain constants (e.g., intensity and wavelength of the initial excitation). To characterize microstructures we also need to introduce scaled microdeformations

$$\Phi_1 \equiv \frac{l_1}{L}\varphi_1, \qquad \Phi_2 \equiv \frac{l_2}{L}\varphi_2. \tag{23}$$

In terms of dimensionless variables, the equation of motion at the macroscale (20) reads

$$U_{TT} = U_{XX} + \frac{A_1}{\rho_0 c^2}\frac{l_1}{U_0}(\Phi_1)_X + \frac{A_2}{\rho_0 c^2}\frac{l_2}{U_0}(\Phi_2)_X, \tag{24}$$

and the corresponding micromotions are governed by

$$\frac{I_1}{L^2\rho_0}\frac{l_1}{L}(\Phi_1)_{TT} = \frac{C_1}{L^2\rho_0 c^2}\frac{l_1}{L}(\Phi_1)_{XX} - \frac{A_1}{\rho_0 c^2}\frac{U_0}{L}U_X - \frac{B_1}{\rho_0 c^2}\frac{l_1}{L}\Phi_1, \tag{25}$$

and

$$\frac{I_2}{L^2\rho_0}\frac{l_2}{L}(\Phi_2)_{TT} = \frac{C_2}{L^2\rho_0 c^2}\frac{l_2}{L}(\Phi_2)_{XX} - \frac{A_2}{\rho_0 c^2}\frac{U_0}{L}U_X - \frac{B_2}{\rho_0 c^2}\frac{l_2}{L}\Phi_2, \tag{26}$$

respectively. As it can be seen, contributions of microstructures and their motion can be separated clearly if the difference of their characteristic scales, l_1 and l_2, is large enough.

5. Dispersion analysis

In order to study dispersive effects, we derive the dispersion relations by assuming the solutions in the form of harmonic waves

$$u(x,t) = \hat{u}e^{i(kx-\omega t)}, \qquad \varphi_1(x,t) = \hat{\varphi}_1 e^{i(kx-\omega t)},$$
$$\varphi_2(x,t) = \hat{\varphi}_2 e^{i(kx-\omega t)}, \tag{27}$$

where k is the wavenumber, ω is the frequency, and $i^2 = -1$. Substituting relations (27) into Eqs. (10)–(12) we get

$$\begin{pmatrix} \rho_0 c^2 k^2 - \rho_0\omega^2 & -iA_1 k & 0 \\ iA_1 k & C_1 k^2 - I_1\omega^2 + B_1 & -iA_{12}k \\ 0 & iA_{12}k & C_2 k^2 - I_2\omega^2 + B_2 \end{pmatrix} \begin{pmatrix} \hat{u} \\ \hat{\varphi}_1 \\ \hat{\varphi}_2 \end{pmatrix} = 0. \tag{28}$$

In order to get nontrivial solutions the determinant of this system must vanish. This leads to the dispersion relation

$$(c^2k^2 - \omega^2)(c_1^2k^2 - \omega^2 + \omega_1^2)(c_2^2k^2 - \omega^2 + \omega_2^2) - c_{A12}^2\omega_2^2k^2(c^2k^2 - \omega^2) - c_{A1}^2\omega_1^2k^2(c_2^2k^2 - \omega^2 + \omega_2^2) = 0, \tag{29}$$

where parameters

$$c_1^2 = \frac{C_1}{I_1}, \quad c_2^2 = \frac{C_2}{I_2}, \quad c_{A1}^2 = \frac{A_1^2}{\rho_0 B_1}, \quad c_{A12}^2 = \frac{A_{12}^2}{I_1 B_2}, \quad \omega_1^2 = \frac{B_1}{I_1}, \quad \omega_2^2 = \frac{B_2}{I_2}, \tag{30}$$

have been introduced. The parameters c_i and c_{Ai} represent characteristic velocities in microstructures, and ω_i are characteristic frequencies.

Dispersion relations for concurrent microstructures are derived in similar way. For Eqs. (14)–(16) and (20)–(21) we get

$$(c^2k^2 - \omega^2)(c_1^2k^2 - \omega^2 + \omega_1^2)(c_2^2k^2 - \omega^2 + \omega_2^2) + c_{A12}^2\omega_2^2k^2(-c_0^2k^2 + \omega^2) - c_{A1}^2\omega_1^2k^2(c_2^2k^2 - \omega^2 + \omega_2^2) - c_{A2}^2k^2\omega_2^2(c_1^2k^2 - \omega^2 + \omega_1^2) = 0, \tag{31}$$

and

$$(c^2k^2 - \omega^2)(c_1^2k^2 - \omega^2 - \omega_1^2)(c_2^2k^2 - \omega^2 + \omega_2^2) - c_{A2}^2\omega_2^2k^2(c_1^2k^2 - \omega^2 + \omega_1^2) - c_{A1}^2\omega_1^2k^2(c_2^2k^2 - \omega^2 + \omega_2^2) = 0, \tag{32}$$

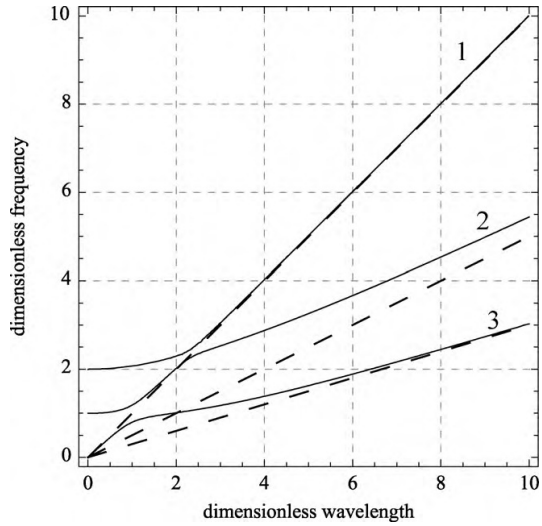

Fig. 3. Dispersion curves of Eq. (34) for $\gamma_{A1} = \gamma_{A12} = 0.4$, $\gamma_1 = 0.5$, $\gamma_2 = 0.3$, and $\eta_2 = 2$: (1,2) optical branches, (3) acoustical branch; dashed lines, asymptotes to dispersion curves.

respectively. In these equations the velocity $c_{A2}^2 = A_2^2/(\rho_0 B_2)$ has been introduced. To reduce the number of coefficients, the dimensionless quantities

$$\xi = \frac{ck}{\omega_1}, \qquad \eta = \frac{\omega}{\omega_1} \tag{33}$$

are used. Introducing the latter into Eqs. (29), (31) and (32) yields the dispersion relations in dimensionless form

$$(\xi^2 - \eta^2)(\gamma_1^2\xi^2 - \eta^2 + \eta_1^2)(\gamma_2^2\xi^2 - \eta^2 + \eta_2^2) - \gamma_{A12}^2\eta_2^2\xi^2(\xi^2 - \eta^2) - \gamma_{A1}^2\xi^2(\gamma_2^2\xi^2 - \eta^2 + \eta_2^2) = 0, \tag{34}$$

$$(\xi^2 - \eta^2)(\gamma_1^2\xi^2 - \eta^2 + \eta_1^2)(\gamma_2^2\xi^2 - \eta^2 + \eta_2^2) - \gamma_{A12}^2\eta_2^2\xi^2(\xi^2 - \eta^2) - \gamma_{A1}^2\xi^2(\gamma_2^2\xi^2 - \eta^2 + \eta_2^2) - \gamma_{A2}^2\eta_2^2\xi^2(\gamma_1^2\xi^2 - \eta^2 + \eta_1^2) = 0, \tag{35}$$

and

$$(\xi^2 - \eta^2)(\gamma_1^2\xi^2 - \eta^2 + \eta_1^2)(\gamma_2^2\xi^2 - \eta^2 + \eta_2^2) - \gamma_{A2}^2\eta_2^2\xi^2(\gamma_1^2\xi^2 - \eta^2 + \eta_1^2) - \gamma_{A1}^2\xi^2(\gamma_2^2\xi^2 - \eta^2 + \eta_2^2) = 0, \tag{36}$$

respectively. New parameters denote velocity ratios and dimensionless frequencies

$$\gamma_1 = \frac{c_1}{c}, \quad \gamma_2 = \frac{c_2}{c}, \quad \gamma_{A1} = \frac{c_{A1}}{c}, \quad \gamma_{A2} = \frac{c_{A2}}{c}, \quad \gamma_{A12} = \frac{c_{A12}}{c}, \quad \eta_1 = 1, \quad \eta_2 = \frac{\omega_2}{\omega_1}. \tag{37}$$

The characteristic set of dispersion curves is shown in Fig. 3. For simplicity we look first at the dispersion curves given by hierarchical microstructure (34). The dispersion relation (34) represents three branches which in general are distinct (see Fig. 3). While lower curve is called acoustical, the two higher frequency curves are called optical and they reflect internal modes of oscillation (Mindlin, 1964). The acoustical curve starts at the origin with a slope $\eta = (1 - \gamma_{A1}^2)^{1/2}\xi$, then it approaches $\eta = (\gamma_1^2 - \gamma_{A12}^2)^{1/2}\xi$ and $\eta = \gamma_2\xi$ in the short wave limit. The middle optical curve starts at $\eta = \eta_1$ with a slope $\eta = \xi$ and then approaches $\eta = \gamma_1\xi$ in the short

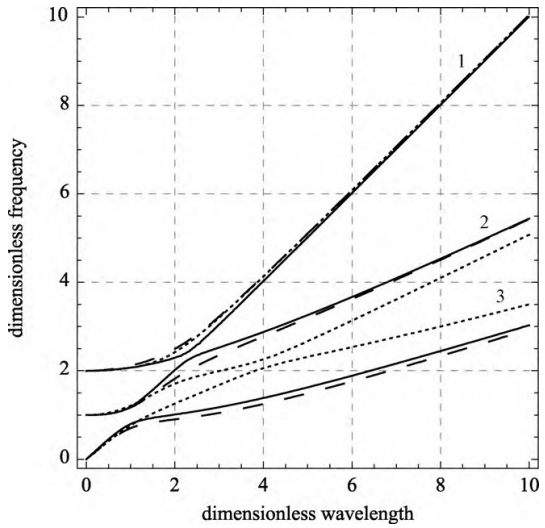

Fig. 4. Comparison of dispersion curves of Eqs. (34)–(36) for $\gamma_{A1} = \gamma_{A2} = \gamma_{A12} = 0.4$, $\gamma_1 = 0.5$, $\gamma_2 = 0.3$, and $\eta_2 = 2$: solid lines, hierarchical model (34); dashed lines, concurrent model (35); dotted lines, concurrent model (36).

wave limit. The second optical curve starts at $\eta = \eta_2$ and approaches $\eta = \xi$. The asymptotical values $\eta = \xi$, $\eta = \gamma_1\xi$ and $\eta = \gamma_2\xi$ are represented by dashed lines in Fig. 3. Although the dispersion relations (34)–(36) are at the first sight similar, there are certain differences in the dispersion curves (see Fig. 4). The important similarities between the models is that all three models are represented by three dispersion curves and in the short wave limit the corresponding curves in different models approach the same values - $\eta = \xi$ for the highest curve, $\eta = \gamma_1\xi$ for the middle curve and $\eta = \gamma_2\xi$ for the lowest curve. While the differences between concurrent model (35) (represented by dashed line in Fig. 4) and hierarchical model (represented by solid line in Fig. 4) are very subtle, the concurrent model (36) (represented by dotted line in Fig. 4) has noticeable differences in acoustical and middle optical curve. The acoustical curve starts with a slope $\eta = (1 - \gamma_{A1}^2 - \gamma_{A2}^2)^{1/2}\xi$, then it approaches $\eta = \gamma_1\xi$ and $\eta = \gamma_2\xi$ in the short wave limit. The middle optical curve starts with a slope $\eta = (1 - \gamma_{A2}^2)^{1/2}\xi$ and then approaches $\eta = \gamma_2\xi$ and $\eta = \gamma_1\xi$ in the short wave limit (cf. asymptotes in Fig. 3).

6. Conclusions

The Mindlin's idea on describing a microstructure is enlarged to multiple scales by using the concept of internal variables. The models and the corresponding dispersion relations are physically well grounded and display essential differences for medium-range wavelengths. This opens possibilities to distinguish the microstructured solids by measuring the wave-field characteristics. It is clear that the complexity of microstructure can be increased by means of the combination of simple microstructure models considered above. Nonlinear terms may be introduced at any level of description as well as at the coupling. The analysis of corresponding wave profiles is in progress.

Acknowledgement

Support of the Estonian Science Foundation under grant No. 7037 is gratefully acknowledged.

References

Berezovski, A., Engelbrecht, J., Maugin, G.A., 2009. One-dimensional microstructure dynamics. In: Ganghoffer, J.-F., Pastrone, F. (Eds.), Mechanics of Microstructured Solids: Cellular Materials, Fibre Reinforced Solids and Soft Tissues. Springer, Berlin, pp. 21–28.

Capriz, G., 1989. Continua with Microstructure. Springer, Heidelberg.

Chen, W., Fish, J., 2001. A dispersive model for wave propagation in periodic heterogeneous media based on homogenization with multiple spatial and temporal scales. ASME J. Appl. Mech. 68, 153–161.

Engelbrecht, J., Berezovski, A., Pastrone, F., Braun, M., 2005. Waves in microstructured materials and dispersion. Philos. Mag. 85, 4127–4141.

Engelbrecht, J., Pastrone, F., Braun, M., Berezovski, A., 2006. Hierarchies of waves in nonclassical materials. In: Delsanto, P.-P. (Ed.), Universality of Nonclassical Nonlinearity: Applications to Non-Destructive Evaluations and Ultrasonics. Springer, Berlin, pp. 29–47.

Engelbrecht, J., Cermelli, P., Pastrone, F., 1999. Wave hierarchy in microstructured solids. In: Maugin, G.A. (Ed.), Geometry, Continua and Microstructure. Hermann Publ., Paris, pp. 99–111.

Eringen, A.C., Suhubi, E.S., 1964. Nonlinear theory of simple microelastic solids I & II. Int. J. Eng. Sci. 2, 189–203, 389–404.

Erofeeyev, V.I., 2003. Wave Processes in Solids with Microstructure. World Scientific, Singapore.

Kunin, I.A., 1982. Elastic Media with Microstructure I. One-Dimensional Models. Springer, Berlin.

Kunin, I.A., 1983. Elastic Media with Microstructure II. Three-Dimensional Models. Springer, Berlin.

Metrikine, A.V., Askes, H., 2002. One-dimensional dynamically consistent gradient elasticity models derived from a discrete microstructure—part 1: generic formulation. Eur. J. Mech. A Solids 21, 555–572.

Metrikine, A.V., 2006. On causality of the gradient elasticity models. J. Sound Vibr. 297, 727–742.

Mindlin, R.D., 1964. Microstructure in linear elasticity. Arch. Rat. Mech. Anal. 16, 51–78.

Santosa, F., Symes, W.W., 1991. A dispersive effective medium for wave propagation in periodic composites. SIAM J. Appl. Math. 51, 984–1005.

Srolovitz, D.J., Chen, L.-Q., 2005. Introduction: Microstructure. In: Yip, S. (Ed.), Handbook of Materials Modeling. Springer, Dordrecht, pp. 2083–2086.

Ván, P., Berezovski, A., Engelbrecht, J., 2008. Internal variables and dynamic degrees of freedom. J. Non-Equilib. Thermodyn. 33, 235–254.

Appendix C: CV

CURRICULUM VITAE

1. Personal data

Name	Tanel Peets
Date and place of birth	16 December 1977, Tallinn, Estonia
Nationality	Estonian

2. Contact information

Address	Institute of Cybernetics at TUT, Akadeemia tee 21,12618 Tallinn, Estonia
Phone	+372 6204168
E-mail	tanelp@cens.ioc.ee

3. Education

2006– . . .	Tallinn University of Technology, Faculty of Science, Engineering Physics, PhD studies
2006	Tallinn University of Technology, Faculty of Science, Engineering Physics, MSc
2003	Tallinn University of Technology, Faculty of Information Technology, Electronics and Biomedical Engineering, BEng

4. Special courses

2002	Tallinn Pedagogical University, School pedagogy course

5. Language competence

Estonian	native
English	fluent
Finnish	fluent
French	average
Russian	average

6. Professional employment

2009– ...	Institute of Cybernetics at Tallinn University of Technology, Researcher
2007– ...	Tallinn University of Technology, Faculty of Civil Engineering, Department of Mechanics, Lecturer
2006–2009	Institute of Cybernetics at Tallinn University of Technology, Extraordinary researcher
2006–2006	Institute of Cybernetics at Tallinn University of Technology, Technician
2004–2006	Rocca al Mare School, Teacher (physics)
2003–2005	Estonian Business School, High school, Teacher (physics in English)
2001–2004	Old Town Educational College, Teacher (physics)
1996–2001	OÜ EKE Nora, Consultant

7. Voluntary work

2001–2007	Estonian Scout Association, National Board member, International Commissioner

8. Honours and awards

- 2009, Tanel Peets; The best scientific publication of a young scientist at the Institute of Cybernetics at TUT – Tanel Peets, Merle Randrüüt, Jüri Engelbrecht: On modelling dispersion in microstructured solids. *Wave Motion*, **45**(4) (2008) 471–480

9. Defended thesis

- 2006, Dispersion in microstructured materials, MSc, supervisor Prof. Jüri Engelbrecht, Tallinn University of Technology, Faculty of Science

10. Field of research

- Waves in microstructured solids

11. Scientific work

Papers

1. Arkadi Berezovski, Jüri Engelbrecht and Tanel Peets. Multiscale modelling of microstructured solids. *Mechanics Research Communications*, **37**(6): 531-/534, 2010.

2. Tanel Peets and Kert Tamm. Dispersion analysis of wave motion in microstructured solids. In T.-T. Wu and C.-C. Ma, editors, *IUTAM Symposium on Recent Advances of Acoustic Waves in Solids: Proceedings, Taipei, Taiwan, May 25–28, 2009*, volume 26 of IUTAM Bookseries, pages 349-354. Springer, Dordrecht, 2010.

3. Tanel Peets, Merle Randrüüt and Jüri Engelbrecht. On modelling dispersion in microstructured solids. *Wave Motion*, **45**(4): 471–480, 2008.

Abstracts

1. Tanel Peets. Internal scales and dispersive properties of microstructured materials. In: Book of Abstracts. The Seventh IMACS International Conference on Nonlinear Evolution Equations and Wave Phenomena: Computation and Theory, Athens, Georgia, April 04–07, 2011. Thiab Taha (Editor), Athens: University of Georgia, 2011, page 64.

2. Tanel Peets. Dispersion analysis of wave motion in microstructured solids. In: IUTAM Symposium on Recent Advances of Acoustic Waves in Solids : May 25–28, 2009, Institute of Applied Mechanics, National Taiwan University, Taipei, Taiwan, 2009, page 39

Conferences

1. Tanel Peets, Internal scales and dispersive properties of microstructured materials, The Seventh IMACS International Conference on Nonlinear Evolution Equations and Wave Phenomena: Computation and Theory, The University of Georgia, Athens, USA, April 04–07, 2011.

2. Tanel Peets (speaker), Kert Tamm, Dispersion Analysis on Wave Motion in Microstructured Solids, Symposium on Recent Advances of Acoustic Waves in Solids, Taiwan, May 25–28, 2009 (invited presentation).

3. Tanel Peets, Dispersiooni modelleerimine mikrostruktuuriga materjalide jaoks (Modelling of dispersion in microstructured solids), XIII Estonian Mechanics days, Tallinn, Sept 15–16, 2008.

ELULOOKIRJELDUS

1. Isikuandmed

Nimi	Tanel Peets
Sünniaeg ja -koht	16.12.1977, Tallinn, Eesti
Kodakondsus	Eesti

2. Kontaktandmed

Aadress	TTÜ Küberneetika Instituut, Akadeemia tee 21, 12618 Tallinn
Telefon	+372 6204168
E-post	tanelp@cens.ioc.ee

3. Haridus

2006 - ...	Tallinna Tehnikaülikool, Matemaatika-loodusteaduskond, tehniline füüsika, doktoriõpe
2006	Tallinna Tehnikaülikool, Matemaatika-loodusteaduskond, tehniline füüsika, MSc
2003	Tallinna Tehnikaülikool, infotehnoloogia teaduskond, elektroonika ja biomeditsiinitehnika, BEng

4. Täiendõpe

2002 Tallinna Pedagoogikaülikooli Täiendõppekeskus, koolipedagoogika

5. Keelteoskus

eesti keel	emakeel
inglise keel	kõrgtase
soome keel	kõrgtase
prantsuse keel	kesktase
vene keel	kesktase

6. Teenistuskäik

2009 - ...	Tallinna Tehnikaülikooli Küberneetika Instituut, teadur
2007 - ...	Tallinna Tehnikaülikool, ehitusteaduskond, mehaanikainstituut, tunnitasuline õppejõud
2006 - 2009	Tallinna Tehnikaülikooli Küberneetika Instituut, erakorraline teadur
2006 - 2006	Tallinna Tehnikaülikooli Küberneetika Instituut,Tehnik
2004 - 2006	Rocca al Mare Kool, õpetaja (füüsika)
2003 - 2005	Estonian Business School, Gümnaasium, õpetaja (füüsika inglise keeles)
2001 - 2004	Vanalinna Hariduskolleegium, õpetaja (füüsika)
1996 - 2001	OÜ EKE Nora, konsultant

7. Vabatahtlik töö

2001 - 2007	Eesti Skautide Ühing, juhatuse liige, välissuhete juht

8. Autasud

- 2009, Tanel Peets; TTÜ Küberneetika Instituudi aasta parim teaduspublikatsioon noorte kategoorias -Tanel Peets, Merle Randrüüt, Jüri Engelbrecht: On modelling dispersion in microstructured solids. *Wave Motion*, **45**(4) (2008) 471 - 480.

9. Kaitstud lõputöö

- 2006, Dispersioon mikrostruktuursetes materjalides, MSc, juhendaja Prof. Jüri Engelbrecht, Tallinna Tehnikaülikool, Matemaatika-loodusteaduskond

10. Teadustöö põhisuunad

- Lainelevi mikrostruktuuriga tahkistes

11. Teadustegevus

Teadusartiklite, konverentsiteeside ja konverentsiettekannete loetelu on toodud ingliskeelse elulookirjelduse juures.

DISSERTATIONS DEFENDED AT
TALLINN UNIVERSITY OF TECHNOLOGY ON
NATURAL AND EXACT SCIENCES

1. **Olav Kongas.** Nonlinear dynamics in modeling cardiac arrhytmias. 1998.

2. **Kalju Vanatalu.** Optimization of processes of microbial biosynthesis of isotopically labeled biomolecules and their complexes. 1999.

3. **Ahto Buldas.** An algebraic approach to the structure of graphs. 1999.

4. **Monika Drews.** A metabolic study of insect cells in batch and continuous culture: application of chemostat and turbidostat to the production of recombinant proteins. 1999.

5. **Eola Valdre.** Endothelial-specific regulation of vessel formation: role of receptor tyrosine kinases. 2000.

6. **Kalju Lott.** Doping and defect thermodynamic equilibrium in ZnS. 2000.

7. **Reet Koljak.** Novel fatty acid dioxygenases from the corals *Plexaura homomalla* and *Gersemia fruticosa*. 2001.

8. **Anne Paju.** Asymmetric oxidation of prochiral and racemic ketones by using sharpless catalyst. 2001.

9. **Marko Vendelin.** Cardiac mechanoenergetics *in silico*. 2001.

10. **Pearu Peterson.** Multi-soliton interactions and the inverse problem of wave crest. 2001.

11. **Anne Menert.** Microcalorimetry of anaerobic digestion. 2001.

12. **Toomas Tiivel.** The role of the mitochondrial outer membrane in *in vivo* regulation of respiration in normal heart and skeletal muscle cell. 2002.

13. **Olle Hints.** Ordovician scolecodonts of Estonia and neighbouring areas: taxonomy, distribution, palaeoecology, and application. 2002.

14. **Jaak Nõlvak.** Chitinozoan biostratigrapy in the Ordovician of Baltoscandia. 2002.

15. **Liivi Kluge.** On algebraic structure of pre-operad. 2002.

16. **Jaanus Lass.** Biosignal interpretation: Study of cardiac arrhytmias and electromagnetic field effects on human nervous system. 2002.

17. **Janek Peterson.** Synthesis, structural characterization and modification of PAMAM dendrimers. 2002.

18. **Merike Vaher.** Room temperature ionic liquids as background electrolyte additives in capillary electrophoresis. 2002.

19. **Valdek Mikli.** Electron microscopy and image analysis study of powdered hardmetal materials and optoelectronic thin films. 2003.

20. **Mart Viljus.** The microstructure and properties of fine-grained cermets. 2003.

21. **Signe Kask.** Identification and characterization of dairy-related *Lactobacillus*. 2003.

22. **Tiiu-Mai Laht.** Influence of microstructure of the curd on enzymatic and microbiological processes in Swiss-type cheese. 2003.

23. **Anne Kuusksalu.** 2–5A synthetase in the marine sponge *Geodia cydonium*. 2003.

24. **Sergei Bereznev.** Solar cells based on polycristalline copper-indium chalcogenides and conductive polymers. 2003.

25. **Kadri Kriis.** Asymmetric synthesis of C2-symmetric bimorpholines and their application as chiral ligands in the transfer hydrogenation of aromatic ketones. 2004.

26. **Jekaterina Reut.** Polypyrrole coatings on conducting and insulating substracts. 2004.

27. **Sven Nõmm**. Realization and identification of discrete-time nonlinear systems. 2004.

28. **Olga Kijatkina.** Deposition of copper indium disulphide films by chemical spray pyrolysis. 2004.

29. **Gert Tamberg.** On sampling operators defined by Rogosinski, Hann and Blackman windows. 2004.

30. **Monika Übner.** Interaction of humic substances with metal cations. 2004.

31. **Kaarel Adamberg.** Growth characteristics of non-starter lactic acid bacteria from cheese. 2004.

32. **Imre Vallikivi.** Lipase-catalysed reactions of prostaglandins. 2004.

33. **Merike Peld.** Substituted apatites as sorbents for heavy metals. 2005.

34. **Vitali Syritski.** Study of synthesis and redox switching of polypyrrole and poly(3,4-ethylenedioxythiophene) by using *in-situ* techniques. 2004.

35. **Lee Põllumaa.** Evaluation of ecotoxicological effects related to oil shale industry. 2004.

36. **Riina Aav.** Synthesis of 9,11-secosterols intermediates. 2005.

37. **Andres Braunbrück.** Wave interaction in weakly inhomogeneous materials. 2005.

38. **Robert Kitt.** Generalised scale-invariance in financial time series. 2005.

39. **Juss Pavelson.** Mesoscale physical processes and the related impact on the summer nutrient fields and phytoplankton blooms in the western Gulf of Finland. 2005.

40. **Olari Ilison.** Solitons and solitary waves in media with higher order dispersive and nonlinear effects. 2005.

41. **Maksim Säkki.** Intermittency and long-range structurization of heart rate. 2005.

42. **Enli Kiipli.** Modelling seawater chemistry of the East Baltic Basin in the late Ordovician–Early Silurian. 2005.

43. **Igor Golovtsov.** Modification of conductive properties and processability of polyparaphenylene, polypyrrole and polyaniline. 2005.

44. **Katrin Laos.** Interaction between furcellaran and the globular proteins (bovine serum albumin ?-lactoglobulin). 2005.

45. **Arvo Mere.** Structural and electrical properties of spray deposited copper indium disulphide films for solar cells. 2006.

46. **Sille Ehala.** Development and application of various on- and off-line analytical methods for the analysis of bioactive compounds. 2006.

47. **Maria Kulp.** Capillary electrophoretic monitoring of biochemical reaction kinetics. 2006.

48. **Anu Aaspõllu.** Proteinases from *Vipera lebetina* snake venom affecting hemostasis. 2006.

49. **Lyudmila Chekulayeva.** Photosensitized inactivation of tumor cells by porphyrins and chlorins. 2006.

50. **Merle Uudsemaa.** Quantum-chemical modeling of solvated first row transition metal ions. 2006.

51. **Tagli Pitsi.** Nutrition situation of pre-school children in Estonia from 1995 to 2004. 2006.

52. **Angela Ivask.** Luminescent recombinant sensor bacteria for the analysis of bioavailable heavy metals. 2006.

53. **Tiina Lõugas.** Study on physico-chemical properties and some bioactive compounds of sea buckthorn (*Hippophae rhamnoides* L.). 2006.

54. **Kaja Kasemets.** Effect of changing environmental conditions on the fermentative growth of *Saccharomyces cerevisae* S288C: auxo-accelerostat study. 2006.

55. **Ildar Nisamedtinov.** Application of 13C and fluorescence labeling in metabolic studies of *Saccharomyces* spp. 2006.

56. **Alar Leibak.** On additive generalisation of Voronoï's theory of perfect forms over algebraic number fields. 2006.

57. **Andri Jagomägi.** Photoluminescence of chalcopyrite tellurides. 2006.

58. **Tõnu Martma.** Application of carbon isotopes to the study of the Ordovician and Silurian of the Baltic. 2006.

59. **Marit Kauk.** Chemical composition of CuInSe 2 monograin powders for solar cell application. 2006.

60. **Julia Kois.** Electrochemical deposition of CuInSe2 thin films for photovoltaic applications. 2006.

61. **Ilona Oja Acik.** Sol-gel deposition of titanium dioxide films. 2007.

62. **Tiia Anmann.** Integrated and organized cellular bioenergetic systems in heart and brain. 2007.

63. **Katrin Trummal.** Purification, characterization and specificity studies of metalloproteinases from *Vipera lebetina* snake venom. 2007.

64. **Gennadi Lessin.** Biochemical definition of coastal zone using numerical modeling and measurement data. 2007.

65. **Enno Pais.** Inverse problems to determine non-homogeneous degenerate memory kernels in heat flow. 2007.

66. **Maria Borissova.** Capillary electrophoresis on alkylimidazolium salts. 2007.

67. **Karin Valmsen.** Prostaglandin synthesis in the coral *Plexaura homomalla*: control of prostaglandin stereochemistry at carbon 15 by cyclooxygenases. 2007.

68. **Kristjan Piirimäe.** Long-term changes of nutrient fluxes in the drainage basin of the gulf of Finland – application of the PolFlow model. 2007.

69. **Tatjana Dedova.** Chemical spray pyrolysis deposition of zinc sulfide thin films and zinc oxide nanostructured layers. 2007.

70. **Katrin Tomson.** Production of labelled recombinant proteins in fed-batch systems in *Escherichia coli*. 2007.

71. **Cecilia Sarmiento.** Suppressors of RNA silencing in plants. 2008.

72. **Vilja Mardla.** Inhibition of platelet aggregation with combination of antiplatelet agents. 2008.

73. **Maie Bachmann.** Effect of Modulated microwave radiation on human resting electroencephalographic signal. 2008.

74. **Dan Hüvonen.** Terahertz spectroscopy of low-dimensional spin systems. 2008.

75. **Ly Villo.** Stereoselective chemoenzymatic synthesis of deoxy sugar esters involving *Candida antarctica* lipase B. 2008.

76. **Johan Anton.** Technology of integrated photoelasticity for residual stress measurement in glass articles of axisymmetric shape. 2008.

77. **Olga Volobujeva.** SEM study of selenization of different thin metallic films. 2008.

78. **Artur Jõgi.** Synthesis of 4'-substituted 2,3'-dideoxynucleoside analogues. 2008.

79. **Mario Kadastik.** Doubly charged Higgs boson decays and implications on neutrino physics. 2008.

80. **Fernando Pérez-Caballero.** Carbon aerogels from 5-methylresorcinol-formaldehyde gels. 2008.

81. **Sirje Vaask.** The comparability, reproducibility and validity of Estonian food consumption surveys. 2008.

82. **Anna Menaker.** Electrosynthesized conducting polymers, polypyrrole and poly(3,4-ethylenedioxythiophene), for molecular imprinting. 2009.

83. **Lauri Ilison.** Solitons and solitary waves in hierarchical Korteweg-de Vries type systems. 2009.

84. **Kaia Ernits.** Study of In2S3 and ZnS thin films deposited by ultrasonic spray pyrolysis and chemical deposition. 2009.

85. **Veljo Sinivee.** Portable spectrometer for ionizing radiation "Gammamapper". 2009.

86. **Jüri Virkepu.** On Lagrange formalism for Lie theory and operadic harmonic oscillator in low dimensions. 2009.

87. **Marko Piirsoo.** Deciphering molecular basis of Schwann cell development. 2009.

88. **Kati Helmja.** Determination of phenolic compounds and their antioxidative capability in plant extracts. 2010.

89. **Merike Sõmera.** Sobemoviruses: genomic organization, potential for recombination and necessity of P1 in systemic infection. 2010.

90. **Kristjan Laes.** Preparation and impedance spectroscopy of hybrid structures based on CuIn3Se5 photoabsorber. 2010.

91. **Kristin Lippur.** Asymmetric synthesis of 2,2'-bimorpholine and its 5,5'-substituted derivatives. 2010.

92. **Merike Luman.** Dialysis dose and nutrition assessment by an optical method. 2010.

93. **Mihhail Berezovski.** Numerical simulation of wave propagation in heterogeneous and microstructured materials. 2010.

94. **Tamara Aid-Pavlidis.** Structure and regulation of BDNF gene. 2010.

95. **Olga Bragina.** The role of Sonic Hedgehog pathway in neuro- and tumorigenesis. 2010.

96. **Merle Randrüüt.** Wave propagation in microstructured solids: solitary and periodic waves. 2010.

97. **Marju Laars.** Asymmetric organocatalytic Michael and aldol reactions mediated by cyclic amines. 2010.

98. **Maarja Grossberg.** Optical properties of multinary semiconductor compounds for photovoltaic applications. 2010.

99. **Alla Maloverjan.** Vertebrate homologues of Drosophila fused kinase and their role in Sonic Hedgehog signalling pathway. 2010.

100. **Priit Pruunsild.** Neuronal Activity-Dependent Transcription Factors and Regulation of Human BDNF Gene. 2010.

101. **Tatjana Knazeva.** New Approaches in Capillary Electrophoresis for Separation and Study of Proteins. 2011.

102. **Atanas Katerski.** Chemical Composition of Sprayed Copper Indium Disulfide Films for Nanostructured Solar Cells. 2011.

103. **Kristi Timmo.** Formation of Properties of CuInSe2 and Cu2ZnSn(S,Se)4 Monograin Powders Synthesized in Molten KI. 2011.

104. **Kert Tamm.** Wave Propagation and Interaction in Mindlin-Type Microstructured Solids: Numerical Simulation. 2011.

105. **Adrian Popp.** Ordovician Proetid Trilobites in Baltoscandia and Germany. 2011.

106. **Ove Pärn.** Sea Ice Deformation Events in the Gulf of Finland and This Impact on Shipping. 2011.

107. **Germo Väli.** Numerical Experiments on Matter Transport in the Baltic Sea. 2011.

108. **Andrus Seiman.** Point-of-Care Analyser Based on Capillary Electrophoresis. 2011.

109. **Olga Katargina.** Tick-Borne Pathogens Circulating in Estonia (Tick-Borne Encephalitis Virus, *Anaplasma phagocytophilum, Babesia* Species): Their Prevalence and Genetic Characterization. 2011.

110. **Ingrid Sumeri.** The Study of Probiotic Bacteria in Human Gastrointestinal Tract Simulator. 2011.

111. **Kairit Zovo.** Functional Characterization of Cellular Copper Proteome. 2011.

112. **Natalja Makarytsheva.** Analysis of Organic Species in Sediments and Soil by High Performance Separation Methods. 2011.

113. **Monika Mortimer.** Evaluation of the Biological Effects of Engineered Nanoparticles on Unicellular Pro- and Eukaryotic Organisms. 2011.

114. **Kersti Tepp.** Molecular System Bioenergetics of Cardiac Cells: Quantitative Analysis of Structure-Function Relationship. 2011.

115. **Anna-Liisa Peikolainen.** Organic Aerogels Based on 5-Methylresorcinol. 2011.

116. **Leeli Amon.** Palaeoecological Reconstruction of Late-Glacial Vegetation Dynamics in Eastern Baltic Area: A View Based on Plant Macrofossil Analysis. 2011.